HIGH LIGHT STRESS IN PHOTOSYNTHESIS: THE ROLE OF OXIDATIVE POST-TRANSLATIONAL MODIFICATIONS IN SIGNALING AND REPAIR

A Thesis
Presented to
The Academic Faculty

by

Tina Michelle Dreaden Kasson

In Partial Fulfillment
of the Requirements for the Degree
Doctor of Philosophy in the
School of Chemistry and Biochemistry

Georgia Institute of Technology
December 2012

*Tandem mass spectrometry experiments in Figures 2.7 and 3.5 were conducted by Sascha Rexroth (Department of Biology, Ruhr-Universität, Bochum, Germany).

HIGH LIGHT STRESS IN PHOTOSYNTHESIS: THE ROLE OF OXIDATIVE POST-TRANSLATIONAL MODIFICATIONS IN SIGNALING AND REPAIR

Approved by:

Prof. Bridgette A. Barry, Advisor
School of Chemistry and Biochemistry
Georgia Institute of Technology

Prof. David M. Collard
School of Chemistry and Biochemistry
Georgia Institute of Technology

Prof. Wendy L. Kelly
School of Chemistry and Biochemistry
Georgia Institute of Technology

Prof. Adegboyega (Yomi) K. Oyelere
School of Chemistry and Biochemistry
Georgia Institute of Technology

Prof. Ingeborg Schmidt-Krey
School of Biology; School of
Chemistry and Biochemistry
Georgia Institute of Technology

Date Approved: July 27, 2012

To my Mom, Dad, and Baby Brother

ACKNOWLEDGMENTS

I dedicate this thesis to my amazing family. I wish to thank my parents for their selfless encouragement, support, and love. I am thankful for my little brother, Erik, who inspires me to be a better scientist every day. I would like to thank my grandmother, who always believed in hard work and academic excellence. I am especially grateful for the patience and support of my husband, Kristopher. I would never have made it this far without all of you by my side.

I wish to acknowledge my advisor, Prof. Bridgette Barry, for her advice, patient encouragement, and inspirational excitement about research. I would also like to acknowledge Prof. Inga Schmidt-Krey for the much needed support concerning both research and life. I am grateful to my lab members, Dr. Adam Offenbacher, Dr. Cynthia Pagba, James Keough, Melissa Martinez, Brandon Polander, Zhanjun Guo, and Atlee Watson for the countless insightful conversations over the years. I would like to acknowledge my collaborators, Prof. Sascha Rexroth, Prof. Jun Chen, Matthew Johnson, Laura Kim, and Maureen Metcalf. I also wish to thank my thesis committee, Prof. Wendy Kelly, Prof. David Collard, and Prof. Yomi Oyelere for their guidance and helpful suggestions.

TABLE OF CONTENTS

LIST OF TABLES

LIST OF FIGURES

Chapter 3

Chapter 4

Chapter 5

LIST OF ABBREVIATIONS

2D	Two-dimensional
2D-GE	Two-dimensional gel electrophoresis
ApoB-100	Apoliprotein B-100
A. thaliana	*Arabidopsis thaliana*
ATP synthase	Adenosine 5'-triphosphate synthase
AU	Absorbance units
B5A	5-(Biotinamido)-pentylamine
BCIP/ NBT	5-Bromo-4-chloro-3-indolyl phosphate/ nitro blue tetrazolium
CCD	Charge-coupled device
Chl	Chlorophyll
^{3}Chl	Triplet chlorophyll
CN-PAGE	Clear native- polyacrylamide gel electrophoresis
DCBQ	2,6-Dichlorobenzoquinone
DDM	*n*-Dodecyl-β-D-maltoside
DMPC	Dimyristoylphosphatidylcholine
ELISA	Enzyme-linked immunosorbant assay
EM	Electron microscopy
EPR	Electron paramagnetic resonance
ESI MS	Electrospray ionization mass spectrometry
FFT	Fast fourier transform
FPLC	Fast protein liquid chromatography
FT	Fourier transform
FT-MS	Fourier transform mass spectrometry

FT-Raman	Fourier transform Raman
FtsH	Filamentation temperature-sensitive h
HEPES	4-(2-Hydroxyethyl)-piperazine-1-ethanesulfonic acid
HPLC	High performance liquid chromatography
LC-MS/MS	Liquid chromatography tandem mass spectrometry
LDL	Low density lipoprotein
LHCII	Light harvesting complex II
LPR	Lipid-to-protein ratio
MES	2-(*N*-Morpholino)-ethanesulfonic acid
MS/ MS	Tandem mass spectrometry
m/z	Mass/ charge
MSP	Manganese stabilizing protein
MWCO	Molecular weight cut-off
NCBI	National Center for Biotechnology Information
ND	Not determined
NFK	*N*-Formylkynurenine
OD	Optical density
OEC	Oxygen-evolving complex
$^1O_2$	Singlet oxygen
$^3O_2$	Triplet (ground state) oxygen
Pheo	Pheophytin
PsbO	33-kDa protein, manganese-stabilizing protin
PTM	Post-translational modification
PSI	Photosystem I
PSII	Photosystem II

PVDF	Polyvinylidene fluoride
Q_A	Plastoquinone Q_A
Q_B	Plastoquinone Q_B
ROS	Reactive oxygen species
Rubisco	Ribulose-1,5-bisphosphate carboxylase oxygenase
SDS-PAGE	Sodium dodecyl-sulfate polyacryalamide gel electrophoresis
SEC	Size exclusion chromatography
SOD	Superoxide dismutase
Synechosystis 6803	*Synechocystis* sp. PCC 6803
T. elongates	*Thermosynechococcus elongates*
TEM	Transmission electron microscopy
TFA	Trifluoroacetic acid
TM	Thylakoid membranes
TMA	Tetramethyl ammonium chloride
Trp	Tryptophan
Tris	Tris(hydroxylmethyl)aminoethane
T. vulcanus	*Thermosynechococcus vulcanus*
TW PSII	Tris-washed photosystem II
UV	Ultraviolet
UVRR	Ultraviolet resonance Raman
YD	Tyrosine D
YZ	Tyrosine Z

SUMMARY

Increased focus on the development of artificial photosynthetic systems and alternative energy sources has led to interest in how photosynthetic organisms adapt to stressful environmental conditions. Plants, algae, and cyanobacteria are particularly sensitive to high light intensity. Although repair mechanisms are in place to prevent long-term damage and inhibition from light stress, signals for initiation of key steps in repair are largely unknown. Post-translational modifications (PTMs) of amino acids have been proposed to participate in the signaling pathways. This thesis describes the identification and functional characterization of an oxidative PTM of tryptophan to *N*-formylkynurenine (NFK) in the Photosystem II (PSII) enzyme. PSII catalyzes the photo-induced water oxidation reaction in oxygenic photosynthesis. *In vitro* and *in vivo* biochemical studies suggest that NFK plays a role in protecting PSII from light-induced stress and functions as a signal in repair. This work has led to a new model of the signal and repair process. Preliminary work on 2D crystallization of an intact plant PSII complex is also presented. These experiments show promise for on-going structural studies by electron crystallography. PSII structure determination under native and light-stressed conditions may provide insight into conformational and sub-complex composition changes that accompany light stress and repair.

CHAPTER 1

INTRODUCTION

1.1 Photosystem II, photoinhibition, and oxidative stress

1.1.1 Oxygenic photosynthesis and PSII

Biological photosynthetic systems have come to the forefront of energy research. Oxygenic photosynthesis is a naturally clean and efficient process that maintains Earth's aerobic atmosphere. The carbon- containing compounds produced during carbon fixation provide a primary source of biomass for most ecological systems. Thus, better understanding of how photosynthetic plants, algae, and cyanobacteria adapt to climate change, increasing CO_2 emissions, and environmental stress is a key topic in energy research.

Temperature elevation and heightened solar intensity are direct results from greenhouse gas accumulation and ozone depletion. Photosynthetic plants and microorganisms are particularly sensitive to excess illumination. Photoinhibition is the phenomenon used to describe the decrease in photosynthetic activity and efficiency during exposure to high light (1). Irreversible damage to the reaction center proteins occurs, which triggers removal and replacement of damaged components (2). This cycle of damage and repair prevents long-term activity loss and enables recovery from damage induced under photo-oxidative conditions.

The Photosystem II (PSII) enzyme complex catalyzes the light-induced water oxidation and electron transfer reactions in the thylakoid membrane (Figure 1.1C) (3). The cyanobacterial PSII structure in *Thermosynechococcus vulcanus* (*T. vulcanus*) was

solved to 1.9 Å resolution (4-9). The higher plant PSII structure containing D1, D2, CP47, and cytochrome *b* was solved to 8 Å resolution (10). The PSII monomer has a molecular weight of ~350 kDa and is composed of more than 20 subunits (4). PSII contains both membrane- spanning intrinsic and extrinsic subunits (4). Cyanobacterial and plant PSII enzymes differ in the identities of the extrinsic and light- harvesting/ antennae polypeptides (11,12). The extrinsic polypeptides are bound to the lumenal surface of the thylakoid membrane and are required for optimal activity (Figure 1.1A) (13). PsbO, or the 33-kDa manganese stabilizing protein (MSP), is the only extrinsic protein conserved in both cyanobacteria and plants (12). Chlorophyll molecules located in "antennae" proteins capture and transfer light energy to the central reaction center where charge separation occurs. The membrane- embedded Light Harvesting Complex II (LHCII) proteins flank the PSII complex at the periphery and bind antennae chlorophyll molecules in plants (11). In cyanobacteria, phycobilin-containing phycobilisome proteins attach to the outer surface of the thylakoid membrane to harness light energy (11).

The PSII "core complex" is composed of the D1, D2, CP43, CP47, and extrinsic polypeptides (Figure 1.1B-C). The "core complex" proteins are the minimal essential components required for optimal water oxidation and electron transfer. The D1 and D2 polypeptides form the reaction center core and house the Mn_4CaO_5 active site and redox cofactors (4). The cofactors involved in electron transfer include redox-active chlorophylls, pheophytin, plastoquinones Q_A and Q_B, and Tyr_z (Figure 1.1C) (4). Calcium and chloride cofactors are also essential for optimal activity (13). Electrons ultimately derived from water oxidized at the Mn_4CaO_5 cluster are transferred from PSII onto the cytochrome b_6f complex via doubly- reduced Q_B (13). The CP43 and CP47 proteins

located on either side of D1 and D2 bind chlorophyll molecules and contain flexible loops that protrude into the lumen (Figure 1.1B) (4). Site-directed mutations of many residues in these loops have indicated their importance in assembly and photoinhibition (14).

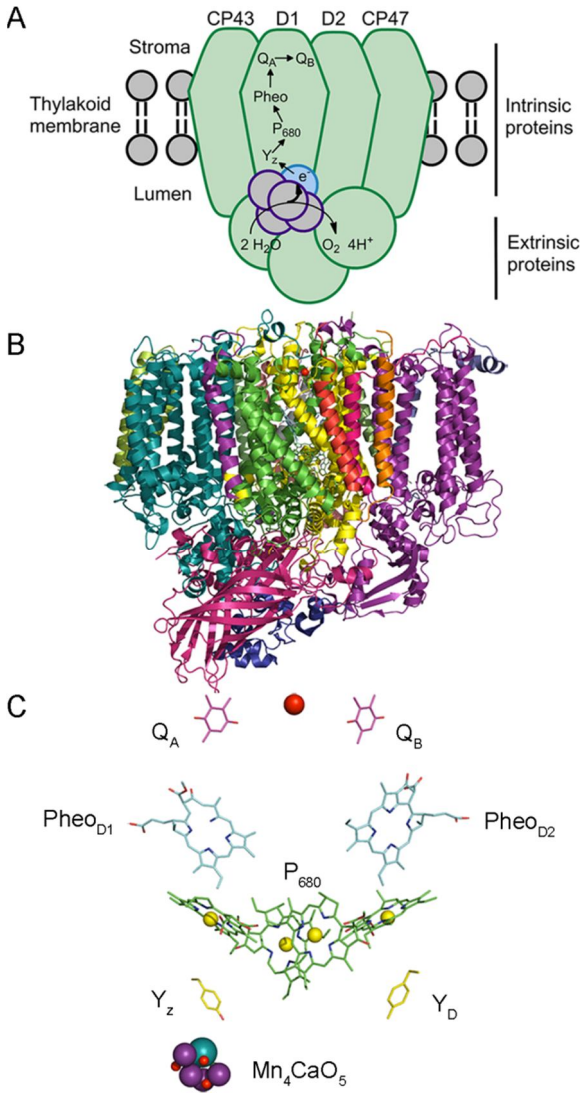

Figure 1.1. PSII model, X-ray structure, and electron transfer cofactors. (A) model of the PSII core complex monomer in the thylakoid membrane. The core polypeptides, water oxidation reaction at the Mn_4CaO_5 cluster, and electron transfer cofactors (Yz, P_{680}, Pheo, Q_A, and Q_B) are labeled. (B) PSII monomer from the *T. vulcanus* 1.9 Å resolution crystal structure (4) (PDB 3ARC). (C) PSII Mn_4CaO_5 cluster and electron transfer cofactors. The images shown in (B) and (C) were rendered in the PyMOL Molecular Graphics System, Version 1.5.0.1 (Schrödinger, LLC).

1.1.2 Photoinhibition, repair, and reactive oxygen species (ROS)

Plants and cyanobacteria are exposed to various levels of high light under physiological conditions. Repair mechanisms become activated under overwhelming light stress conditions to compensate for these environmental stresses. The D1 polypeptide, which binds the redox cofactors, is the primary target of photo-induced damage under excess illumination and exhibits a high rate of turnover (15). During turnover, D1 is quickly degraded and replaced by a new copy (15). Partial PSII complex disassembly and re-assembly are required for D1 replacement (2). The filamentation temperature- sensitive (FtsH) protease is the primary protease proposed to play a role in proteolysis of damaged D1 proteins (16-18). The signals for repair remain unanswered questions. However, post-translational oxidations of amino acids have been proposed to mediate initiation (18).

Various reactive oxygen species (ROS) are generated as a result of electron transfer reactions in photosynthesis (19). Formation of ROS is accelerated during photoinhibition, when the rate of light energy absorption exceeds the photosynthetic output capacity (20). ROS react with amino acid side chains and induce post-translational modifications (PTMs). PTMs perform a variety of essential functions, including cell regulation (21) and catalysis (22). Oxidative modifications also act as markers for damaged protein turnover (23).

Post-translational N- and C-terminal processing of PSII intrinsic subunits has been described (24-28). Increase in oxidative modifications of PSII reaction center proteins was observed in response to high light stress conditions in *Arabidopsi*s (29). The majority of the Trp oxidation products in the *Arabidopsis* thylakoid membrane

complexes were observed in PSII (29). Trp side chains in PSII react with ROS to generate many types of oxidative modifications (Figure 1.2) (30,31).

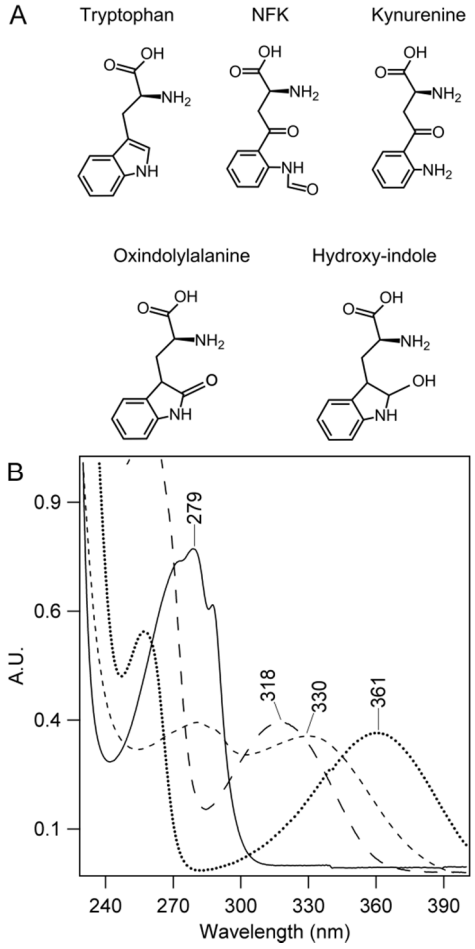

Figure 1.2. Chemical structures and optical absorption spectra of tryptophan and tryptophan oxidation products. The top row of (A) shows the chemical structures of tryptophan, NFK, and kynurenine. The bottom row shows oxindolylalanine and hydroxy-indole. (B) Optical absorption spectra of model tryptophan (solid line), NFK (coarse dashed line), and kynurenine (dotted line). For comparison, the absorption spectrum of PSII peptides containing NFK-365 in CP43 is also shown in (B) (fine dashed line).

1.1.3 Tryptophan oxidation to *N*-formylkynurenine (NFK)

Trp conversion to NFK has been detected in a variety of other proteins, including mitochondrial ATP Synthase (31), apolipoprotein B-100 (apoB-100) (32), MopE, and α-

crystallin (33) (Table 1.1). Studies of NFK formation in PSII and mitochondrial proteins show that the reaction is a very specific, ROS-mediated conversion (31,34). These results suggest that NFK formation plays a specialized functional role. NFK accumulates in PSII membranes during exposure to high light intensity stress, supporting a role in photoinhibition (31). In agreement with this hypothesis, substitution of the NFK-modified Trp (Trp-365) to alanine, cysteine, and leucine in the CP43 protein of *Synechocystis* sp. PCC 6803 (*Synechocystis* 6803) increases the rate of photoinhibition *in vivo* (30). General oxidations of amino acid side chains, such as Trp oxidation to NFK, have been proposed to play signaling roles in D1 turnover in repair (18). NFK may act as a trigger for proteolysis during photoinhibition in PSII (30,31). Although NFK has been identified in a number of proteins, few studies have assessed the functional relevance.

1.2 Detection of NFK

1.2.1 Mass spectrometry

Oxidation of the Trp side chain to NFK involves indole ring cleavage and addition of two oxygen atoms (35) (Figure 1.2A). Tandem mass spectrometry (MS/ MS) sequencing can be used to identify Trp residues modified to NFK by searching for the resulting +32 *m/z* mass increase (31,36). Other known Trp oxidations are distinguished from NFK by different mass shifts (Figure 1.2A). Kynurenine is another common Trp modification that results from the de-formylation of NFK under acidic conditions (30) (Figure 1.2A). Oxindolylalanine and hydroxyindole are singly- oxidized Trp derivatives

with mass shifts of +16 and +18 *m/z* (30). A proteomic approach with MS/ MS has been used to identify NFK and other Trp modifications in many types of proteins (Table 1.1).

Table 1.1. Overview of NFK modifications and methods of identification

Protein	Modified residue	Method of detection	Reference
PSII (CP43 subunit)	Trp-365	HPLC, MS/ MS, optical absorption, UVRR	(31)
PSII (D1 subunit)	Trp-317	HPLC, MS/ MS, optical absorption	(37)
PSII (CP24 subunit)	Trp-177	HPLC, MS/ MS, optical absorption	(31)
PSII (LHCII subunit)	Trp-128	MS/ MS	(38)
Apoliprotein B-100	N.D.	HPLC, Flourescence	(32)
Myoglobin	Trp-7, Trp-14	Western, MS/ MS	(39)
Aconitase-2 (mitochondria)	Trp-373, Trp-657	2D-GE, MS/ MS	(36)
ATP Synthase (alpha subunit)	Trp-503	2D-GE, MS/ MS	(34)
Frataxin	Trp-155	MS/ MS	(40)
Microsomes	N.D.	Flourescence	(41)
Rubisco	N.D.	Flourescence	(41)
Crystallin	N.D.	Flourescence	(33)
Troponin I	Trp-161	MS/ MS	(42)
Actin	Trp-79, Trp-340	MS/ MS	(42)

"Flourescence" indicates fluorescence spectroscopy; "Western" indicates Western blot

As previously observed in PSII, multiple types of oxidations can occur to the same Trp residue (30). Trp-365 (Trp-352 in *Synechocystis* 6803) in the CP43 subunit of PSII was modified to kynurenine, oxindolylalanine, and hydroxy-indole (30). This residue is highly conserved in cyanobacteria and plants (30). Our recent analysis in spinach PSII concluded that the same residue was modified to NFK (31).

Oxindolylalanine and hydroxy-indole were proposed reaction intermediates involved in kynurenine product formation (30).

1.2.2 UV spectroscopy

NFK has a unique optical signature that enables its detection in proteins (Figure 1.2B), fine-dashed line. NFK models (Figure 1.2B, fine-dashed line) can be synthesized by formylation of commercially available kynurenine (Sigma-Aldrich, St. Louis, MO) (43,44). Compared to natural Trp with a maximum absorption peak ~280 nm (Figure 1.2B, solid line), NFK has a red-shifted peak at ~320 nm (Figure 1.2B, course dashed line). Kynurenine can also be distinguished from Trp and NFK, with a λ_{max} ~360 nm (Figure 1.2B, dotted line). Oxindolylalanine and hydroxy-indole are also characterized by absorption spectra with maximum absorption peaks less than 300 nm (45,46).

NFK's red-shifted absorption enables optical detection and separation from non NFK-containing peptides. Detection of NFK-modified peptides in a complex mixture of un-modified peptides can be accomplished by monitoring elution at red-shifted wavelengths (31). Since un-modified natural peptides do not absorb at wavelengths longer than ~280- 290 nm, only peptides that contain NFK will be detected as peaks in the chromatogram (31). The fine dashed line in Figure 1.2B shows the absorption spectrum, derived from the 350 nm HPLC chromatogram, of a PSII peptide containing an NFK (31).

1.2.3 NFK covalently binds amines and hydrazines

NFK in proteins can bind to primary amines (31) and hydrazine (41,47). This property of NFK was used to purify NFK-containing PSII peptides for MS/MS sequencing (31). A primary amine linked to a biotin group was used for these experiments (31). The biotin handle enabled enrichment by avidin affinity chromatography (31). Binding was predicted to occur at the *N*-formyl nitrogen to form a ring- conjugated amidine (31). This type of purification could be used for sequence determination of NFK- modified peptides in any protein.

1.3 ROS generate NFK in PSII

Trp side chains in proteins can react with many types of ROS to generate NFK, including singlet oxygen ($^1O_2$) (38,48), ozone (O_3) (49), and hydroxyl radicals ($HO^{\bullet}$) (33). The electron transfer reactions and photosensitizing pigments are responsible for ROS generation during light stress in the thylakoid membranes of plants and cyanobacteria (20). Depending on the mechanism of photoinhibition, different types of ROS are produced in PSII. The roles that these ROS play in photoinhibition are also unclear. Several models of photoinhibition have also been proposed.

1.3.1 Charge recombination reactions in PSII lead to triplet chlorophyll and $^1O_2$

PSII catalyzes the photo-oxidation of two molecules of water to O_2 and four H^+. The green pigments that enable light energy utilization are called chlorophyll (chl). Each chl molecule contains a phorphyrin ring, Mg^{2+}, and a phytol tail. Initial light excitation of the primary donor chlorophyll P_{680} initiates electron transfer to pheophytin (Pheo) (Figure 1.1A and C). The result is the charge separated state $P_{680}^{+\bullet}Pheo^{-\bullet}$. On the PSII acceptor side, reduced $Pheo^{-\bullet}$ then rapidly transfers the electron to plastoquinone Q_A, then to the terminal acceptor Q_B (Figure 1.1A and C). The mobile Q_B acceptor is then exchanged with the plastoquinone pool in the membrane. On the donor side, a redox active tyrosine Y_z reduces $P_{680}^{+\bullet}$ (Figure 1.1A and C). The catalytic Mn_4O_5Ca cluster on the lumenal surface oxidizes a water molecule to reduce $Y_z^{+\bullet}$ (Figure 1.1). Four photons of light are required to oxidize two molecules of water at the active site.

In the presence of excess light and photoinhibition, alterations to PSII that slow the forward secondary electron transfer reactions can result in recombination between $P_{680}^{+\bullet}$ and $Pheo^{-\bullet}$. Over-reduction (50) and alterations in the midpoint potential (51) of Q_A can promote the back-electron flow (50). Recombination reactions between $Pheo^{-\bullet}$ and $P680^{+\bullet}$ promote formation of triplet chlorophyll (^{3}chl), $^3P_{680}$ (50,51). Energy transfer from triplet chlorophyll to ground state molecular oxygen ($^3O_2$) evolved nearby at the oxygen evolving complex (OEC), or Mn_4O_5Ca cluster, leads to the highly reactive singlet oxygen ($^1O_2$) (51). $^1O_2$ yield increases during photoinhibition and has been detected with EPR spin traps (52).

1.3.2 ^{3}Chl and $^1O_2$ are generated in the light-harvesting complex II (LHCII)

In addition to charge combination reactions, the light-harvesting antennae proteins are also a source of ^{3}chl and $^1O_2$ in higher plant PSII. A primary function of the antennae proteins is to capture light energy and transfer it to the reaction centers. In plants, the abundant LHCII proteins located on the periphery of PSII bind the majority of the chl *a* and chl *b* molecules in the thylakoid membrane. Chl molecules can act as photosensitizers in the antennae (53). Radical spin traps have detected $^1O_2$ during illumination of isolated LHCII (53). The $^1O_2$ was attributed to energy transfer from ^{3}chl to O_2 (53).

Chl molecules are energetically coupled in the protein matrix of the antennae. They are also coupled to carotenoids, which are protective $^1O_2$ quenchers (54). Damaged or incorrectly assembled antennae proteins can cause weak coupling of chl- carotenoid triplet energy transfer (55). A correlation between photoinhibition and uncoupling of both chl *a* and *b* was demonstrated in isolated thylakoids (55). Chl *b* is only present in the antennae proteins. Uncoupling of chl can result in increased $^1O_2$ production from inefficient quenching.

1.3.3 Trp reacts with $^1O_2$ to form NFK in PSII

NFK modifications have been described in the CP43 (31), D1 (37), and LHCII (38) subunits of PSII (31). Tandem mass spectrometry (MS/MS) determined the positions of the modifications at Trp-365 in CP43 and Trp-317 in D1 (31). The type of ROS

involved in Trp oxidation to NFK was proposed to be $^1O_2$ (31,38). Charge recombination may produce $^3P_{680}$ in the reaction center proteins, leading to $^1O_2$ production (31). Trp-365 (CP43) and Trp-317 (D1) are located ~17 and 24 Å away from the OEC, where the ROS are produced (Figure 1.3) (4).

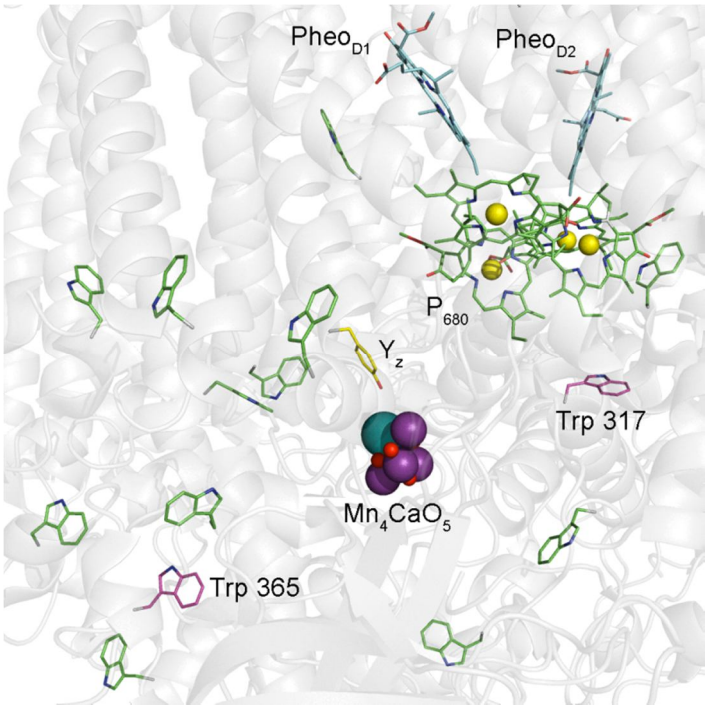

Figure 1.3. Locations of NFK- modified tryptophans in the 1.9 Å PSII crystal structure from *T. vulcanus* (4) PDB 3ARC. The Mn_4CaO_5 cluster, Yz, $Pheo_{D1}$, and $Pheo_{D2}$ are labeled. W365 (CP43) and W317 (D1) are colored in magenta. These residues were shown to be oxidized to NFK. The side chains of all Trp residues within 25 Å of the Mn_4CaO_5 cluster are shown in green (D1 protein: W97, W105; D2 protein: W191, W328; CP43 protein: W189, W223, W291, W359, W387, W425; Cytochrome c_{550} protein: W130). The image was rendered in the PyMOL Molecular Graphics System, Version 1.5.0.1 (Schrödinger, LLC).

The NFK formation in CP43 was detected in both dark- maintained spinach thylakoid and detergent solubilized PSII membranes (31). The presence of NFK in the thylakoid membranes ruled out any detergent- induced experimental artifact as

contributing to the NFK formation. Because the thylakoid and PSII membrane preparations were kept in the dark, light- induced electron transfer reactions that might generate $^1O_2$ were also prevented. This outcome supports that the NFK formation may have a precise physiological role in PSII. Experimental artifacts induced by sample handling were also ruled out as contributing to mitochondrial NFK modifications (56). In further support, there was no correlation between methionine oxidation, a known artifact of sample handling, and Trp modification (56).

Photosensitizing ^{3}chl was also proposed to be responsible for $^1O_2$ involved in conversion of Trp-132 to NFK in LHCII (38). Soft light illumination of thylakoid membranes induced production of highly reactive $^1O_2$, and the NFK modification (38). In this instance, the chl molecules act as photosensitizers to generate $^1O_2$. In addition to NFK modifications, ROS also induced protein aggregation and truncation, as assessed by 2-dimensional gel electrophoresis (2D-GE) and MS/MS (38). The ROS are also directly involved in cleavage of the antennae proteins from the N-terminal end (57). Protein truncation can induce changes in protein conformation and initiate weakened chl-chl or chl-carotenoid coupling (55). This pathway could promote NFK formation during photoinhibition. Although functional LHCII forms trimers (58), monomerization occurs during light stress (59). Only the LHCII monomers are targeted for proteolysis (60). NFK formation in the trimer could trigger the monomerization event under these conditions. Alternatively, NFK formation in the monomer could provide a signal for proteolysis of the targeted monomer, a process which is also controlled by light (60).

1.3.4 NFK modifications in PSII are induced by illumination

NFK modifications in PSII are light-induced. High light illumination results in an approximate two- fold increase in yield of CP43 NFK-365 in oxygen-evolving PSII membranes (31). Because PSII does not evolve oxygen in the dark, production of ROS is also suppressed in the absence of light. Removal of the OEC where $^1O_2$ originates also inhibits accumulation of NFK in CP43. This evidence supports that the $^1O_2$ involved in NFK formation in PSII originates at the OEC. It is not surprising to find NFK present in PSII maintained under dark conditions, however, because photodamage and protein turnover occur under any light intensity. Thus, detection of a low yield of NFK suggests that NFK modifications occur naturally under moderate conditions, not merely under extreme light stress.

Upon a modest ionic strength increase during illumination, a second NFK modification was detected in the D1 polypeptide (NFK-317) (Figure 1.3). Accumulation of CP43 NFK-365 was suppressed under these conditions. An ionic strength-induced conformational change in the flexible loop regions was suggested to account for this effect. Different PSII conformational states may result in various discrete NFK modifications. Although multiple NFKs exist, the modifications are not random. The targeted pathways suggest a specific functional role (discussed below).

1.3.5 Other ROS (H_2O_2, $HO^{\bullet}$, and $O_2^{\bullet-}$) in PSII

The combined generation of O_2 at the OEC together with the strong oxidation and reduction potential in PSII suggests that many other types of ROS are produced under conditions of light stress (20,61). Because the light-induced NFK accumulation occurred only in the presence of active oxygen evolution, ROS produced from photodamage occurring on the donor side should be eliminated as potential sources of NFK. However, the same ROS ($O_2^{\bullet-}$, H_2O_2, and $HO^{\bullet}$) have been attributed to NFK formation by different mechanisms on both the donor and acceptor side of PSII (20). On the donor side, release of the extrinsic proteins and OEC stimulated H_2O_2 production, which was explained by increased solvent accessibility leading to alternate water oxidation side reactions (62). The one electron oxidation and reduction of H_2O_2 then resulted in $O_2^{\bullet-}$ and $HO^{\bullet}$, respectively (reviewed in 20). In contrast, other work has demonstrated O_2 reduction on the acceptor side can result in $O_2^{\bullet-}$ under light stress conditions (20). Dismutation to H_2O_2, followed by a single electron reduction, then produces $HO^{\bullet}$ (20). Of these other ROS, $HO^{\bullet}$ is the only other potential source of reactant for NFK formation and cannot be ruled out.

1.4 Functional roles of NFK in PSII

1.4.1 NFK as a $^1O_2$ scavenger

Antioxidant systems are in place to protect PSII from damaging ROS. Enzymatic scavengers superoxide dismutase (SOD) and catalase eliminate reactive $O_2^{\bullet-}$ and H_2O_2

generated from electron transport (63). Non-enzymatic scavengers, such carotenoids and prenylquinols, protect from $^1O_2$ (63). The carotenoids physically quench $^1O_2$ by excitation energy transfer, which is important in the PSII reaction center (64). The prenylquinols, such as α-tocopherol, chemically react with $^1O_2$ to form a hydroperoxide intermediate that hydrolyzes to a quinone (65).

Specific Trp residues in CP43 and D1 may function as scavengers of $^1O_2$ in the reaction center. α-Tocopherol scavengers are predicted to reside close to the edge of the membrane (66). Their location enables them to chemically quench $^1O_2$ that is out of reach of β-carotene in the membrane. The reaction of α-tocopherol with $^1O_2$ is irreversible, which means that these molecules must be continuously re-synthesized. The chemical reaction of Trp with $^1O_2$ is also irreversible. The CP43 NFK-modified sidechain is similarly located close to the membrane edge in a lumenal loop region (Figure 1.3). In PSII, Trp may function as a ROS scavenger during excess light stress when α-Tocopherol cannot effectively scavenge the high yield of $^1O_2$ being produced. Small PSII intrinsic proteins have been proposed to play a similar direct role in enzymatic scavenging of $O_2^{\bullet-}$ (67).

1.4.2 NFK as a photosensitizer

Once produced as a PTM in PSII, NFK may also act as a photodynamic sensitizer (68). NFK can be formed by UV irradiation of proteins (69,70), and then serve as a UV-A absorbing chromophore. UV irradiation of NFK forms either an excited singlet state, in which an intra-molecular hydrogen bond can occur, or a long-lived triplet state (71).

An unusually red-shifted fluorescence is observed from NFK, which has been attributed to intra-molecular proton transfer between the hydrogen bonded formamide and ortho-carbonyl groups. The yield of the red shifted fluorescence increased in non-polar solvents (72). The NFK triplet state can react with oxygen to produce ROS species (68,73) or can directly oxidize substrates (69). Thus, UV- mediated photodamage to PSII could potentially utilize NFK as the photosensitizer (74) to further promote the repair cycle by generation of more ROS.

1.4.3 NFK in D1 turnover and repair

Degradation and replacement of the D1 protein is a key step in repair from light stress (2). Although the other polypeptides turn over at an increased rate during photoinhibition, compared to normal light-saturated conditions, the D1 protein is the primary site of photodamage and accordingly exhibits a much higher turnover rate. The steps involved in this repair cycle are demonstrated in Figure 1.4 (2). The first step is partial PSII complex disassembly (Figure 1.4, step 2), which is required for protease access to D1. The extrinsic polypeptides, OEC, and CP43 are removed in this initial step. New D1 synthesis (Figure 1.4, step 4) occurs concomitantly with damaged D1 proteolysis (Figure 1.4, step 3). The D2 and CP47 polypeptides remain complexed in the membrane. New D1 is then adjoined to the partial complex (Figure 1.4, step 5). The final step is PSII re-assembly to re-activate oxygen- evolving activity (Figure 1. 4, step 6).

Despite decades of research, key steps involved in the repair cycle remain elusive. Particularly, the signals for PSII disassembly, D1 proteolysis, and D1 translation are

unknown. Post-translational oxidations of amino acids have been proposed as signals (18). The Filamentation temperature-sensitive H (FtsH) protease is the primary protease proposed to be involved in D1 degradation (18). In *Arabidopsis*, FtsH alone mediates D1 proteolysis during photoinhibition (75). The FtsH protease is a weak unfoldase (76). Oxidation of Trp to NFK may trigger a conformational change to enable disassembly and trigger proteolysis (Figure 1.4).

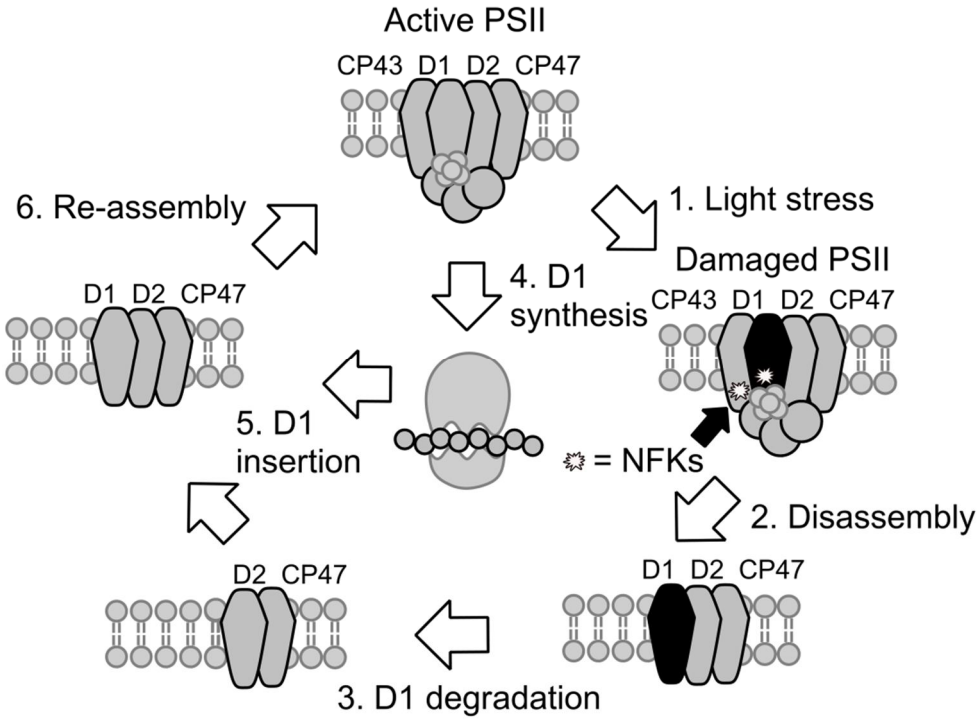

Figure 1.4. NFK in the D1 repair cycle. In step 1, the D1 polypeptide is damaged by exposure to high light illumination. NFK formation occurs. In step 2, the damaged PSII complex is partially disassembled. CP43, the OEC, and the extrinsic subunits are removed to enable access to the damaged D1 protein. Damaged D1 is degraded and removed in step 3. In steps 4 and 5, a new D1 polypeptide is synthesized and inserted into the partial D2-CP47 complex. Re-assembly of the complex in step 6 re-activates photosynthetic activity.

1.4.4 UV radiation in oxidative stress and NFK formation

With increasing ozone depletion, effects of increasing UV-B radiation on plants are emerging as an important area of research. Aromatic amino acids are susceptible to UV-B light and can be directly photo-oxidized or indirectly modified by endogenous photosensitizing pathways (77). Fluorescence spectroscopy was used to probe UV-B induced Trp oxidation in cucumber leaves (41). To compare NFK formation in membrane proteins and soluble proteins, microsomes and ribulose-1,5-bisphosphate carboxylase oxygenase (Rubisco) were analyzed (41). The shift in fluorescence from 333- 343 nm to wavelengths longer than 400 nm upon UV-B light exposure was indicative of Trp oxidation to NFK (41). The yield of NFK was significantly less in Rubisco than microsomal membranes, indicating that Trp may be more susceptible to oxidation in a hydrophobic environment (41). Although ROS were involved in Trp oxidation, it was not clear whether $^1O_2$ or $HO^{\bullet}$ was the reactant involved (41). The addition of hydrazine prior to the UV-B treatment inhibited formation of the blue fluorescing product, suggesting that NFK binds to hydrazine to form a hydrazone (41,47). In PSII, NFK was similarly shown to bind to amines to form a stable amidine (31).

1.5 NFK in non-photosynthetic proteins

NFK was first reported in hen egg white lysozyme (49). Since then, NFK modifications have been observed in a diverse range of proteins. A common feature of many oxidatively-modified proteins is the ability to perform redox chemistry. Accordingly, several NFK modifications have been identified within proteins of the

photosynthetic and mitochondrial electron transport chains (Table 1.1). Normal respiration involving oxidative phosphorylation in the mitochondria produces ROS as by-products (78). Other modifications occur in proteins that are exposed to a high concentration of ROS generated nearby, such as the ATP Synthase (34).

1.5.1 Ozone induces NFK formation in lysozyme

Ozonation of Trp residues in lysozyme provided insight into their functional significance in hen egg white lysozyme (49). Two residues, Trp-108 and Trp-111, were converted to NFK in the presence of ozone (exposure time undefined) (49) without any loss of lytic activity (49). The shift in Trp optical absorption from 280 nm to 320 nm was used as a marker for Trp to NFK conversion (49). Prolonged ozonation (exposure time undefined) induced further oxidation of the remaining four Trp residues (Trp-28, Trp-62, Trp-63, and Trp-123), along with functional inactivation (49). The findings lead to conclusion that Trp-108 and Trp-111 were located on a surface-exposed region on the surface of the protein (49). The results of the study concluded that those particular Trp residues do not participate in maintenance of a functional protein conformation (49). An alternative interpretation could be that the Trp residues do not participate in the ligand binding required for biological activity (49). The other four Trp residues (Trp-28, Trp-62, Trp-63, and Trp-123), on the contrary, were determined to play structural roles or participate in ligand binding (49).

1.5.2 NFK in mitochondrial proteins: oxidative stress and redox chemistry

An evaluation of the normal human heart mitochondrial proteome found that NFK modifications were targeted to a discrete subcategory of proteins involved in redox metabolism (56). A total of 51 NFK modifications were identified, with an over-represented proportion located in Complex I (NADH Dehydrogenase) and Complex V (ATP Synthase) (56). Complexes I and III (Cytochrome bc_1) are the major sites of ROS production in the mitochondria (79). Single electron reduction of molecular oxygen by both complexes produces the superoxide anion radical ($O_2^{\bullet -}$) (79). Superoxide is rapidly converted to hydrogen peroxide (H_2O_2) by SOD (79). Although the reactivity of Trp with H_2O_2 is low (80), the decomposition to hydroxyl radicals ($HO^{\bullet}$) can occur via a metal catalyzed Fenton reaction (81). $HO^{\bullet}$ has a high reactivity with Trp (80). As demonstrated in the α-crystallin proteins, $HO^{\bullet}$ can oxidize Trp side chains to NFK (33). Interestingly, there was no correlation between the locations of the Trp oxidations and methionine (Met) oxidations, a known experimental artifact (56). The extensive mitochondrial analysis concluded that the NFK modifications occur naturally in absence of any induced oxidative stress within proteins capable of redox chemistry (56). These enzymes that facilitate the electron transfer pathway in normal respiration produce the reactive oxygen that result in NFK modifications.

In mitochondria, ATP Synthase is located close to the electron transport chain, making it a ROS target. Trp oxidation to NFK was also observed in the alpha subunit of ATP Synthase in a bacterium, *Podospora anserina* (*P. anserina*) (34). ATP Synthase is located in the plasma membrane of bacteria, which lack mitochondria. The oxidation was targeted to a single residue (Trp-503), supporting a non-random mechanism of formation

(34). Two other Trp side chains were also similarly surface-exposed and should have been oxidized if the modification occurred by indiscriminate pathways (34). The yield of NFK was reduced by ~30% when mitochondrial isolation was performed in the presence of an iron chelator, Desferal (34). This result provided further support for the involvement of $HO^{\bullet}$ in NFK formation in the mitochondria. NFK was suggested to function as an irreversible marker for removal of damaged proteins (34), an essential function in mitochondrial regulation. As an irreversible marker, turnover of the NFK-oxidized protein should also occur.

Two specific NFK modifications were identified in the mitochondrial aconitase-2 enzyme (36) (Table 1.1). The reaction chemistry involved was not discussed in the proteomic study. However, aconitase-2 contains a [4Fe-4S] metallo-cluster (82). An electron paramagnetic resonance (EPR) spectroscopic study detected $HO^{\bullet}$ from the proposed reaction of H_2O_2 with the metal cluster (83). Aconitase-2 exhibits a high degree of post translational carbonylation in the presence of ROS and is frequently used as a biomarker for oxidative stress. The metallo-enzyme may actively protect the mitochondrial respiratory machinery from oxidative stress. A study in *A. thaliana* found that impaired assembly of [4Fe-4S] clusters in mitochondrial enzymes, including aconitase, resulted in increased production of ROS (84). Increased transcription of aconitase and other proteins known to play a role in oxidative stress were also up-regulated (84). The results concluded that Fe-S cluster-containing enzymes protect from potentially deleterious oxidative damage (84). The NFK-modified Trp residues identified in aconitase could function as intrinsic protein antioxidants (85).

Frataxin is another mitochondrial protein with proposed functions in ROS metabolism, Fe-S cluster biosynthesis, and iron uptake (86). Reduced expression results in the most common hereditary ataxia, Friedreich's Ataxia (86). This condition leads to iron accumulation and an environment susceptible to Fenton reactions (86). Frataxin is also a ROS target and highly susceptible to oxidative modifications (40). Despite the high degree of carbonylation, only Trp-155 was modified to NFK (40). This residue is highly conserved and exists as a point mutation in heterozygotes with Friedreich's Ataxia (87). $HO^{\bullet}$ mediated oxidation of frataxin did not significantly inhibit functional activity, and frataxin- mediated ROS protection was still detected (40). The findings support that Trp oxidation to NFK is essential for proper protein function.

1.5.3 Immunological detection of NFK in proteins and cells

Experimental difficulties involved in identification of Trp oxidation products by proteomic methods prompted development of an antiserum for NFK (39). Photosensitizers, Rose Bengal and riboflavin, were used to generate $^1O_2$ in horse heart myoglobin and milk proteins, respectively (39). $^1O_2$ reacted with Trp side chains to form NFK, which was detected by Western blot and enzyme-linked immunosorbent assay (ELISA) analysis (39). The validity of the antiserum was corroborated by MS/MS sequencing. Both Trp residues in myoglobin were modified to NFK (Table 1.1). The relative ease of NFK detection by immunochemical methods enables the identification and quantitation of NFK in both large proteins and under various stress conditions.

The NFK antiserum was also used to detect modifications within keratinocyte cells by confocal fluorescent microscopy (88). Illumination in the presence of a photosensitizer confirmed co-localization of NFK within the Golgi and mitochondria (88). However, the limit of detection for naturally- occurring NFK modifications in absence of a photosensitizer was not illustrated. This type of study would provide relevant insight into the utility of the antiserum for tracking the fate of NFK-modified protein in live cells.

1.5.4 Trp oxidation and copper coordination

The MopE protein is an example in which Trp oxidation plays an essential role in metal binding (89). In *Methylococcus capsulatus*, MopE is predicted to participate in copper uptake (90), an important role in regulation and activity of the methane monooxygenases (91). The 1.35 Å crystal structure revealed that the amino nitrogen atom of kynurenine (Figure 1.2A), an oxidative modification of Trp-130, provided an essential ligand to a mononuclear copper site (89). Two histidine imidazoles and an oxygen from a water molecule provided the other three ligands (89). Un-oxidized Trp in heterologously expressed MopE did not bind copper, supporting the physiological role of the PTM (89). Lack of the modification in heterologous protein lead the authors to speculate that the modification was enzymatically catalyzed (89). However, the *in vivo* role of local ROS was not discussed (89). This work demonstrates solid support for participation of oxidized Trp modifications in essential physiological roles. NFK is formed as a stable intermediate in the formation of kynurenine (Figure 1.2B). One could speculate that NFK

could perform a similar function in other proteins as a transient intermediate to regulate metal uptake. Other similarly functioning Trp modifications may have eluded detection in heterologously expressed proteins.

1.5.5 NFK and crystallin

The crystallins constitute a large proportion of the proteins in the eye lens. Metabolic turnover of damaged proteins in the eye is very slow. Thus, the crystallins are extremely long-lived, with half lives on the order of decades. Stress-induced oxidative modifications play a role in cross-linking and aggregation (92). These changes that accumulate with age lead to loss of lens opacity, or cataracts (87). In a study of $HO^{\bullet}$ mediated oxidation to crystallin proteins, Trp oxidation to NFK did not lead to the covalent cross-linking associated with cataracts (33). The loss of intrinsic Trp fluorescence (λ_{em} = 325 nm) concomitant with the appearance of a new red-shifted peak (λ_{em}= 435) was used to assess the complete conversion of Trp to NFK (33). $HO^{\bullet}$ stress is relevant *in vivo* and can be naturally generated by photochemical (93) or Fenton-type mechanisms (94) in the lens. Histidine oxidation, in contrast to Trp oxidation, was a precursor for formation of higher molecular weight cross-links (33). As discussed above, Trp may act as a non-catalytic ROS scavenger.

1.5.6 NFK formation in apoB-100

NFK formation in the apolipoprotein B-100 (apoB-100) was initiated through a Trp radical intermediate formed from electron donation to Cu^{2+} (32) (Table 1.1). ApoB-100 is a major component of low density lipoprotein (LDL). Copper and iron are critical in LDL oxidation (95). Oxidized LDL is a key risk factor in atherosclerosis (96), and apoB-100 reduction of Cu^{2+} to Cu^{+} is implicated in the progression (97). In the investigation of LDL oxidation, Trp oxidation to NFK, kynurenine, and tryptamine occurred upon addition of Cu^{2+} (32). Trp oxidation was monitored by specific HPLC absorbance and fluorescence profiles of pronase E digests (32). Trp oxidation and Cu^{+} were required for LDL oxidation, implicating the relevance of the reaction (97). Because Trp does not form radicals in solution with Cu^{2+}, the primary sequence and environment of the apoB-100 protein must alter the redox properties of Trp to enable the reaction to occur (98).

1.5.8 X-ray radiation generates ROS and NFK in an animal model

Oxidative stress and protein oxidation play a chief role in mammalian ageing and disease development (99). Thus, the utilization of animal models for the study of ROS mechanisms is pertinent. An established rat model was used to examine Trp oxidation *in vivo* (99). X-ray radiation was employed to induce acute oxidative stress, and NFK formation was assessed in rat skeletal muscles, actin and troponin I (Table 1.1) (42). Another aim of the investigation was to identify and quantify NFK modifications within a complex mixture of proteins, which was accomplished by gas phase fractionation on an

LTQ Orbitrap mass spectrometer (42). One Trp in troponin I (Trp-161) and two Trp (Trp-79 and Trp-340) in actin were oxidized to NFK (42). While Trp-79 is surface exposed and expected to readily react with ROS, the other Trp side chains are shielded within the hydrophobic interior of the protein (42). The oxidation of these buried residues suggests that the superficial oxidations induce a conformational change or structural unfolding that enables exposure to the surface (42).

1.6 Thesis overview

Oxidative stress is a natural consequence of photosynthetic oxygen evolution and redox enzyme processes. Trp oxidation to NFK is a specific, ROS-mediated reaction. This thesis work describes the identification and functional characterization of NFK in oxygen evolving PSII. Although proteomics studies have confirmed NFK modifications in many types of proteins, limited knowledge on the biochemical significance exists. Based on the current knowledge of NFK, ROS, and repair, we propose a model describing a role for NFK in signaling for turnover of damaged proteins in PSII during photoinhibition and repair. NFK may play a similar role in replacement of damaged proteins in other systems.

In vitro studies in thylakoids and PSII membranes are used to establish a correlation between oxidative stress, NFK formation, and photoinhibition. The *in vivo* effect of preventing Trp oxidation to NFK is assessed by site-directed mutation in *Synechocystis* 6803. This work provides insight into the role of NFK in photosynthetic oxygen evolution and photoinhibition.

1.7 References

1. Adir, N., Zer, H., Shochat, S., and Ohad, I. (2003) Photoinhibition- a historical perspective. *Photosynth. Res.* **76**, 343-370

2. Nixon, P. J., Michoux, F., Yu, J., Boehm, M., and Komenda, J. (2010) Recent advances in understanding the assembly and repair of photosystem II. *Ann. Bot.* **106**, 1-16

3. Nelson, N., and Yocum, C. F. (2006) Structure and function of photosystems I and II. *Annu. Rev. Plant Biol.* **57**, 521-565

4. Umena, Y., Kawakami, K., Shen, J.-R., and Kamiya, N. (2011) Crystal structure of oxygen-evolving photosystem II at a resolution of 1.9 Å. *Nature* **473**, 55-60

5. Ferreira, K. N., Iverson, T. M., Maghlaoui, K., Barber, J., and Iwata, S. (2004) Architecture of the photosynthetic oxygen-evolving center. *Science* **303**, 1831-1838

6. Guskov, A., Kern, J., Gabdulkhakov, A., Broser, M., Zouni, A., and Saenger, W. (2009) Cyanobacterial photosystem II at 2.9 Å resolution and the role of quinones, lipids, channels and chloride. *Nat. Struct. Mol. Biol.* **16**, 334-342

7. Kamiya, N., and Shen, J.-R. (2003) Crystal structure of oxygen-evolving photosystem II from *Thermosynechococcus vulcanus* at 3.7 Å resolution. *Proc. Natl. Acad. Sci. U. S. A.* **100**, 98-103

8. Loll, B., Kern, J., Saenger, W., Zouni, A., and Biesiadka, J. (2005) Towards complete cofactor arrangement in the 3.0 Å resolution structure of photosystem II. *Nature* **438**, 1040-1044

9. Zouni, A., Witt, H.-T., Kern, J., Fromme, P., Krauß, N., Saenger, W., and Orth, P. (2001) Crystal structure of photosystem II from *Synechococcus elongatus* at 3.8 Å resolution. *Nature* **409**, 739-743

10. Rhee, K.-H., Morris, E. P., Barber, J., and Kühlbrandt, W. (1998) Three-dimensional structure of the plant photosystem II reaction center at 8 Å resolution. *Nature* **396**, 283-286

11. Grossman, A. R., Bhaya, D., Apt, K. E., and Kehoe, D. M. (1995) Light-harvesting complexes in oxygenic photosynthesis: diversity, control, and evolution. *Annu. Rev. Genet.* **29**, 231-288

12. Roose, J. L., Wegener, K. M., and Pakrasi, H. B. (2007) The extrinsic proteins of photosystem II. *Photosynth. Res.* **92**, 369-387

13. Yocum, C. F. (2008) The calcium and chloride requirements of the O_2 evolving complex. *Coord. Chem. Rev.* **252**, 296-305

14. Bricker, T. M., and Frankel, L. K. (2002) The structure and function of CP47 and CP43 in photosystem II. *Photosynth. Res.* **72**, 131-146

15. Ohad, I., Kyle, D. J., and Arntzen, C. J. (1984) Membrane protein damage and repair: removal and replacement of inactivated 32-kilodalton polypeptides in chloroplast membranes. *J. Cell Biol.* **99**, 481-485

16. Ito, K., and Akiyama, Y. (2005) Cellular functions, mechanism of action, and regulation of FtsH protease. *Annu. Rev. Microbiol.* **59**, 211-231

17. Komenda, J., Barker, M., Kuviková, S., de Vries, R., Mullineaux, C. W., Tichy, M., and Nixon, P. J. (2006) The FtsH protease slr0228 is important for quality control of photosystem II in the thylakoid membrane of *Synechocystis* sp. PCC 6803. *J. Biol. Chem.* **281**, 1145-1151

18. Nixon, P. J., Barker, M., Boehm, M., de Vries, R., and Komenda, J. (2005) FtsH-mediated repair of the photosystem II complex in response to light stress. *J. Exp. Bot.* **56**, 357-363

19. Asada, K. (1999) The water cycle in chloroplasts: scavenging of active oxygens and dissipation of excess photons. *Annu. Rev. Plant Physiol. Plant Mol. Biol.* **50**, 601-639

20. Pospíšil, P. (2009) Production of reactive oxygen species by photosystem II. *Biochim. Biophys. Acta* **1787**, 1151-1160

21. Allen, J. F. (1992) Protein phosphorylation in regulation of photosynthesis. *Biochim. Biophys. Acta* **1098**, 275-335

22. Janes, S. M., Mu, D., Wemmer, D., Smith, A. J., Kaur, S., Maltby, D., Burlingame, A. L., and Klinman, J. P. (1990) A new redox cofactor in eukaryotic enzymes: 6-hydroxydopa at the active site of bovine serum amine oxidase. *Science* **248**, 981-987

23. Stadtman, E. R. (1990) Covalent modification reactions are marking steps in protein turnover. *Biochemistry* **29**, 6323-6331

24. Whitelegge, J. P., Gundersen, C. B., and Faull, K. F. (1998) Electrospray-ionization mass spectrometry of intact intrinsic membrane proteins. *Protein Sci.* **7**, 1423-1430

25. Whitelegge, J. P., Faull, K. F., Gundersen, C. B., and Gómez, S. M. (1999) Imaging the native covalent state of thylakoid proteins by electrospray-ionization mass spectrometry. in *Photosynthesis: Mechanisms and Effects* (Garab, G. ed.), Kluwer Academic Publishers, Dordrecht, Netherlands. pp 4381 -4384

26. Bowyer, J. R., Packer, J. C. L., McCormack, B. A., Whitelegge, J. P., Robinson, C., and Taylor, M. A. (1992) Carboxyl-terminal processing of the D1 protein and photoactivation of water-splitting in photosystem II. *J. Biol. Chem.* **267**, 5424-5433

27. Liao, D. I., Qian, J., Chisholm, D. A., Jordan, D. B., and Diner, B. A. (2000) Crystal structures of the photosystem II D1 C-terminal processing protease. *Nat. Struct. Biol.* **7**, 749-753

28. Sharma, J., Panico, M., Shipton, C. A., Nilsson, F., Morris, H. R., and Barber, J. (1997) Primary structure characterization of the photosystem II D1 and D2 subunits. *J. Biol. Chem.* **272**, 33158-33166

29. Galetskiy, D., Lohscheider, J. N., Kononikhin, A. S., Popov, I. A., Nikolaev, E. N., and Adamska, I. (2011) Mass spectrometric characterization of photooxidative protein modifications in *Arabidopsis thaliana* thylakoid membranes. *Rapid Commun. Mass Spectrom.* **25**, 184-190

30. Anderson, L. B., Maderia, M., Ouellette, A. J. A., Putnam-Evans, C., Higgins, L., Krick, T., MacCoss, M. J., Lim, H., Yates, J. R., III, and Barry, B. A. (2002) Posttranslational modifications in the CP43 subunit of photosystem II. *Proc. Natl. Acad. Sci. U. S. A.* **99**, 14676-14681

31. Dreaden, T. M., Chen, J., Rexroth, S., and Barry, B. A. (2011) *N*-Formylkynurenine as a marker of high light stress in photosynthesis. *J. Biol. Chem.* **286**, 22632-22641

32. Gießauf, A., van Wickern, B., Simat, T., Steinhart, H., and Esterbauer, H. (1996) Formation of *N*-formylkynurenine suggests the involvement of apolipoprotein B-100 centered tryptophan radicals in the initiation of LDL lipid peroxidation. *FEBS Lett.* **389**, 136- 140

33. Guptasarma, P., Balasubramanian, D., Matsugo, S., and Saito, I. (1992) Hydroxyl radical mediated damage to proteins, with special reference to the crystallins. *Biochemistry* **31**, 4296-4303

34. Rexroth, S., Poetsch, A., Rögner, M., Hamann, A., Werner, A., Osiewacz, H. D., Schäfer, E. R., Seelert, H., and Dencher, N. A. (2012) Reactive oxygen species target specific tryptophan site in the mitochondrial ATP Synthase. *Biochim. Biophys. Acta* **1817**, 381-387

35. Davies, M. J. (2003) Singlet oxygen-mediated damage to proteins and its consequences. *Biochem. Biophys. Res. Commun.* **305**, 761-770

36. Hunzinger, C., Wozny, W., Schwall, G. P., Poznanović, S., Stegmann, W., Zengerling, H., Schoepf, R., Groebe, K., Cahill, M. A., Osiewacz, H. D., Jägemann, N., Bloch, M., Dencher, N. A., Krause, F., and Schrattenholz, A. (2006) Comparative profiling of the mammalian mitochondrial proteome: multiple aconitase-2 isoforms including *N*-formylkynurenine modifications as part of a protein biomarker signature for reactive oxidative species. *J. Proteome Res.* **5**, 625-633

37. Dreaden Kasson, T. M., and Barry, B. A. (2012) Light-induced oxidative Stress, *N*-formylkynurenine, and oxygenic photosynthesis *Plos ONE* **Accepted**

38. Rinalducci, S., Campostrini, N., Antonioli, P., Righetti, P. G., Roepstorff, P., and Zolla, L. (2005) Formation of truncated proteins and high-molecular-mass aggregates upon soft illumination of photosynthetic proteins. *J. Proteome Res.* **4**, 2327-2337

39. Ehrenshaft, M., Silva, S. d. O., Perdivara, I., Bilski, P., Sik, R. H., Chignell, C. F., Tomer, K. B., and Mason, R. P. (2009) Immunological detection of *N*-formylkynurenine in oxidized proteins. *Free Radic. Biol. Med.* **46**, 1260-1266

40. Correia, A. R., Ow, S. Y., Wright, P. C., and Gomes, C. M. (2009) The conserved Trp155 in human frataxin as a hotspot for oxidative stress related chemical modifications. *Biochem. Biophys. Res. Commun.* **390**, 1007-1011

41. Caldwell, C. R. (1993) Ultraviolet-induced photodegradation of cucumber (*Cucumis sativus L.*) microsomal and soluble protein tryptophanyl residues *in vitro*. *Plant Physiol.* **101**, 947-953

42. Fedorova, M., Todorovsky, T., Kuleva, N., and Hoffmann, R. (2010) Quantitative evaluation of tryptophan oxidation in actin and troponin I from skeletal muscles using a rat model of acute oxidative stress. *Proteomics* **10**, 2692-2700

43. Simat, T., Meyer, K., and Steinhart, H. (1994) Synthesis and analysis of oxidation of carbonyl condensation compounds of tryptophan. *J. Chromatogr. A* **661**, 93-99

44. Jacobson, K. B. (1978) New substrate for formylkynurenine formidase: *N*', N^{α}-diformylkynurenine. *Arch. Biochem. Biophys.* **186**, 84-88

45. Zhao, H., Sagert, J., Hwang, D. S., and Waite, J. H. (2009) Glycosylated hydroxytryptophan in a mussel adhesive protein from *Perna viridis*. *J. Biol. Chem.* **284**, 23344-23352

46. Huang, H. V., Bond, M. W., Hunkapiller, M. W., and Hood, L. E. (1983) Cleavage at tryptophanyl residues with dimethylsulfoxide hydrochloric acid and cyanogen bromide. *Methods Enzymol.* **91**, 318-324

47. Fujimori, E. (1981) Blue fluorescence and crosslinking of photooxidized proteins. *FEBS Lett.* **135**, 257-260

48. Gracanin, M., Hawkins, C. L., Pattison, D. I., and Davies, M. J. (2009) Singlet-oxygen-mediated amino acid and protein oxidation: formation of tryptophan peroxides and decomposition products. *Free Radic. Biol. Med.* **47**, 92-102

49. Previero, A., Coletti-Previero, M.-A., and Jollès, P. (1967) Localization of non-essential tryptophan residues for biological activity of lysozyme. *J. Mol. Biol.* **24**, 261-268

50. Vass, I., Styring, S., Hundal, T., Koivuniemi, A., Aro, E.-M., and Andersson, B. (1992) Reversible and irreversible intermediates during photoinhibition of

photosystem II: stable reduced Q_A species promote chlorophyll triplet formation. *Proc. Natl. Acad. Sci. U. S. A.* **89**, 1408-1412

51. Krieger-Liszkay, A., Fufezan, C., and Trebst, A. (2008) Singlet oxygen production in photosystem II and related protection mechanism. *Photosynth. Res.* **98**, 551-564

52. Hideg, E., Spetea, C., and Vass, I. (1994) Singlet oxygen and free radical production during acceptor-induced and donor-side photoinhibition: studies with spin-trapping EPR spectroscopy *Biochim. Biophys. Acta* **1186**, 143-152

53. Rinalducci, S., Pedersen, J. Z., and Zolla, L. (2004) Formation of radicals from singlet oxygen produced during photoinhibition of isolated light-harvesting proteins of photosystem II. *Biochim. Biophys. Acta* **1608**, 63-73

54. Dall'Osto, L., Fiore, A., Cazzaniga, S., Giuliano, G., and Bassi, R. (2007) Different roles of α- and β- branch xanthophylls in photosystem assembly and photoprotection. *J. Biol. Chem.* **282**, 35056-35068

55. Santabarbara, S., Neverov, K. V., Garlaschi, F. M., Zucchelli, G., and Jennings, R. C. (2001) Involvement of uncoupled antenna chlorophylls in photoinhibition in thylakoids. *FEBS Lett.* **491**, 109-113

56. Taylor, S. W., Fahy, E., Murray, J., Capaldi, R. A., and Ghosh, S. S. (2003) Oxidative post-translational modification of tryptophan residues in cardiac mitochondrial proteins. *J. Biol. Chem.* **278**, 19587-19590

57. Zolla, L., and Rinalducci, S. (2002) Involvement of active oxygen species in degradation of light-harvesting proteins under light stresses. *Biochemistry* **41**, 14391-14402

58. Kühlbrandt, W., Wang, D. N., and Fujiyoshi, Y. (1994) Atomic model of plant light- harvesting complex by electron crystallography. *Nature* **367**, 614-621

59. Garab, G., Cseh, Z., Kovács, L., Rajagopal, S., Várkonyi, Z., Wentworth, M., Mustárdy, L., Dér, A., Ruban, A. V., Papp, E., Holzenburg, A., and Horton, P. (2002) Light-induced trimer to monomer transition in the main light-harvesting antenna complex of plants: thermo-optic mechanism. *Biochemistry* **41**, 15121-15129

60. Yang, D.-H., Paulsen, H., and Andersson, B. (2000) The N-terminal domain of the light-harvesting chlorophyll *a/b*-binding protein complex (LHCII) is essential for its acclimative proteolysis. *FEBS Lett.* **466**, 385-388

61. Nishiyama, Y., Allakhverdiev, S. I., and Murata, N. (2006) A new paradigm for the action of reactive oxygen species in the photoinhibition of photosystem II. *Biochim. Biophys. Acta* **1757**, 742-749

62. Hillier, W., and Wydrzynski, T. (1993) Increases in peroxide formation by the photosystem II oxygen-evolving reactions upon removal of the extrinsic 16, 22, and 33 kDa proteins are reversed by $CaCl_2$ addition. *Photosynth. Res.* **38**, 417-423

63. Pospíšil, P. (2012) Molecular mechanisms of production and scavenging of reactive oxygen species by photosystem II. *Biochim. Biophys. Acta* **1817**, 218-231

64. Telfer, A. (2005) Too much light? How β-carotene protects the photosystem II reaction centre. *Photochem. Photobiol. Sci.* **4**, 950-956

65. Gruszka, J., Pawlak, A., and Kruk, J. (2008) Tocochromanols, plastoquinol, and other biological prenyllipids as singlet oxygen quenchers- determination of singlet oxygen quenching rate constants and oxidation products. *Free Radic. Biol. Med.* **45**, 920-928

66. Kruk, J., Strzalka, K., and Leblanc, R. M. (1992) Monolayer study of plastoquinones, α-tocopherol quinone, their hydroquinone forms and their interaction with monogalatosyldiacylglycerol- charge transfer complexes in a mixed monolayer. *Biochim. Biophys. Acta* **1112**, 19-26

67. Pospíšil, P. (2011) Enzymatic function of cytochrome b_{559} in photosystem II. *J. Photochem. Photobiol. B-Biol.* **104**, 341-347

68. Walrant, P., and Santus, R. (1974) *N*-Formylkynurenine, a tryptophan photooxidation product, as a photodynamic sensitizer *Photochem. Photobiol.* **19**, 411-417

69. Pileni, M.-P., Walrant, P., and Santus, R. (1976) Electronic properties of *N*-formylkynurenine and related compounds. *J. Phys. Chem.* **80**, 1804-1809

70. Pirie, A. (1971) Formation of *N*'-formylkynurenine in proteins from lens and other sources by exposure to sunlight. *Biochem. J.* **125**, 203- 208

71. Pileni, M. P., Santus, R., and Land, E. J. (1978) 265-nm laser flash photolysis of some ortho-substituted anilides and related *N*-formylkynurenine derivatives. *Photochem. Photobiol.* **27**, 671-681

72. Pileni, M. P., Walrant, P., and Santus, R. (1976) On the possible excited state proton transfer in *N*-formylkynurenine derivatives *Chem. Phys. Lett.* **42**, 89-92

73. Igarashi, N., Onoue, S., and Tsuda, Y. (2007) Photoreactivity of amino acids: tryptophan-induced photochemical events *via* reactive oxygen species generation. *Anal. Sci.* **23**, 943-948

74. Sarvikas, P., Hakala, M., Pätsikkä, E., Tyystjärvi, T., and Tyystjäarvi, E. (2006) Action spectrum of photoinhibition in leaves of wild type and npq1-2 and npq4-1 mutants of *Arabidopsis thaliana*. *Plant Cell Physiol.* **47**, 391-400

75. Huesgen, P. F., Schuhmann, H., and Adamska, I. (2006) Photodamaged D1 protein is degraded in *Arabidopsis* mutants lacking the Deg2 protease. *FEBS Lett.* **580**, 6929-6932

76. Herman, C., Prakash, S., Lu, C. Z., Matouschek, A., and Gross, C. A. (2003) Lack of a robust unfoldase activity confers a unique level of substrate specificity to the universal AAA protease FtsH. *Mol. Cell* **11**, 659-669

77. Walrant, P., and Santus, R. (1974) Ultraviolet and *N*-formylkynurenine- sensitized photoactivation of bovine carbonic anhydrase: and internal photodynamic effect. *Photochem. Photobiol.* **20**, 455-460

78. Balaban, R. S., Nemoto, S., and Finkel, T. (2005) Mitochondria, oxidants, and aging. *Cell* **120**, 483-495

79. Inoue, M., Sato, E. F., Nishikawa, M., Park, A.-M., Kira, Y., Imada, I., and Utsumi, K. (2003) Mitochondrial generation of reactive oxygen species and its role in aerobic life. *Curr. Med. Chem.* **10**, 2495-2505

80. Ji, J. A., Zhang, B. Y., Cheng, W., and Wang, Y. J. (2009) Methionine, tryptophan, and histidine oxidation in a model protein, PTH: mechanisms and stabilization. *J. Pharm. Sci.* **98**, 4485-4500

81. Thomas, C., Mackey, M. M., Diaz, A. A., and Cox, D. P. (2009) Hydroxyl radical is produced via the Fenton reaction in submitochondrial particles under oxidative stress: implications for diseases associated with iron accumulation. *Redox Rep.* **14**, 102-108

82. Beinert, H., and Kennedy, M. C. (1993) Aconitase, a two-faced protein: enzyme and iron regulatory factor. *FASEB J.* **7**, 1442-1449

83. Vásquez-Vivar, J., Kalyanaraman, B., and Kennedy, M. C. (2000) Mitochondrial aconitase is a source of hydroxyl radical - an electron spin resonance investigation. *J. Biol. Chem.* **275**, 14064-14069

84. Busi, M. V., Maliandi, M. V., Valdez, H., Clemente, M., Zabaleta, E. J., Araya, A., and Gomez-Casati, D. F. (2006) Deficiency of *Arabidopsis thaliana* frataxin alters activity of mitochondrial Fe-S proteins and induces oxidative stress. *Plant J.* **48**, 873-882

85. Nyström, T. (2005) Role of oxidative carbonylation in protein quality control and senescence. *EMBO J.* **24**, 1311-1317

86. Delatycki, M. B., Williamson, R., and Forrest, S. M. (2000) Friedreich ataxia: an overview. *J. Med. Genet.* **37**, 1-8

87. Cossée, M., Dürr, A., Schmitt, M., Dáhl, N., Trouillas, P., Allinson, P., Kostrzewa, M., Nivelon-Chevallier, A., Gustavson, K.-H., Kohlschütter, A., Müller, U., Mandel, J.-L., Brice, A., Koenig, M., Cavalcanti, F., Tammaro, A., De Michele, G., Filla, A., Cocozza, S., Labuda, M., Montermini, L., Poirier, J., and Pandolfo, M. (1999) Friedreich's ataxia: point mutations and clinical presentation of compound heterozygotes. *Ann. Neurol.* **45**, 200-206

88. Ehrenshaft, M., Bonini, M. G., Feng, L., Chignell, C. F., and Mason, R. P. (2010) Partial colocalization of oxidized, *N*-formylkynurenine-containing proteins in mitochondria and golgi of keratinocytes dagger. *Photochem. Photobiol.* **86**, 752-756

89. Helland, R., Fjellbirkeland, A., Karlsen, O. A., Ve, T., Lillehaug, J. R., and Jensen, H. B. (2008) An oxidized tryptophan facilitates copper binding in *Methylococcus capsulatus*-secreted protein MopE. *J. Biol. Chem.* **283**, 13897-13904

90. Karlsen, O. A., Berven, F. S., Stafford, G. P., Larsen, O., Murrell, J. C., Jensen, H. B., and Fjellbirkeland, A. (2003) The surface-associated and secreted MopE protein of *Methylococcus capsulatus* (Bath) responds to changes in the concentration of copper in the growth medium. *Appl. Environ. Microbiol.* **69**, 2386-2388

91. Hakemian, A. S., and Rosenzweig, A. C. (2007) The biochemistry of methane oxidation. in *Annu. Rev. Biochem*, Annual Reviews, Palo Alto. pp 223-241

92. Davies, M. J., and Truscott, R. J. W. (2001) Photo-oxidation of proteins and its role in cataractogenesis. *J. Photochem. Photobiol. B-Biol.* **63**, 114-125

93. Zigler, J. S., and Goosey, J. D. (1981) Photosensitized oxidation in the ocular lens: evidence for photosensitizers endogenous to the human lens. *Photochem. Photobiol.* **33**, 869-874

94. Zigler, J. S., Jernigan, H. M., Garland, D., and Reddy, V. N. (1985) The effects of "oxygen radicals" generated in the medium on lenses in organ culture: inhibition of damage by chelated iron. *Arch. Biochem. Biophys.* **241**, 163-172

95. Steinbrecher, U. P., Parthasarathy, S., Leake, D. S., Witztum, J. L., and Steinberg, D. (1984) Modification of low density lipoprotein by endothelial cells involves lipid peroxidation and degradation of low density lipoprotein phospholipids. *Proc. Natl. Acad. Sci. U. S. A.* **81**, 3883-3887

96. Steinberg, D., Parthasarathy, S., Carew, T. E., Khoo, J. C., and Witztum, J. L. (1989) Beyond cholesterol. Modifications of low density lipoprotein that increase its atherogenicity. *New Engl. J. Med.* **320**, 915-924

97. Lynch, S. M., and Frei, B. (1993) Mechanisms of copper- dependent and iron-dependent oxidative modification of human low density lipoprotein. *J. Lipid Res.* **34**, 1745-1753

98. Gießauf, A., Steiner, E., and Esterbauer, H. (1995) Early destruction of tryptophan residues of apolipoprotein B is a vitamin E independent process during

copper mediated oxidation of LDL. *Biochim. Biophys. Acta-Lipids Lipid Metab.* **1256**, 221-232

99. Berlett, B. S., and Stadtman, E. R. (1997) Protein oxidation in aging, disease, and oxidative stress. *J. Biol. Chem.* **272**, 20313-20316

CHAPTER 2

N-FORMYLKYNURENINE AS A MARKER OF HIGH LIGHT STRESS IN PHOTOSYNTHESIS

by

Tina Michelle Dreaden Kasson[1], Jun Chen[2], Sascha Rexroth[3], and Bridgette A. Barry[1]

[1]School of Chemistry and Biochemistry and the Petit Institute for Bioengineering and Bioscience, Georgia Institute of Technology, Atlanta, GA 30332

[2]Present address: Dalian National Laboratory for Clean Energy, Dalian Institute of Chemical Physics, Chinese Academy of Science, Dalian 116023, China

[3] Department of Biology, Ruhr-Universität, Bochum, Germany

This research was originally published in *The Journal of Biological Chemistry*.

Tina M. Dreaden, Jun Chen, Sascha Rexroth, and Bridgette A. Barry. *N*-formylkynurenine as a marker of high light stress in photosynthesis. *J. Biol. Chem*. 2011; 286: 22632-22641.

*Tandem mass spectrometry experiments in Figure 2.7 were performed by Sascha Rexroth (Department of Biology, Ruhr-Universität, Bochum, Germany).

2.1 Abstract

PSII is the membrane protein complex that catalyzes the photo-induced oxidation of water at a manganese-calcium active site. Light-dependent damage and repair occur in PSII under conditions of high light stress. The core reaction center complex is composed of the D1, D2, CP43, and CP47 intrinsic polypeptides. In this study, a new chromophore formed from the oxidative PTM of tryptophan was identified in the CP43 subunit. Tandem mass spectrometry peptide sequencing was consistent with the oxidation of the CP43 tryptophan side chain, Trp-365, to produce NFK. Characterization with ultraviolet-visible absorption and ultraviolet resonance Raman spectroscopies supported this assignment. An optical assay suggested that the yield of NFK increased two fold (2.2 ± 0.5) under high light illumination. A concomitant 2.4 ± 0.5 fold decrease was observed in the steady state rate of oxygen evolution under the same high light conditions. NFK is the product formed from reaction of tryptophan with highly reactive singlet oxygen, which can be produced under high-light stress in PSII. Reactive oxygen species (ROS) reactions lead to oxidative damage to the reaction center, D1 protein turnover, and inhibition of electron transfer. Our results are consistent with a role for the CP43 NFK modification in photoinhibition.

2.2 Introduction

Oxygenic photosynthesis is the enzyme-catalyzed conversion of light energy to biochemical energy, and this process occurs in the membranes of plants, algae, and cyanobacteria. In oxygenic photosynthesis, PSII catalyzes the light-driven oxidation of

water and reduction of plastoquinone. On the acceptor side of PSII, electrons are transferred sequentially to two quinone molecules, Q_A and Q_B (1). On the donor side, a Mn_4CaO_5 active site is the binding site for water and the site of oxygen production. Each monomer is composed of 20 protein subunits, chlorophylls, carotenoids, and redox-active plastoquinones (2). Calcium and chloride are required for activity under physiological conditions (3). The chloride binding site has been assigned near the active site (2).

The D1, D2, CP43, and CP47 polypeptides form the intrinsic core complex of PSII. The D1 and D2 membrane spanning proteins bind the electron transfer cofactors active in water oxidation (4). This central heterodimeric core is symmetrically flanked by the CP43 and CP47 proteins, which bind light-harvesting antennae chlorophyll (chl) molecules (5). Each of these core polypeptides is composed of intrinsic membrane-spanning helices, as well as several hydrophilic loops that protrude into the interior lumen of the thylakoid membrane (2). The lumenal loop regions of CP43 have been implicated as important in assembly and protection from photoinhibition (see 5 and references therein).

The active site of water oxidation, the Mn_4CaO_5 cluster, is located on the lumenal surface and is protected by three extrinsic polypeptides (6). In plants, these extrinsic proteins, the 18-kDa, 24-kDa, and the psbO (or the 33-kDa, manganese stabilizing protein, MSP), are essential for maximal oxygen evolution under physiological conditions (6). Both cyanobacterial and plant PSII contain an intrinsic cytochrome b_{559} (7), while cyanobacterial PSII also contains an extrinsic cytochrome c_{550} (2,8-11). The structure of cyanobacterial PSII has been solved to 1.9 Å resolution (2,8-11). In contrast, the resolution of a plant PSII structure remains at 8 Å resolution (12).

Given its structural and functional complexity, many aspects of PSII function remain elusive. In particular, the roles of PTMs of amino acid side chains are not thoroughly understood. The biological relevance of PTMs is evident in their wide range of functions, including roles in cellular regulation (13,14) and catalysis (15). Modifications of the intrinsic subunits of PSII have been described previously (16,17). For example, in the D1 subunit, the N-terminal methionine is removed, the N-terminal amino acid is acylated, and the carboxyl terminus is processed by a specific lumenal protease, CtpA (18,19). In CP43, fourteen amino acids are cleaved from the N-terminus, which is then N-acetylated. In D2 and CP47, amino terminal residues are removed, and the subunits are also N-acetylated. In addition, in a PSII reaction center preparation, in which CP47 and CP43 have been removed with chaotropes, a susceptibility to oxidation of D1/D2 has been reported (20). A proteomics-based study of *Arabidopsis* has shown an increased prevalence of oxidative modifications under high light stress (21). Despite improvements in PSII structure resolution, detection of PTMs based on available X-ray structures is not yet possible.

Other PTMs of PSII proteins have been identified, including oxidation of tryptophan to kynurenine (Figure 2.1A) (22), reduction of aspartic acid to aspartyl aldehyde (23), acyl activation of glutamic acid to a species that binds primary amines (24), as well as numerous phosphorylations (25). Core PSII subunits contain multiple unidentified PTM residues that covalently bind amines (23,26,27). These reactions were attributed to reactive, carbonyl-containing amino acid side chains close to the active site, and covalent binding was proposed to occur via a Schiff base complex. The addition of chloride was observed to inhibit amine binding, suggesting that the binding sites were

near the water oxidizing complex (28,29). Importantly, amines are well-known inhibitors of photosynthetic water oxidation (28,29), this reactivity was found in plants and cyanobacteria, and experiments showed that amines were oxidized to produce aldehydes (26,27). These experiments imply that the amine-binding residues may play a role in the structure, function, or assembly of PSII.

In addition to kynurenine, another known PTM of tryptophan in proteins is *N*-formylkynurenine (NFK). NFK may bind amines and is created as a stable double oxidation intermediate in the formation of kynurenine (Figure 2.1A) (21,30-32). In this work, we use tandem mass spectrometry (MS/MS) and UV resonance Raman (UVRR) to show that PSII contains NFK. The unique ~325 nm absorption band of NFK is employed in the purification of NFK-containing CP43 peptides. By MS/MS peptide sequencing, NFK is identified as a +32 *m/z* modification of Trp-365 in CP43. A vibrational band at 1044 cm^{-1} is observed, which is characteristic of the oxidized indole ring in NFK. Quantitative analysis of the HPLC chromatogram was compared to the amount of inhibition under high light conditions. This comparison suggests that the CP43 NFK modification can be induced by high light stress in PSII membrane preparations.

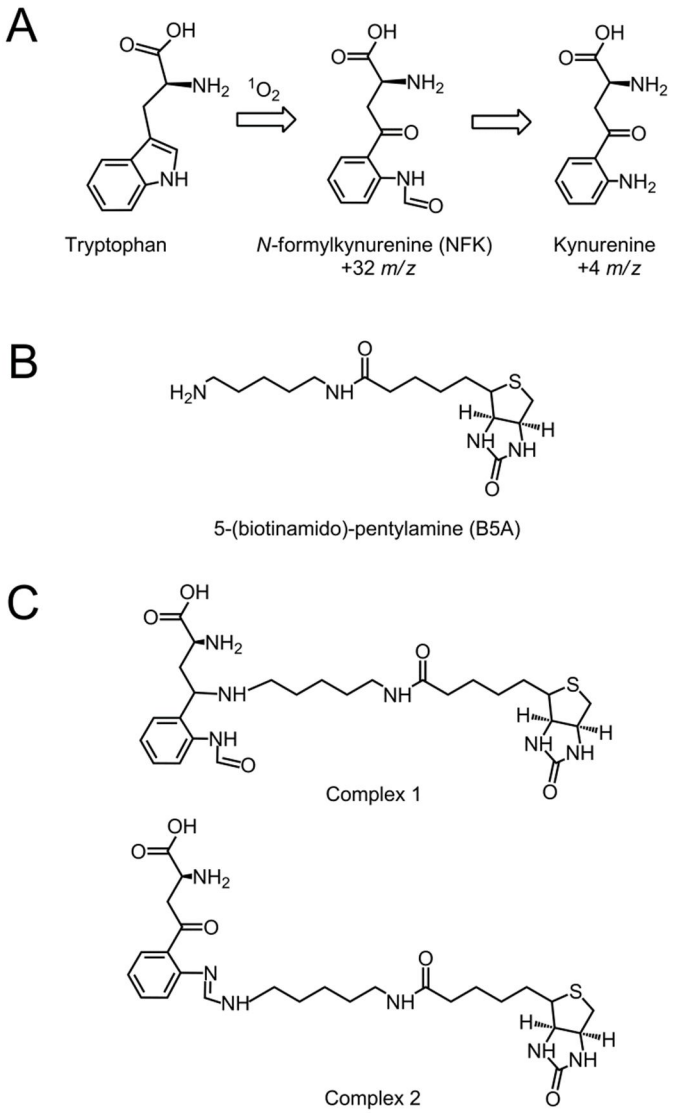

Figure 2.1. Structures of NFK and the PSII labeling reagent. (A) Oxidation of tryptophan to form NFK and kynurenine. (B) B5A reagent used for derivatization. (C) Possible covalent complexes of B5A with NFK.

2.3 Materials and Methods

2.3.1 PSII Preparations and oxygen evolution measurements

PSII was isolated from spinach (33) with the modifications previously described (27). Unless otherwise noted, all procedures were performed at 4 °C and under dim green light illumination. Chlorophyll (34) and oxygen assays (35) were performed, and steady-state rates of oxygen evolution were ≥ 600 μmol O_2/ (mg chl•h).

The 18- and 24-kDa extrinsic subunits were removed by treatment with 2 M NaCl for 30 minutes in the dark (36). Removal of psbO and the Mn_4Ca cluster (Figure 2.2, step 1) was performed by incubation with 800 mM tris(hydroxymethyl)aminomethane (Tris)-NaOH, pH 8.0 for 45 minutes at room temperature in the light (37). These Tris-washed (TW) PSII membranes were washed three times with a buffer of 400 mM sucrose, 50 mM 4-(2-hydroxyethyl)-1-piperazineethanesulfonic acid (HEPES)-NaOH, pH 7.5 and finally resuspended in the same buffer to yield a chlorophyll concentration of 2-4 mg/mL. Samples were stored at -70 °C.

2.3.2 PSII derivatization with B5A

TW PSII membranes (~6 mg of chlorophyll) were derivatized by incubation (Figure 2.2, step 2) with 4 mM of a primary amine-biotin conjugate, B5A (Invitrogen, Carlsbad, CA) (Figure 2.1B). The chlorophyll concentration was 1 mg/mL, and the incubation was performed for 30 minutes at room temperature in the light (27). As a control, TW PSII samples were also incubated in parallel under identical conditions, except B5A was omitted from the sample solution. B5A binding to PSII was confirmed by Western blot (38) of a urea-SDS-PAGE gel (39) containing derivatized PSII and by

detection with an avidin-alkaline phosphatase conjugate (38). B5A-derivatized samples were subjected either to direct *in-situ* trypsin digestion (Figure 2.2, step 4B) or 2D electrophoresis, followed by in-gel digestion (Figure 2.2, steps 3 and 4C).

2.3.3 *In-situ* trypsin digestion of PSII

The samples employed were either intact PSII (Figure 2.5), TW PSII (Figure 2.2, step 4A), or B5A labeled TW PSII (Figure 2.2, step 4B). Labeled TW PSII samples were centrifuged at 108,800 x g for 20 minutes to remove non-covalently bound B5A. The unlabeled TW control was treated similarly. PSII samples were reconstituted to 3 mg/mL in 50 mM HEPES-NaOH, pH 7.5 buffer. For the *in-situ* trypsin digest, 1 μg of porcine trypsin (Sequencing grade, Promega, Madison, WI) in 25 mM ammonium biocarbonate was added per 0.15 μg chloropyll. Samples were incubated for ~20 hours at room temperature under constant agitation. Undigested protein was pelleted by centrifugation at 108,800 x g for 20 minutes. The tryptic peptides released into the supernatant were then lyophilized and stored at -20 ºC. Tryptic cleavage of peptides was confirmed by SDS-PAGE comparison of intact and digested PSII samples (39,40).

2.3.4 HPLC purification of NFK- containing peptides

Tryptic peptides were separated by reverse phase chromatography (Figure 2.2, steps 5A and B) on a Beckman (Brea, CA) Gold HPLC system equipped with a 125 solvent module, a 168 photodiode array detector (1 cm path length, 2 nm scan interval), and 32 Karat Software, version 7.0. Lyophilized samples were reconstituted in 50 μL of 5% acetonitrile/ 0.1% trifluoroacetic acid (TFA). The samples were filtered with an

Acrodisc (Pall, Ann Arbor, MI) 0.2 µm nylon filter and loaded onto an Alltech (Deerfield, IL) Prosphere C18 column (4.6 mm x 250 mm, 300 Å pore size, 5 µm diameter packing). Buffer A was H_2O/ 0.1% TFA, and buffer B was acetonitrile/ 0.1% TFA. Peptides were eluted from the column over a 60 minute period with a gradient of 10-60% buffer B. The elution profile was monitored at 350 nm. Column chromatography was performed at room temperature and at a flow rate of 1 mL/ minute. Where appropriate, 1 mL fractions with absorption peaks at 350 nm (Figures 2.3 and 2.5) were lyophilized and stored at -20 ºC. Injection of a trypsin blank (no PSII) gave no significant 350 nm peaks (data not shown).

2.3.5 2D electrophoresis and in- gel digestions of PSII proteins

To ensure that the red-shifted absorption spectra derive from a peptide-derived chromophore, Coomassie dye and bromophenol blue were omitted from the gel purification experiments. B5A-derivatized, TW PSII membranes (~13 mg chlorophyll) were solubilized and separated in the first dimension as previously described (24). These CN-PAGE gels were run like Blue Native gels (41), without Coomassie dye in the buffers. The PSII dimer band deficient in light-harvesting complexes (24) was excised and run in the second dimension by Tricine-SDS-PAGE (Figure 2.2, step 3) (42). Bands were visualized with a zinc-imidazole negative stain (43). Protein bands were excised from the second dimension gels and cut into 1 mm^3 cubes. Residual zinc was removed by incubation with 50 mM EDTA for five minutes. A tryptic digest was generated (Figure 2.2, step 4C) with 2.5 µg/ mL of porcine trypsin (Promega, Madison, WI), as described by Rexroth *et al*. (44). Once extracted from the gel, samples were dried completely by

lyophilization and either stored at -20 °C or loaded directly onto an avidin affinity column.

2.3.6 Avidin affinity chromatography

For selective purification of biotinylated peptides (B5A-derivatized), lyophilized peptide samples from *in-situ* or in-gel digests were reconstituted in 100 µL binding buffer (50 mM NaCl, 150 mM HEPES, pH 7.0) and loaded onto monomeric avidin resin spin columns (45) (Figure 2.2, steps 6A and B). Peptides were allowed to bind overnight at room temperature and eluted with a 50% acetonitrile/ 0.1% TFA solution (45). An ELISA-like test (46) was used to quantify eluted peptides by comparison to a biotinylated insulin standard in concentrations ranging from 10 µM to 1 pM. Affinity purified samples were lyophilized and stored at -20 °C.

2.3.7 UVRR of amino acids, chlorophyll a, and β-carotene

UVRR measurements were conducted by methods previously described (47,48). Spectra of the amino acids (Sigma-Aldrich, St. Louis, MO), histidine (20 mM), phenylalanine (20 mM), tyrosine (1 mM), and tryptophan (1 mM), were conducted in 5 mM HEPES buffer, pH 7.5. The UVRR spectra were collected with a 250 µW, 229 nm beam excitation and a 21 minute exposure time (Figure 2.9). Chlorophyll *a* (Sigma-Aldrich) was dissolved in absolute ethanol at a concentration of 0.5 mg/mL. β-carotene (Sigma-Aldrich) was dissolved in a 80:20 acetone:water mixture at a concentration of 1 mg/mL. The UVRR spectra were collected with a 360 µW, 325 nm laser beam for a 30 minute exposure time (Figure 2.10).

2.3.8 Synthesis of the model compound, NFK

NFK (Figure 2.1A) was synthesized by formylation of commercially available kynurenine (95% purity, Sigma Aldrich, St. Louis, MO). The method has been previously described (49) and is known to produce a mixture of the single formylated NFK, and a double formylated compound, *N', N*$^{\alpha}$-formylkynurenine (50). ESI MS analysis was used to characterize the product. A Micromass Quattro LC, a triple quadrupole tandem mass spectrometer, was employed. The MH^+ peaks observed were 236.8 and 265.0 *m/z*, consistent with the predicted MH^+ masses for the singly and doubly formulated NFK at 237.2 and 265.2 *m/z*. The relative intensities of the two peaks were approximately 1:2 (236.8:265:0), consistent with the expectation that a mixture of the singly and doubly formulated species was produced. The electronic spectra of the singly and doubly formylated compounds have been reported to be indistinguishable (50).

2.3.9 UV-visible spectrophotometry

Optical spectra in Figures 2.4C and 2.6 were recorded at room temperature from 200-750 nm on a Hitachi (U3000) spectrophotometer. The quartz cuvettes contained 200 µL, the slit width was 2 nm, and the scan speed was 120 nm min^{-1}. The optical spectra in Figures 2.4A and B were derived from the chromatogram through the use of a Beckman System Gold® HPLC (Brea, CA), equipped with a 125 solvent module, a 168 photodiode array detector (1 cm path length, 2 nm scan interval), and 32 Karat Software, version 7.0. Peptide samples were suspended in 200 µL of 50% acetonitrile/ 0.1% trifluoroacetic acid. The model compounds, 40 µM *L*-tryptophan (Sigma-Aldrich, St. Louis, MO), *L*-kynurenine (Sigma-Aldrich, St. Louis, MO), and NFK (synthesis described above) were

suspended either in H_2O or 50% acetonitrile/ 0.1% TFA. Reduction of NFK with $NaBH_4$ was performed by incubation of 40 μM NFK with 400 μM $NaBH_4$ for 30 minutes at room temperature (51). Reduction of a NFK-B5A mixture with 400 μM $NaBH_4$ was performed using 40 μM NFK and 160 μM B5A.

2.3.10 UVRR spectroscopy

A Renishaw (Hoffman Estates, IL) microprobe resonance Raman spectrometer was employed, as described (47,48). A 15x objective was used to focus the laser beam on the sample and to collect backscattered radiation. Experiments were conducted at room temperature, and the slit width was 50 μm.

To reduce the fluorescence background, PSII peptides were both HPLC and affinity purified (Figure 2.2, steps 5B and 6A). Lyophilized peptide samples were suspended in water/ 0.1% TFA to increase solubility. A 3 μL peptide sample and a 360 μW, 325 nm probe beam from a He-Cd laser (KIMMON, Tokyo, Japan) were used. The 325 nm probe was chosen to give resonance enhancement of the PSII chromophore. The total exposure time for each spectrum was two minutes (47), and data from three individual experiments were averaged. The spectral resolution was 6 cm^{-1}.

A 220 μW, 229 nm probe beam from a frequency-doubled Ar-ion laser (Cambridge LEXEL 95, Fremont, CA) was used to record Raman spectra of the model compounds, kynurenine and NFK, which were dissolved in water. These samples were recirculated at a flow rate ~4.5 m/s through a 120 μm diameter nozzle, which formed a jet (47). The total exposure time for each spectrum was two minutes (47). The spectral resolution was 10 cm^{-1}.

2.3.11 Peptide sequencing with MS/ MS

Lyophylized peptide samples were reconstituted in 50 µL buffer A (99.9% water, 0.1% TFA) and analyzed on a Waters nanoHPLC C18 column (75 µm x 150 mm, 130 Å, 1.7 µm). For reverse phase chromatography, a gradient of buffer A (99.9 % H_2O, 0.1 % TFA) and buffer B (99.9 % acetonitrile, 0.1 % TFA) was used. For MS analysis, a Thermo LTQ Orbitrap mass spectrometer was operated in a duty cycle consisting of one 400-2000 *m/z* FT-MS and four MS/MS LTQ scans.

2.3.12 MS/ MS data analysis

For analysis of the LC-MS/MS data, the Sequest algorithm (52), implemented in the Bioworks software (Thermo Scientific, Waltham, MA), was applied for peptide identification versus a database. The database consisted of all spinach protein sequences present in National Center for Biotechnology Information (NCBI). For detection of modified peptides, a tryptophan modification of 31.98928 *m/z* was used as a parameter during the search.

2.3.13 Photoinhibition experiments

Photoinhibition experiments were conducted with intact PSII (22,53,54). Samples were illuminated with white light from a Dolan-Jenner (Boxborough, MA) Fiber-Lite illuminator. The applied light intensity was ~9,000 µmol photons m^{-2} s^{-1}) when measured with a Li-Cor (Lincoln, NE) Light Meter (model LI-189, with a ~8 cm diameter sensor) before the sample. The light intensity was ~7,000 µmol photons m^{-2} s^{-1}) when measured after an empty sample tube. During illumination, PSII samples were maintained at 25 ºC

by immersion in a water bath. The same two hour illumination experiment was also conducted without the water bath. During this time, the temperature was observed to increase to 37 ºC. As dark controls, PSII samples were incubated for two hours either at room temperature (~ 25 ºC) or at 37 ºC.

These conditions are similar to those described in the literature. For example, in spinach PSII membranes, at 25 ºC, and a light intensity of 4,000 μmol photons m^{-2} s^{-1}), the half-time for oxygen evolution was reported as ~30 minutes (55). In spinach thylakoid membranes, at 20 ºC, and a light intensity of 7,000 μmol photons m^{-2} s^{-1}, the half-time was ~25 minutes (56). A light intensity of 5,000 μmol photons m^{-2} s^{-1} at 25 ºC was used for studies of photoinhibition and degradation of the spinach CP43 subunit in spinach PSII membranes (57).

For quantitation of the amount of NFK induced by photoinhibition, the intact PSII samples were digested with trypsin, and an HPLC assay was performed. Briefly, tryptic peptides were injected onto a C18 column, and the elution was monitored with a diode array detector, as described above. To quantitate the yield of the NFK-containing peptide, the area of the 350 nm peak was calculated using instrument software. This value was normalized to the total integrated area in the 220 nm chromatogram (0-50 min). This normalization provides an internal standard and corrects for any changes in the yield of tryptic peptides. Experiments were performed 3-7 times, and the values were averaged. Oxygen evolution experiments (35) were performed under the same conditions, i.e., after a two hour dark incubation or a two hour illumination (with water bath at 25^{o}C). Measurements were performed six times, and the values were averaged.

2.4 Results

2.4.1 Isolation of the amine- binding chromophore

Following purification from spinach (33), PSII membranes were depleted of the 18-kDa, 24-kDa, and psbO extrinsic polypeptides, as well as the Mn_4CaO_5 cluster (36,37). These modifications allow access to the sterically-hindered core complex where covalent amine-binding occurs (Figure 2.2, step 1) (26,27). TW PSII membranes were reacted with a primary amine-biotin conjugate, B5A (Figure 2.1B) by incubation in light (Figure 2.2, step 2). Previous work demonstrated that PSII core subunits form stable covalent adducts with amines under these conditions, and binding was attributed to reactive carbonyl groups in PTMs (23,26,27). In our experiments, the biotin-linked amine allowed the selective purification of peptides by avidin affinity chromatography (Figure 2.2, steps 6A & B). Binding of B5A was confirmed by Western blot of a sodium dodecyl sulfate-polyacrylamide gel (SDS-PAGE) of B5A-derivatized PSII and by detection with an avidin-alkaline phosphatase conjugate (data not shown) (38).

Following derivatization, *in-situ* digestion was employed to release modified, surface exposed peptides. This method was used previously to identify surface-exposed phosphorylation sites in *Arapidopsis* thylakoid membranes (58). B5A-derivatized TW PSII was trypsin digested overnight (Figure 2.2, step 4B), cleaved peptides were separated from undigested PSII by centrifugation, and the peptides were subjected to HPLC (Figure 2.2, step 5B). When a 10-60% acetonitrile/ 0.1% TFA gradient was used and the peptide elution was monitored at 350 nm, three fractions with unique red-shifted absorption peaks were observed (Figure 2.3A). The fractions had retention times of ~28

min (fraction 1), ~35 min (fraction 2), and ~36 min (fraction 3). Unlabeled peptides gave a similar 350 nm chromatogram (Figure 2.3B). These peaks were also present in intact PSII membranes (Figure 2.5).

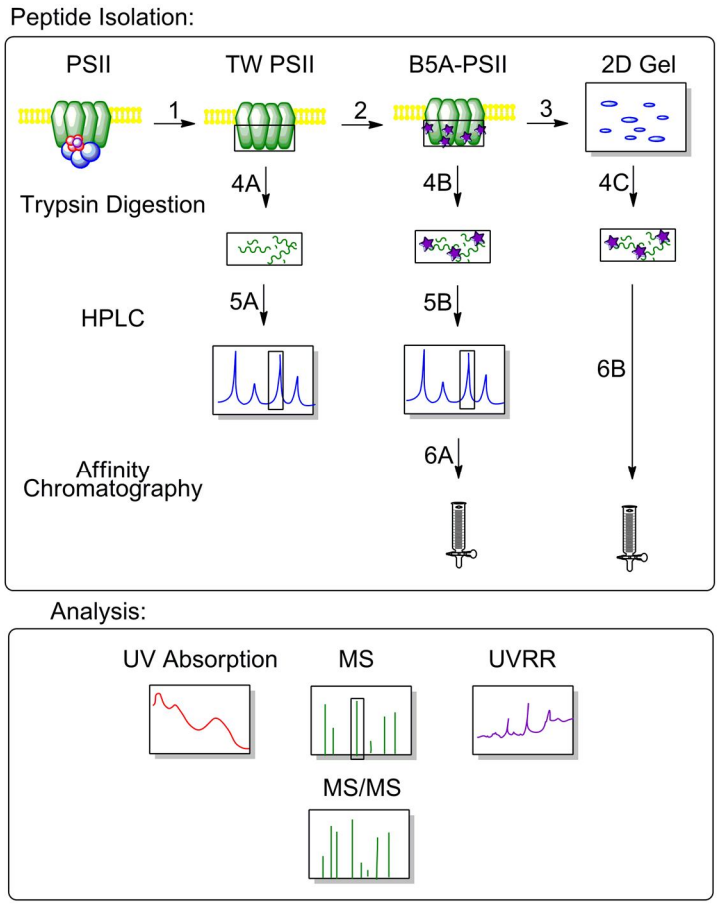

Figure 2.2. Overview of peptide isolation and analysis. Peptide isolation by *in-situ* digestion: In step 1, intact PSII was Tris-washed (TW) to remove the extrinsic subunits and the Mn_4CaO_5 cluster. The TW PSII was either directly trypsin digested *in-situ* (step 4A) or derivatized with B5A (step 2), and then subjected to digestion (step 4B). Both sets of peptides were separated by HPLC (steps 5A and B). For some experiments, HPLC purified peptides were subjected to avidin affinity chromatography (step 6A). Peptide isolation by 2D gel electrophoresis: B5A-derivatized peptides were electrophoresized in two dimensions (step 3), in-gel digested, and then extracted from the gel (step 4C). For some experiments, the extracted peptides were subjected to avidin affinity chromatography (step 6B). Analysis: HPLC-purified peptides were characterized by their optical UV absorption. HPLC and affinity purified peptides were analyzed by MS/MS and UVRR spectroscopy.

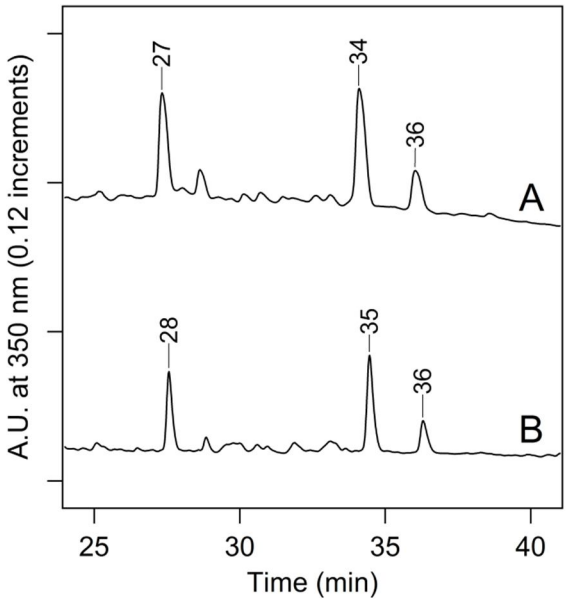

Figure 2.3. HPLC separation of peptides derived from TW PSII by *in situ* trypsin digestion. The chromatograms were monitored at 350 nm and show three fractions with the retention times noted. In (A), TW PSII was unlabeled. In (B), TW PSII was B5A-labeled. Chromatograms were displaced by an arbitrary amount on the y axis for comparison. Each y-axis tick mark represents 120 milli-absorbance units.

The absorption spectra of these unlabeled and B5A-labeled fractions are shown in Figure 2.4A and B, respectively. As derived from the HPLC detector, the spectra all exhibited maxima between 326 and 336 nm. Small shifts may be due to overlap with a 280 nm shoulder, which is indicative of tyrosine absorption (59). The spectra of the fractions also showed strong 220 nm absorption from the peptide bond (60), but no visible absorption, which is characteristic of photosynthetic pigments. The observation of these 220 and 280 nm absorption bands supports the conclusion that the fractions contain peptides, which have been post-translationally modified to produce a chromophore with a ~325 nm absorption maximum.

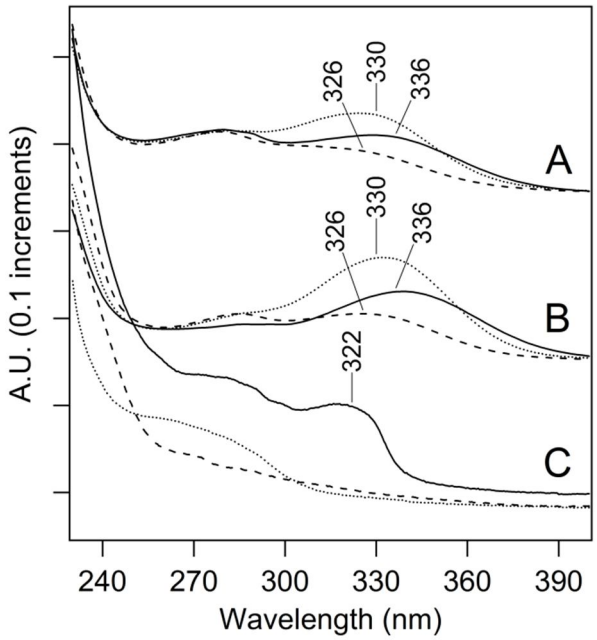

Figure 2.4. Absorption spectra of peptides, derived from tryptic digestion of TW PSII. In (A) and (B), the peptides were separated by HPLC. The 350 nm chromatogram exhibited three fractions with approximate retention times of 28 (fraction 1), 35 (fraction 2), and 36 (fraction 3) min (Figure 2.3). (A) Absorption spectra of fraction 1 (solid line), fraction 2 (dotted line), and fraction 3 (dashed line) from samples in which PSII was not treated with B5A. (B) Absorption spectra of fraction 1 (solid line), fraction 2 (dotted line), and fraction 3 (dashed line) from samples in which PSII was treated with B5A. Fraction 1 corresponds to a CP43 peptide. (C) Absorption spectra of 2D gel-purified, B5A labeled-CP43 peptides before (dotted line) and after (solid line) affinity chromatography. The data in the dashed black line in (C) is the spectrum of B5A alone. Spectra shown in (A) and (B) were derived from the HPLC chromatogram and are an arbitrary y scale. The spectra shown in (C) were measured on a Hitachi spectrophotometer.

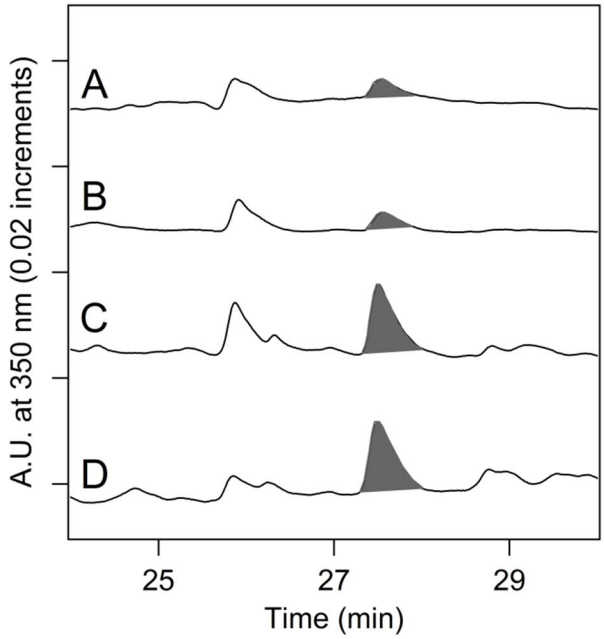

Figure 2.5. HPLC chromatograms of tryptic peptides from intact PSII membranes. The shaded peak at ~27 minutes corresponds to fraction 1 and contains a CP43 peptide with Trp-365 modified to NFK. Elution was monitored at 350 nm. PSII was maintained in the dark at room temperature (~25 ºC) (A) or 37 ºC (B) for two hours. PSII was illuminated with white light (C and D) at a light intensity of ~7,000 μmol photons m^{-2} s^{-1}) for two hours. In (C), the temperature under illumination was maintained at 25 ºC. In (D), the temperature under illumination was allowed to increase to 37^{o}C. Chromatograms were displaced in the y-direction for comparison, and the y-axis tick marks correspond to 20 milli-absorbance units. As an internal standard, the chromatograms were normalized to the total 220 nm absorption, which was integrated from 0-50 min. The 350 nm peak at 26 min is not observed in tryptic digests of TW PSII (Figure 2.3).

To identify the 325 nm chromophore in the peptide samples, a comparison was made to model compounds. Some oxidative tryptophan products, such as hydroxytryptophan, dioxyindolylalanine, and oxyindolylalanine, absorb near 295 nm, only slightly red-shifted from the tryptophan absorption band (61,62). However, other PTMs of tryptophan, including NFK and kynurenine (Figure 2.1A), show more red-shifted absorption (51,63). To compare with the peptide spectra, NFK was synthesized

by formylation of commercially available kynurenine. As shown in Figure 2.6A, NFK had an absorption peak at ~320 nm (Figure 2.6A, red), while kynurenine had a longer wavelength absorption maximum at ~365 nm (Figure 2.6A, blue). Both spectra were red-shifted compared to the tryptophan absorption maximum at ~280 nm (Figure 2.6A, black). The absorption maximum of NFK was slightly solvent dependent, showing a shift from 318 to 324 nm when water (Figure 2.6A, solid red) was compared to 50% acetonitrile/0.1% TFA (Figure 2.6A, dashed red). The peptide spectra (Figure 2.4A and B) exhibited a clear similarity with the NFK spectrum (Figure 2.6A, red), making NFK a candidate for the PTM.

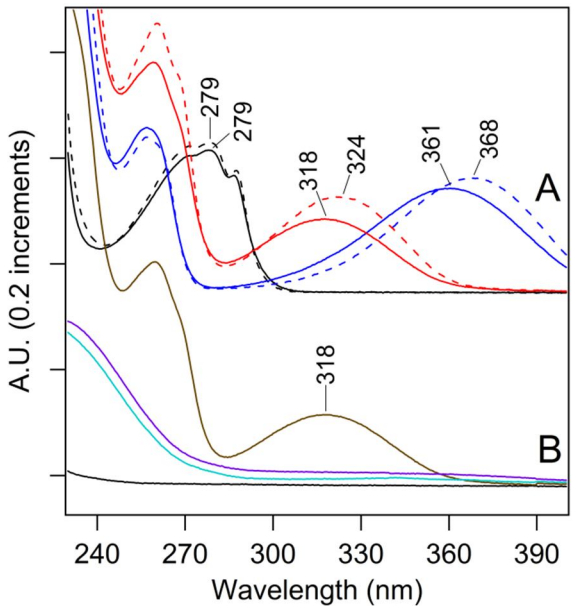

Figure 2.6. Absorption spectra of model compounds. (A) Spectra of 40 µM tryptophan in water (black, solid line) and in 50% acetonitrile/ 0.1% TFA (black, dashed line). Spectra of 40 µM kynurenine in water (blue, solid line) and in 50% acetonitrile/ 0.1% TFA (blue, dashed line). Spectra of 40 µM NFK in water (red, solid line) and in 50% acetonitrile/ 0.1% TFA (red, dashed line). (B) Spectra of a mixture of 40 µM NFK and 160 µM B5A (brown) and when treated with 400 µM $NaBH_4$ in water (cyan). Spectrum of 160 µM B5A when treated with 400 µM $NaBH_4$ in water (red). Spectrum of 40 µM NFK when treated with 400 µM $NaBH_4$ (violet) in water. Spectra shown in (A) and (B) were displaced by an arbitrary amount on the y-axis for comparison.

2.4.2 MS/ MS identifies a NFK modification in the CP43 subunit

HPLC fractions 1-3 were purified by a second round of chromatography, avidin affinity (Figure 2.2, step 6A). Applying LC-MS/MS analysis to the purified peptide samples resulted in unambiguous identification of a CP43 peptide, ^{363}AP[W*]LEPLRGPNGLDLSR^{379}, in fraction 1 with a p-value of 10^{-7} and displaying a mass shift of +32 *m/z* on Trp-365 (Figure 2.7). These results are indicative of an NFK modification. In fraction 2, a peptide of CP24, ^{169}PDSQSVE[W*]ATPWSR^{184}, with a NFK modification was observed (data not shown). There were no spectra detected consistent with the B5A-labeled peptides, however, suggesting that the adduct of NFK and B5A was not stable under the conditions employed for mass spectrometry.

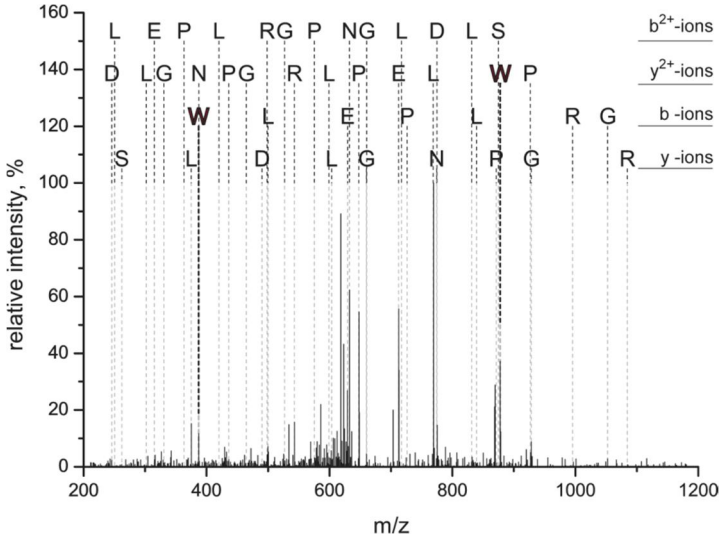

Figure 2.7. MS/MS spectrum assigned to the triply charged CP43 peptide ^{363}AP[W*]LEPLRGPNGLDLSR^{379}. The labels in the figure indicate the N-terminal amino acids for the b-fragments and the C-terminal amino acids for the y-fragments. W is bold face because this residue carries a *+32 m/z* modification. The mass shift of +32 *m/z* can be unambiguously assigned to Trp-365 due to the y^{2+}-ion series and b-ion series. All relevant signals in the MS/MS spectra, which are complex due to the presence of singly, doubly and triply charged fragment ions, can be explained by the peptide sequence. *Tandem mass spectrometry experiments in Figure 2.7 were performed by Sascha Rexroth (Department of Biology, Ruhr-Universität, Bochum, Germany).

2.4.3 2D gel electrophoresis

To confirm that the chromophore arises from a PTM in a PSII peptide, PSII core peptides were purified by 2D gel electrophoresis. For these experiments, B5A-labeled PSII was solubilized and electrophoresized in the first dimension by non-denaturing CN-PAGE (41), which separates the PSII membranes into dimer complexes with varying amounts of light-harvesting proteins (24). All gels were run without Coomassie or bromophenol blue to eliminate possible spectral artifacts from the dyes. The PSII dimer complex, which is deficient in light-harvesting proteins (24), was excised and resolved into individual polypeptides in the second dimension (Figure 2.2, step 3) (42). Due to their similarity in electrophoretic mobility, the CP43 and CP47 protein bands were not fully resolved. MS/MS analysis, following in-gel digestion and peptide extraction (Figure 2.2, step 4C), validated the band identities (data not shown). The identities were also substantiated by previous work (24,64). Although *in-situ* these polypeptides bind many pigment molecules, the non-covalently bound pigments were separated from the proteins under the denaturing gel conditions in the second dimension. Therefore, this experiment eliminated chlorophyll or carotenoid (or their degradation products) as possible sources of the optical absorption.

Before affinity chromatography (Figure 2.2, step 6B), the absorption spectrum of the gel extracted sample exhibited only absorption characteristics of tyrosine containing peptides, with a 280 nm absorption band (59) (Figure 2.4C, dotted line). However, upon affinity purification of the gel-extracted peptide mixture, a ~322 nm peak was observed (Figure 2.4C, solid line). This band resembled the chromophore absorption observed in the HPLC purified peptides (Figure 2.4A and B). The λ_{max} was similar to the spectra

recorded from the HPLC fractions, given the increased scattering background in the gel-extracted samples. Figure 2.4C also shows that the B5A compound itself does not contribute to the optical absorption (Figure 2.4C, dashed line), although affinity chromatography was essential for the selection of the modified peptides.

2.4.4 Proposed structure of the B5A adduct

NFK is expected to react with hydrazines, hydrazides, and amines (65-67). Figure 2.1C presents two possible structures for the B5A-NFK adduct formed in our experiments. The small 2 *m/z* mass difference between the two structures may not be distinguishable by low resolution peptide mass spectrometry. Figure 2.1C, complex 1, is a covalent adduct, formed by nucleophilic addition of the B5A label at the C4 position of NFK and a subsequent reduction reaction. Figure 2.1C, complex 2, is another possibility for the formation of a B5A-derived amidine, in which the nucleophilic addition occurs at the *N*-formyl carbon. While complex 1 should be quite stable during MS and should be observed in MS/MS spectra, complex 2 is expected to break preferentially at the NFK-B5A interface and escape MS/MS detection.

To distinguish between these two possible structures, we considered the effect of reduction on the optical spectrum. As shown in Figure 2.6B, addition of sodium borohydride ($NaBH_4$) and reduction of the C4 carbonyl group eliminated the 318 nm absorption of NFK (compare Figure 2.6A, red and Figure 2.6B, violet). Addition of sodium borohydride to a mixture of NFK and B5A had a similar effect (Figure 2.6B, brown and cyan). This result suggests that reduction of the carbonyl group of NFK will eliminate the 322 nm absorption. Because the 322 nm band was observed in the labeled

peptides, consideration of these optical properties supports an assignment of complex 2 as the covalent adduct.

2.4.5 UVRR spectroscopy of the chromophore

To obtain more information concerning the structure of the B5A peptide complex, UV resonance Raman (UVRR) was employed (68). Figure 2.8A and B are the Raman spectra of kynurenine and NFK model compounds, respectively. These data were obtained with 229 nm excitation. The Raman spectrum of kynurenine could not be acquired at 325 nm, due to a large fluorescence background. The Raman spectrum of NFK, obtained either with 229 or 325 nm probe beams, displayed a band at 1242 cm^{-1}. There was no observable signal from the B5A label alone, either at 229 or 325 nm, due to lack of resonance enhancement (data not shown).

In Figure 2.8B, unique bands assignable to the NFK *N*-formyl group were observed at 1667 and 1242 cm^{-1}. A band between 1040 and 1053 cm^{-1} was observed both in the kynurenine and the NFK Raman spectra (Figure 2.8A and B). These bands are characteristic of the oxidized indole group (31,69). These spectral features were not observed in the UV Raman spectra of the aromatic amino acids, histidine, tryptophan, tyrosine, and phenylalanine (Figure 2.9). For example, unmodified tryptophan exhibited a benzene breathing mode at 1009 cm^{-1} (Figure 2.9B). In addition, these bands were not observed in spectra derived from chl *a* or a carotenoid, after correction for solvent scattering (Figure 2.10).

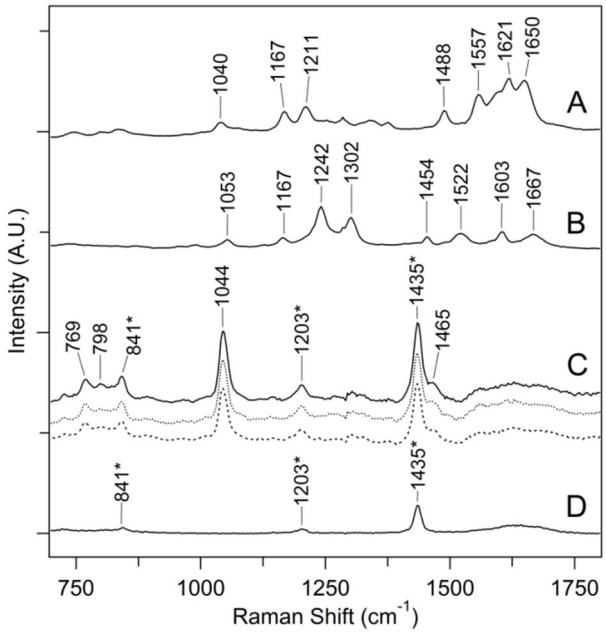

Figure 2.8. UVRR spectra of chromophore-containing PSII peptides and model compounds. Spectra of kynurenine (A) and NFK (B) in water, recorded with 220 μW, 229 nm laser excitation. (C) Spectra of the chromophore-containing peptides from HPLC fractions 1 (solid line), 2 (dotted line), and 3 (bold dotted line) (see Figure 2.3B), recorded with 360 μW, 325 nm laser excitation. The peptides were B5A-derivatized, purified both by HPLC and by affinity chromatography, and suspended in H_2O/ 0.1% TFA. (D) shows the UVRR spectrum of H_2O/ 2% TFA only, and the bands assigned to TFA are indicated with a "*". The spectra were displaced by an arbitrary amount on the y-axis for comparison. Each y-axis tick mark corresponds to 6,500 arbitrary intensity units.

Previous FT-Raman measurements on NFK assigned a band at 1050 cm^{-1} to the ring system, a band at 1604 cm^{-1} to a ring stretching mode, and bands at 1239 and 1685 cm^{-1} to the *N*-formyl group (69). In addition, bands at 1052 and 1050 cm^{-1} were observed for NFK modifications in lysozyme (69) and egg white ovalbumin (31), respectively. Formamide gave rise to Raman bands at 1670, 1599, 1391, 1313, 1098, 1048, and 983 cm^{-1} (70). In anilides, the carbonyl band was observed at higher frequency (1704 cm^{-1} in formanilide), due to delocalization of the unpaired electrons on the formamide nitrogen into the phenyl ring (71).

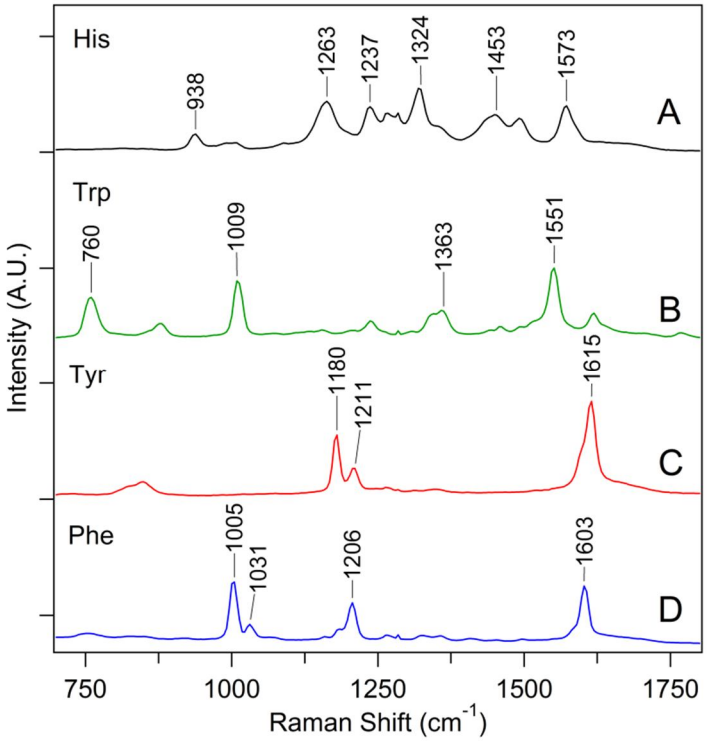

Figure 2.9. UVRR spectra of amino acids. Spectra of histidine (A), tryptophan (B), tyrosine (C), and phenylalanine (D) in HEPES, pH 7.5 were recorded with a 250 µW, 229 nm probe. The total exposure time was 21 minutes. The spectra were displaced by an arbitrary amount on the y-axis for comparison. Each y-axis tick mark represents 20,000 arbitrary intensity units (A.U.).

Because the UV Raman spectrum is specific for the contribution of NFK, the Raman spectrum of derivatized peptide samples was obtained with a 325 nm probe (Figure 2.8C), which resonantly enhances the chromophore. In peptides purified by HPLC only (Figure 2.2, step 5B), a strong fluorescence background obscured the Raman signal. Therefore, samples were subjected to purification by affinity chromatography (Figure 2.2, step 6A), which reduced the background fluorescent signal. The resulting Raman spectra of all three HPLC, 350 nm absorbing fractions were similar (Figure 2.8C). These results imply that all three fractions contain the same PTM. Comparison with the TFA buffer spectrum (Figure 2.8D) showed that bands at 841, 1203, and 1435 cm^{-1} arise

from TFA. The Raman spectra of all three peptide fractions displayed a band at 1044 cm^{-1}, which is consistent with the presence of NFK in all three fractions. The shift from the 1053 cm^{-1} frequency observed in NFK alone (Figure 2.8B) may be due to reaction with the B5A label. No vibrational bands from the *N*-formyl group (1242 and 1667 cm^{-1}) were observed, supporting the interpretation that complex 2 (Figure 2.1C) is the stable structure.

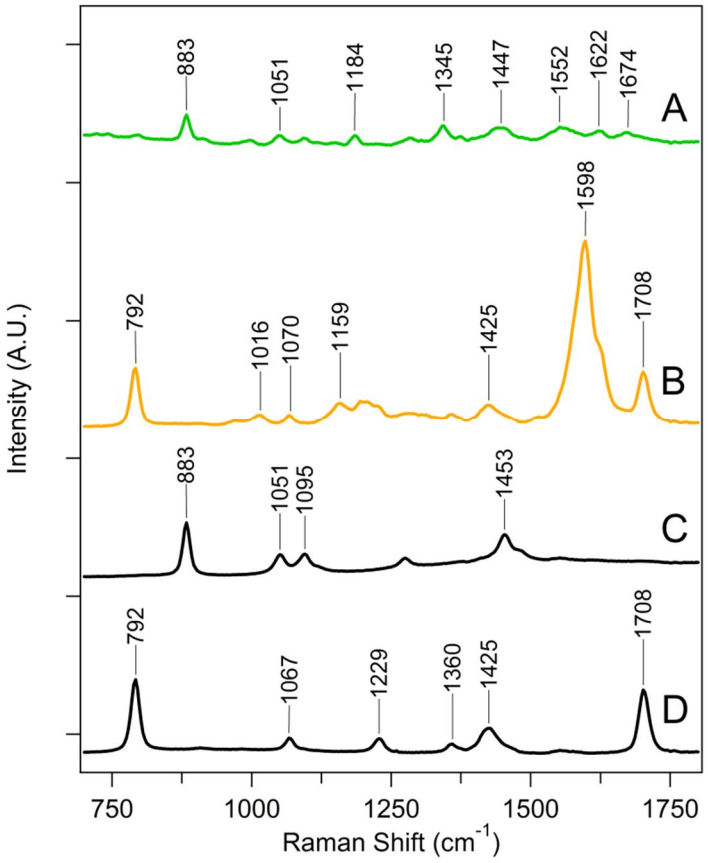

Figure 2.10. UVRR of chlorophyll *a* and β-carotene. Spectra of chlorophyll *a* (A) in ethanol (B) and β-carotene (C) in an 80:20 acetone-water mixture (D) were recorded with a 360 μW, 325 nm laser probe. The total exposure time was 30 minutes. The spectra were displaced by an arbitrary amount on the y-axis for comparison. Each y-axis tick mark represents 400,000 arbitrary intensity units (A.U.).

2.4.6 Yield of NFK in TW PSII

Using an extinction coefficient of 3750 M^{-1} cm^{-1} at 321 nm (63), the yield of NFK in TW PSII can be estimated. For the HPLC experiment, fraction 1 was collected, the sample was concentrated to 200 µl, and the absorption spectrum was measured on a Hitachi spectrophotometer. Starting with 6 mg chl or 24 nmole PSII reaction center (72), the NFK yield (on a reaction center basis) was estimated as ~7% in the HPLC method. For the 2D gel experiment, peptides were extruded from the gel, concentrated to 200 µl, and the absorption spectrum was measured as described above (Figure 2.4C). Starting with 13 mg chl or 52 nmole PSII reaction center (72), the NFK yield was estimated as ~6% in the 2D gel method.

2.4.7 Photoinhibition increases the yield of NFK in intact PSII

Our MS/MS data support the interpretation that NFK is formed by PTM of Trp-365 in the CP43 subunit. NFK can be generated from tryptophan by ROS (73,74). These species, including singlet oxygen ($^1O_2$,), hydrogen peroxide (H_2O_2), superoxide anion (O_2^-), and hydroxyl radical (•OH) (75), have been proposed to be involved with photoinhibition in PSII. However, the mechanism of their involvement remains controversial (reviewed in 76,77). High light conditions have been linked to oxidative modification of *Arabidopsis* PSII in proteomic studies (21). We have previously reported that substitutions at Trp-365 increase the rate of photoinhibition (22). The magnitude of the change depends on light intensity (data not shown) and will be described in a future publication.

To probe for a possible connection between the yield of NFK and photoinhibition, we compared 350 nm chromatograms of tryptic peptides obtained from intact PSII (Figure 2.5). The integrated area of the 350 nm peak, derived from fraction 1, was corrected for the total integrated absorption at 220 nm. This normalization is an internal standard, which corrects for any change in the total yield of tryptic peptides. In this experiment, intact PSII samples were maintained in the dark at room temperature (~25 ºC) (Figure 2.5A) or in the dark at 37 ºC (Figure 2.5B). These dark-maintained, intact PSII samples gave a 350 nm fraction, with a similar retention time to TW PSII fraction 1 (Figure 2.5A and B, shaded peaks and Figure 2.3). The fraction 1 yield in dark maintained PSII was estimated as 0.3% on a reaction center basis. The NFK yield was not significantly altered by an increase in temperature in the dark. Comparison of the integrated areas (Figure 2.5, shaded peaks, fraction 1), derived from dark-maintained PSII at 25 ºC and at 37 ºC, gave a ratio of 1.1 $\pm$ 0.1.

Intact PSII samples were also illuminated with white light for two hours under temperature-controlled conditions at 25 ºC (Figure 2.5C) or under conditions in which the temperature of the sample increased to 37 ºC (Figure 2.6D). An increase in peak height was observed after two hours of illumination. This increase was observed when the temperature was controlled at 25^{o}C (ratio 2.4 $\pm$ 0.8, Figure 2.5C, shaded peak) or when the temperature was allowed to increase to 37 ºC (ratio 2.2 $\pm$ 0.5, Figure 2.5D, shaded peak).

The steady state rate of oxygen evolution was also measured under the same conditions (35). Before illumination, the average rate was 740 $\pm$ 50 µmol O_2 mg chl^{-1} hr^{-1}. After two hours in the dark, the rate was 630 $\pm$ 30 µmol O2 mg^{-1}hr^{-1}. However, with a

2 hour illumination, the rate declined to 270 $\pm$ 60 μmol O_2 mg chl^{-1} hr^{-1}. The 2.4 $\pm$ 0.5 fold decrease in activity is similar to the increase observed in NFK yield. Therefore, these results suggest that the NFK modification at Trp-365 is induced by illumination and high light stress in intact PSII.

2.5 Discussion

2.5.1 Summary

In this paper, we provide evidence that PSII contains a modified form of tryptophan, NFK. Mass spectrometry on purified peptides shows a mass shift of +32 *m/z* for the ^{363}AP[W*]LEPLRGPNGLDLSR^{379} peptide from CP43. This mass shift and peptide sequencing by MS/MS are consistent with a double oxidation of Trp-365. Optical absorption and UV resonance Raman data support the conclusion that CP43 peptides contain NFK. In these experiments, NFK was observed following *in-situ* and in-gel tryptic digestion. The yield of NFK in TW PSII was significant, and the yield increased when intact PSII was subjected to photoinhibitory conditions.

2.5.2 Generation of NFK and NFK in other proteins

NFK has been identified in other proteins by mass spectrometry, including bovine heart mitochondrial proteins (78), rat skeletal muscle proteins (79), bovine α-crystalline (80), and spinach LHCII (32). NFK is formed by the reaction of ROS with tryptophan side chains in proteins (73). One potential reactive species is singlet oxygen, $^1O_2$ (74). Initial reaction of tryptophan with $^1O_2$ has been proposed to form one of two unstable

intermediates. A dioxetane derivative intermediate can form across the C2-C3 indole ring bond; subsequent ring cleavage gives NFK. On the other hand, an intermediate hydroperoxide, formed at the C3 position on the indole ring, can also decompose to form NFK (81). Therefore, we propose that NFK is formed by a reaction between Trp-365 and $^1O_2$.

2.5.3 Other modifications at Trp-365

Other modifications of Trp-365 in the lumenal loop of CP43 (Trp-352 in *Synechocystis sp.* PCC 6803) have been reported previously (22). The data were obtained by tandem mass spectrometry (22) and were consistent with modification of the side chain to kynurenine (+4 *m/z*), oxindolalanine (+16 *m/z*), and a hydroxy-indole derivative (+18 *m/z*). The oxindolalanine and hydroxy-indole derivatives were proposed to be intermediates produced during oxidative cleavage to give kynurenine (22). None of these species are expected to show an absorption maximum at 325 nm (61,62), as observed here for the NFK-containing peptides. NFK can be formed as a stable intermediate during the production of kynurenine (Figure 2.1A) (49). In previous work, kynurenine was observed to be present in PSII which had not been TW and had not been subjected to gel electrophoresis (22). Kynurenine was also observed in PSII, which had been maintained in the dark. Taken together with the results described here, these data support the conclusion that oxidative modification of Trp-365 is relevant *in vivo*.

2.5.4 Analysis of three different HPLC fractions

In this work, three 350 nm absorbing fractions, with reproducible retention times, were observed with HPLC purification of TW PSII peptides. UV resonance Raman studies suggest that all three fractions contained the same, B5A-derivatized NFK chromophore. The NFK modification in CP43 was confirmed by MS/MS of fraction 1. An NFK modification in a light harvesting protein (CP24) was observed in fraction 2. However, the modified peptide detected in fraction 1 was the result of incomplete tryptic digestion. Therefore, it is possible that other fractions contain a different cleavage product of the same CP43 peptide. In addition to 325 nm absorption, all three fractions exhibited a 280 nm peak, which is indicative of tyrosine absorption. It should be noted that the NFK containing CP43 sequence does not contain tyrosine (^{363}AP[W*]LEPLRGPNGLDLSR^{379}). Thus, other tyrosine-containing peptides must be present in all three eluting fractions. Our MS analysis of the fractions provided evidence for ~40 peptides, even after HPLC and affinity purification (data not shown). Such complexity can be attributed to the challenges of MS/MS as applied to membrane associated peptides.

2.5.5 Proposed structure of the B5A- labeled NFK complex

In some of our experiments, a biotinylated amine was used to label the NFK-containing peptide. Amines and hydrazines are expected to label activated carbonyl groups (26 and references therein). In other proteins, it has been suggested that kynurenine and NFK react with hydrazine. These proteins include low-density lipoprotein (LDL) (82), cucumber microsomal membrane proteins (66) and ribulose-1,5-

bisphosphate carboxylase oxygenase (Rubisco) (66). In bovine serum albumin (65) and α-crystallin (65), NFK was proposed to crosslink with lysine residues. On the other hand, in PSII, a complex between kynurenine and a hydrazide labeling reagent was not observed by MS/MS (22).

NFK may react with amines to form an adduct at the C4 position (Figure 2.1C, complex 1). Reaction of the amine and electrophilic carbon produces a Schiff base, which can be reduced to give the stable product shown in complex 1. Previous work has indicated that reducing equivalents are produced during PSII light reactions. These reducing equivalents were observed to stabilize amine-PTM complexes (27). On the other hand, reaction of the amine with the NFK formamide group would give the structure shown in Figure 2.1C, complex 2. Although amide groups do not usually react with amines, a similar product complex was observed between *N*-acetyl-formylkynurenine and dimethyl-*p*-benzoquinonediimine in solution (83). Delocalization of the unpaired electrons on the nitrogen into the aromatic ring may help to activate the formamide carbon (71). It should be noted that we have not observed the labeled NFK adduct by MS/MS. However, our optical and resonance Raman data support binding of the amine label, B5A, at the formamide group, as shown in complex 2. An addition at the *N*-formyl carbon would provide a breaking point during collision induced dissociation, which could lead to the neutral loss of the B5A moiety during MS analysis.

2.5.6 Photoinhibition and high light stress

Examination of CP43 protein sequences in other organisms, both prokaryotes and eukaryotes, indicates strict sequence conservation of Trp-365. This conservation suggests

a functional role for this residue. We hypothesize that Trp-365 may play a role in protection from photoinhibition (22). In PSII, photoinhibition is the light-induced inactivation of photosynthetic activity induced by excess light energy (reviewed in 84). The results are a decreased efficiency in electron transfer, damage and degradation of the D1 and other PSII subunits, and finally repair by *de novo* protein synthesis. When the rate of repair is slower than the rate of degradation, a loss of PSII activity is observed (84). This cycle of damage and repair must be coordinated, and the mechanisms of these reactions have not yet been elucidated.

Photoinhibition may occur by two different mechanisms (reviewed in 77,84,85,86). In the acceptor side photoinhibition model, damage is initiated by charge separation in reaction centers that contain a reduced quinone, Q_A^-. Recombination leads to the product of triplet chlorophyll, ^{3}chl, species (87). Changes in the midpoint potential of Q_A^- may alter the susceptibility of PSII to photoinhibition (reviewed in 85). In donor side photoinhibition, damage is initiated by inactivation of the OEC and water oxidation. Under these conditions, P_{680}^+, which has a high potential, has a long lifetime and can act as an oxidant for prosthetic groups and amino acid residues (reviewed in 85).

2.5.7 ROS and high light stress in PSII

We attribute the formation of NFK to the reaction of Trp-365 with $^1O_2$. In PSII, $^1O_2$ can be formed by photo-excitation of chlorophyll molecules, which results in formation of ^{3}chl (88). ROS and ^{3}chl are generated by charge recombination in acceptor side inhibition (87,89). $^1O_2$ has been detected by spin trapping in photoinhibited PSII (76,90) and by a fluorescence sensor in *Arabidopsis* leaves (91). Chemical trapping in

PSII reaction center preparations, which lack the quinone acceptors, has also detected $^1O_2$ (92). Other ROS species may be formed in donor side photoinhibition (76,90).

While a correlation between ROS production and photodamage is largely accepted, there is no consensus on the specific role of $^1O_2$ (see 90 and references therein). One view suggests direct involvement of ROS in damage and increased turnover of the reaction center D1 protein (93). This can occur directly, because ROS damage can lead to peptide bond cleavage (73). Alternatively, ROS induced modifications could cause a protein conformational change, which allows access of specific proteases to the D1 subunit (22,94,95). Finally, $^1O_2$ may inhibit the D1 repair cycle (for example, see 96). These roles of ROS are not mutually exclusive.

2.5.8 Proposed role for NFK- 365 in photoinhibition

In this paper, we provide evidence that NFK is present in dark maintained PSII, and that the yield of NFK increases by a factor of two under high light intensity in intact PSII. This change was accompanied by a ~2 fold decrease in steady state oxygen evolution rate. Previous preliminary characterization of site directed mutations at Trp-365 reported that the Trp provides photoprotection (22). The 1.9 Å resolution crystal structure (3) of cyanobacterial PSII shows that Trp-365 is ~17 Å from the water oxidizing complex (Figure 2.11). Trp-365 is found in a CP43 loop region, which is in close proximity to the D1 subunit.

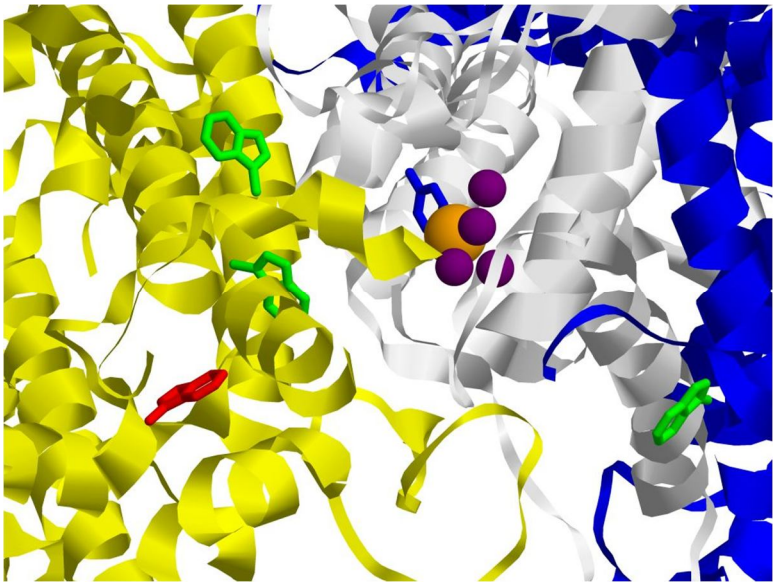

Figure 2.11. Location of CP43 Trp-365, a site of NFK modification, in the PSII structure from the cyanobacterium, *T. vulcanus* (3) (PDB 3ARC). The CP43 protein backbone is shown in yellow, and the D1 and D2 proteins are shown in white and blue, respectively. The Mn_4CaO_5 cluster is displayed in purple and orange; the Tyr_z side chain is shown in blue. Trp residues located within 20 Å of the Mn_4Ca cluster are shown. The side chain of CP43 Trp-365, which is modified to NFK, is shown in red. Trp-359 (CP43), Trp-291 (CP43), and Trp-328 (D2) are shown in green. The measured distances to the Mn_4Ca are 17 Å for Trp-365 (CP43), 16 Å for Trp-359 (CP43), 11 Å for Trp-291 (CP43), and 15 Å for Trp-328 (D2).

Taken together, these observations suggest a role for modification of Trp-365 in the high light induced, damage/repair cycle. This could be accomplished by two different mechanisms. In the first, Trp-365 may act as a ROS scavenger, and in the second, Trp-365 may serve as signal, which facilitates reaction center repair. It should be noted that Trp-359 and 291 in CP43, as well as Trp-328 in D2, are also within 17 Å of the OEC (Figure 2.11). In our MS/MS experiments, we have seen no evidence for NFK modifications of these sidechains, although Trp-359 was observed in the +16 *m/z* form (data not shown).

2.6 Conclusions

We have identified an oxidative modification of tryptophan in the CP43 subunit of PSII. This NFK is a UV absorbing chromophore, which is formed by the oxidation of a Trp side chain by ROS. We propose that NFK plays a role in protection and repair during photoinhibition. The evolutionarily conserved residue may act as a $^1O_2$ scavenger. Alternatively, oxidation of the tryptophan may promote repair by signaling for degradation or enabling efficient removal of the damaged D1.

2.7 Acknowledgments

We thank Prof. Cindy Putnam-Evans for helpful discussions concerning the photoinhibition experiments. We are also grateful to Dr. Adam Offenbacher for the UV resonance Raman spectra of the aromatic amino acid residues.

2.8 References

1. Nelson, N., and Yocum, C. F. (2006) Structure and function of photosystems I and II. *Annu. Rev. Plant Biol.* **57**, 521-565

2. Guskov, A., Kern, J., Gabdulkhakov, A., Broser, M., Zouni, A., and Saenger, W. (2009) Cyanobacterial photosystem II at 2.9 Å resolution and the role of quinones, lipids, channels and chloride. *Nat. Struct. Mol. Biol.* **16**, 334- 342

3. Yocum, C. F. (2008) The calcium and chloride requirements of the O_2 evolving complex. *Coord. Chem. Rev.* **252**, 296-305

4. Nanba, O., and Satoh, K. (1987) Isolation of a photosystem II reaction center consisting of D-1 and D-2 polypeptides and cytochrome *b*-559. *Proc. Natl. Acad. Sci. U. S. A.* **84**, 109-112

5. Bricker, T. M., and Frankel, L. K. (2002) The structure and function of CP47 and CP43 in photosystem II. *Photosynth. Res.* **72**, 131-146

6. Miyao, M., and Murata, N. (1989) The mode of binding of 3 extrinsic proteins of 33-kDa, 23-kDa, and 18-kDa in the photosystem II complex of spinach. *Biochim. Biophys. Acta* **977**, 315- 321

7. MacDonald, G. M., Boerner, R. J., Everly, R. M., Cramer, W. A., Debus, R. J., and Barry, B. A. (1994) Comparison of cytochrome *b*-559 content in photosystem II complexes from spinach and *Synechocystis* species PCC 6803. *Biochemistry* **33**, 4393-4400

8. Zouni, A., Witt, H.-T., Kern, J., Fromme, P., Krauß, N., Saenger, W., and Orth, P. (2001) Crystal structure of photosystem II from *Synechococcus elongatus* at 3.8 Å resolution. *Nature* **409**, 739-743

9. Ferreira, K. N., Iverson, T. M., Maghlaoui, K., Barber, J., and Iwata, S. (2004) Architecture of the photosynthetic oxygen-evolving center. *Science* **303**, 1831-1838

10. Kamiya, N., and Shen, J.-R. (2003) Crystal structure of oxygen-evolving photosystem II from *Thermosynechococcus vulcanus* at 3.7 Å resolution. *Proc. Natl. Acad. Sci. U. S. A.* **100**, 98-103

11. Loll, B., Kern, J., Saenger, W., Zouni, A., and Biesiadka, J. (2005) Towards complete cofactor arrangement in the 3.0 Å resolution structure of photosystem II. *Nature* **438**, 1040-1044

12. Rhee, K.-H., Morris, E. P., Barber, J., and Kühlbrandt, W. (1998) Three-dimensional structure of the plant photosystem II reaction center at 8 Å resolution. *Nature* **396**, 283-286

13. Allen, J. F. (1992) Protein phosphorylation in regulation of photosynthesis. *Biochim. Biophys. Acta* **1098**, 275-335

14. Stadtman, E. R. (1990) Covalent modification reactions are marking steps in protein turnover. *Biochemistry* **29**, 6323-6331

15. Janes, S. M., Mu, D., Wemmer, D., Smith, A. J., Kaur, S., Maltby, D., Burlingame, A. L., and Klinman, J. P. (1990) A new redox cofactor in eukaryotic enzymes: 6-hydroxydopa at the active site of bovine serum amine oxidase. *Science* **248**, 981-987

16. Whitelegge, J. P., Faull, K. F., Gundersen, C. B., and Gómez, S. M. (1999) Imaging the native covalent state of thylakoid proteins by electrospray-ionization mass spectrometry. in *Photosynthesis: Mechanisms and Effects* (Garab, G. ed.), Kluwer Academic Publishers, Dordrecht, Netherlands. pp 4381 -4384

17. Whitelegge, J. P., Gundersen, C. B., and Faull, K. F. (1998) Electrospray-ionization mass spectrometry of intact intrinsic membrane proteins. *Protein Sci.* **7**, 1423-1430

18. Bowyer, J. R., Packer, J. C. L., McCormack, B. A., Whitelegge, J. P., Robinson, C., and Taylor, M. A. (1992) Carboxyl-terminal processing of the D1 protein and photoactivation of water-splitting in photosystem II. *J. Biol. Chem.* **267**, 5424-5433

19. Liao, D. I., Qian, J., Chisholm, D. A., Jordan, D. B., and Diner, B. A. (2000) Crystal structures of the photosystem II D1 C-terminal processing protease. *Nat. Struct. Biol.* **7**, 749-753

20. Sharma, J., Panico, M., Shipton, C. A., Nilsson, F., Morris, H. R., and Barber, J. (1997) Primary structure characterization of the photosystem II D1 and D2 subunits. *J. Biol. Chem.* **272**, 33158-33166

21. Galetskiy, D., Lohscheider, J. N., Kononikhin, A. S., Popov, I. A., Nikolaev, E. N., and Adamska, I. (2011) Mass spectrometric characterization of photooxidative protein modifications in *Arabidopsis thaliana* thylakoid membranes. *Rapid Commun. Mass Spectrom.* **25**, 184-190

22. Anderson, L. B., Maderia, M., Ouellette, A. J. A., Putnam-Evans, C., Higgins, L., Krick, T., MacCoss, M. J., Lim, H., Yates, J. R., III, and Barry, B. A. (2002) Posttranslational modifications in the CP43 subunit of photosystem II. *Proc. Natl. Acad. Sci. U. S. A.* **99**, 14676-14681

23. Anderson, L. B., Ouellette, A. J. A., Eaton-Rye, J., Maderia, M., MacCoss, M. J., Yates, J. R., III, and Barry, B. A. (2004) Evidence for a post-translational modification, aspartyl aldehyde, in a photosynthetic membrane protein. *J. Am. Chem. Soc.* **126**, 8399-8405

24. Rexroth, S., Wong, C. C. L., Park, J. H., Yates, J. R., III, and Barry, B. A. (2007) An activated glutamate residue identified in photosystem II at the interface between the manganese-stabilizing subunit and the D2 polypeptide. *J. Biol. Chem.* **282**, 27802-27809

25. Mamedov, F., Rintamäki, E., Aro, E. M., Andersson, B., and Styring, S. (2002) Influence of protein phosphorylation on the electron-transport properties of photosystem II. *Photosynth. Res.* **74**, 61-72

26. Ouellette, A. J. A., Anderson, L. B., and Barry, B. A. (1998) Amine binding and oxidation at the catalytic site for photosynthetic water oxidation. *Proc. Natl. Acad. Sci. U. S. A.* **95**, 2204-2209

27. Anderson, L. B., Ouellette, A. J. A., and Barry, B. A. (2000) Probing the structure of photosystem II with amines and phenylhydrazine. *J. Biol. Chem.* **275**, 4920-4927

28. Sandusky, P. O., and Yocum, C. F. (1984) The chloride requirement for photosynthetic oxygen evolution: analysis of the effects of chloride and other anions on amine inhibition of the oxygen-evolving complex. *Biochim. Biophys. Acta* **766**, 603-611

29. Sandusky, P. O., and Yocum, C. F. (1986) The chloride requirement for photosynthetic oxygen evolution: factors affecting nucleophilic displacement of chloride from the oxygen-evolving complex. *Biochim. Biophys. Acta* **849**, 85-93

30. Previero, A., Coletti-Previero, M.-A., and Jollès, P. (1967) Localization of non-essential tryptophan residues for biological activity of lysozyme. *J. Mol. Biol.* **24**, 261-268

31. Rokos, H., Wood, J. M., Hasse, S., and Schallreuter, K. U. (2008) Identification of epidermal *L*-tryptophan and its oxidation products by *in vivo* FT-raman spectroscopy further supports oxidative stress in patients with vitiligo. *J. Raman Spectrosc.* **39**, 1214-1218

32. Rinalducci, S., Campostrini, N., Antonioli, P., Righetti, P. G., Roepstorff, P., and Zolla, L. (2005) Formation of truncated proteins and high-molecular-mass aggregates upon soft illumination of photosynthetic proteins. *J. Proteome Res.* **4**, 2327-2337

33. Berthold, D. A., Babcock, G. T., and Yocum, C. F. (1981) A highly resolved, oxygen-evolving photosystem II preparation from spinach thylakoid membranes. *FEBS Lett.* **134**, 231-234

34. Lichtenthaler, H. K. (1987) Chlorophylls and carotenoids- pigments of photosynthetic biomembranes. *Methods Enzymol.* **148**, 350-382

35. Barry, B. A. (1995) Tyrosyl radicals in photosystem II. *Methods Enzymol.* **258**, 303-319

36. Ghanotakis, D. F., Topper, J. N., Babcock, G. T., and Yocum, C. F. (1984) Water-soluble 17-kDa and 23-kDa polypeptides restore oxygen evolution activity by creating a high-affinity binding-site for Ca^{2+} on the oxidizing side of photosystem-II. *FEBS Lett.* **170**, 169-173

37. Yamamoto, Y., Doi, M., Tamura, N., and Nishimura, M. (1981) Release of polypeptides from highly active O_2-evolving photosystem II preparations by tris treatment. *FEBS Lett.* **133**, 265-268

38. Towbin, H., Staehelin, T., and Gordon, J. (1979) Electrophoretic transfer of proteins from polyacrylamide gels to nitrocellulose sheets: procedure and some applications. *Proc. Natl. Acad. Sci. U. S. A.* **76**, 4350-4354

39. Piccioni, R., Bellemare, G., and Chua, N. (1982). in *Methods in Chloroplast Molecular Biology* (Edelman, H., Hallick, R. B., and Chua, N.-H. eds.), Elsevier, Amsterdam. pp 985-1014

40. Bollag, D. M., and Edelstein, S. J. (1991) *Protein Methods*, Wiley-Liss, New York

41. Schägger, H., and von Jagow, G. (1991) Blue native electrophoresis for isolation of membrane-protein complexes in enzymatically active form. *Anal. Biochem.* **199**, 223-231

42. Schägger, H., Cramer, W. A., and von Jagow, G. (1994) Analysis of molecular masses and oligomeric states of protein complexes by blue native electrophoresis and isolation of membrane-protein complexes by 2-dimensional native electrophoresis. *Anal. Biochem.* **217**, 220-230

43. Fernandez-Patron, C., Castellanos-Serra, L., Hardy, E., Guerra, M., Estevez, E., Mehl, E., and Frank, R. W. (1998) Understanding the mechanism of the zinc-ion stains of biomacromolecules in electrophoresis gels: generalization of the reverse-staining technique. *Electrophoresis* **19**, 2398-2406

44. Rexroth, S., Meyer zu Tittingdorf, J. M., Krause, F., Dencher, N. A., and Seelert, H. (2003) Thylakoid membrane at altered metabolic state: challenging the forgotten realms of the proteome. *Electrophoresis* **24**, 2814-2823

45. Sinz, A., Kalkhof, S., and Ihling, C. (2005) Mapping protein interfaces by a trifunctional cross-linker combined with MALDI-TOF and ESI-FTICR mass spectrometry. *J. Am. Soc. Mass. Spectrom.* **16**, 1921-1931

46. Kim, J.-R., Yoon, H. W., Kwon, K. S., Lee, S.-R., and Rhee, S. G. (2000) Identification of proteins containing cysteine residues that are sensitive to oxidation by hydrogen peroxide at neutral pH. *Anal. Biochem.* **283**, 214-221

47. Chen, J., and Barry, B. A. (2008) Ultraviolet resonance Raman microprobe spectroscopy of photosystem II. *Photochem. Photobiol.* **84**, 815-818

48. Chen, J., Bender, S. L., Keough, J. M., and Barry, B. A. (2009) Tryptophan as a probe of photosystem I electron transfer reactions: a UV resonance raman study. *J. Phys. Chem. B* **113**, 11367-11370

49. Simat, T., Meyer, K., and Steinhart, H. (1994) Synthesis and analysis of oxidation of carbonyl condensation compounds of tryptophan. *J. Chromatogr. A* **661**, 93-99

50. Jacobson, K. B. (1978) New substrate for formylkynurenine formidase: *N*', N^{α}-diformylkynurenine. *Arch. Biochem. Biophys.* **186**, 84-88

51. Pirie, A. (1971) Formation of *N*'-formylkynurenine in proteins from lens and other sources by exposure to sunlight. *Biochem. J.* **125**, 203- 208

52. Eng, J. K., McCormack, A. L., and Yates, J. R., III. (1994) An approach to correlate tandem mass spectral data of peptides with amino acid sequences in a protein database. *J. Am. Soc. Mass. Spectrom.* **5**, 976-989

53. Rosenberg, C., Christian, J., Bricker, T. M., and Putnam-Evans, C. (1999) Site-directed mutagenesis of glutamate residues in the large extrinsic loop of the photosystem II protein CP43 affects oxygen-evolving activity and PSII assembly. *Biochemistry* **38**, 15994-16000

54. Knoepfle, N., Bricker, T. M., and Putnam-Evans, C. (1999) Site-directed mutagenesis of basic arginine residues 305 and 342 in the CP43 protein of photosystem II affects oxygen-evolving activity in *Synechocystis* 6803. *Biochemistry* **38**, 1582-1588

55. Henmi, T., Miyao, M., and Yamamoto, Y. (2004) Release and reactive-oxygen-mediated damage of the oxygen-evolving complex subunits of PSII during photoinhibition. *Plant Cell Physiol.* **45**, 243-250

56. Virgin, I., Styring, S., and Andersson, B. (1988) Photosystem II disorganization and manganese release after photoinhibition of isolated spinach thylakoid membranes. *FEBS Lett.* **233**, 408-412

57. Yamamoto, Y., and Akasada, T. (1995) Degradation of antenna chlorophyll-binding protein CP43 during photoinhibition of photosystem II. *Biochemistry* **34**, 9038-9045

58. Vener, A. V., Harms, A., Sussman, M. R., and Vierstra, R. D. (2001) Mass spectrometric resolution of reversible protein phosphorylation in photosynthetic membranes of *Arabidopsis thaliana*. *J. Biol. Chem.* **276**, 6959-6966

59. Edelhoch, H. (1967) Spectroscopic determination of tryptophan and tyrosine in proteins. *Biochemistry* **6**, 1948-1954

60. Ham, J. S., and Platt, J. R. (1952) Far UV spectra of peptides. *J. Chem. Phys.* **20**, 335-336

61. Zhao, H., Sagert, J., Hwang, D. S., and Waite, J. H. (2009) Glycosylated hydroxytryptophan in a mussel adhesive protein from *Perna viridis*. *J. Biol. Chem.* **284**, 23344-23352

62. Huang, H. V., Bond, M. W., Hunkapiller, M. W., and Hood, L. E. (1983) Cleavage at tryptophanyl residues with dimethylsulfoxide hydrochloric acid and cyanogen bromide. *Methods Enzymol.* **91**, 318-324

63. Mehler, A. H., and Knox, W. E. (1950) The conversion of tryptophan to kynurenine in the liver II. The enzymatic hydrolysis of formylkynurenine. *J. Biol. Chem.* **187**, 431-438

64. Kügler, M., Jänsch, L., Kruft, V., Schmitz, U. K., and Braun, H.-P. (1997) Analysis of the chloroplast protein complexes by blue-native polyacrylamide gel electrophoresis (BN-PAGE). *Photosynth. Res.* **53**, 35-44

65. Fujimori, E. (1981) Blue fluorescence and crosslinking of photooxidized proteins. *FEBS Lett.* **135**, 257-260

66. Caldwell, C. R. (1993) Ultraviolet-induced photodegradation of cucumber (*Cucumis sativus L.*) microsomal and soluble protein tryptophanyl residues *in vitro*. *Plant Physiol.* **101**, 947-953

67. Yang, C.-Y., Gu, Z.-W., Yang, H.-X., Yang, M., Gotto, A. M., Jr., and Smith, C. V. (1997) Oxidative modifications of apoB-100 by exposure of low density lipoproteins to HOCl *in vitro*. *Free Radic. Biol. Med.* **23**, 82-89

68. Asher, S. A. (1993) UV resonance raman spectroscopy for analytical, physical, and biophysical chemistry. *Anal. Chem.* **65**, A59-A66

69. Bieker, L., and Schmidt, H. (1979) Raman spectra of *N*-formylkynurenine derivatives of lysozyme produced by ozone oxidation. *FEBS Lett.* **106**, 268--270

70. Puranik, P. G., and Ramiah, K. V. (1959) Infrared and raman spectroscopic studies of the association of formamide. *J. Mol. Spectrosc.* **3**, 486-495

71. Chalapathi, V. V., and Ramiah, K. V. (1968) Integrated absorption intensities of carbonyl band in amides and anilides *J. Mol. Spectrosc.* **26**, 444-453

72. Patzlaff, J. S., and Barry, B. A. (1996) Pigment quantitation and analysis by HPLC reverse phase chromatography: a characterization of antenna size in oxygen-evolving photosystem II preparations from cyanobacteria and plants. *Biochemistry* **35**, 7802-7811

73. Berlett, B. S., and Stadtman, E. R. (1997) Protein oxidation in aging, disease, and oxidative stress. *J. Biol. Chem.* **272**, 20313-20316

74. Gracanin, M., Hawkins, C. L., Pattison, D. I., and Davies, M. J. (2009) Singlet-oxygen-mediated amino acid and protein oxidation: formation of tryptophan peroxides and decomposition products. *Free Radic. Biol. Med.* **47**, 92-102

75. Asada, K. (1999) The water cycle in chloroplasts: scavenging of active oxygens and dissipation of excess photons. *Annu. Rev. Plant Physiol. Plant Mol. Biol.* **50**, 601-639

76. Krieger, A., Rutherford, A. W., Vass, I., and Hideg, E. (1998) Relationship between activity, D1 loss, and Mn binding in photoinhibition of photosystem II. *Biochemistry* **37**, 16262-16269

77. Nishiyama, Y., Allakhverdiev, S. I., and Murata, N. (2006) A new paradigm for the action of reactive oxygen species in the photoinhibition of photosystem II. *Biochim. Biophys. Acta* **1757**, 742-749

78. Hunzinger, C., Wozny, W., Schwall, G. P., Poznanović, S., Stegmann, W., Zengerling, H., Schoepf, R., Groebe, K., Cahill, M. A., Osiewacz, H. D., Jägemann, N., Bloch, M., Dencher, N. A., Krause, F., and Schrattenholz, A. (2006) Comparative profiling of the mammalian mitochondrial proteome: multiple aconitase-2 isoforms including *N*-formylkynurenine modifications as part of a protein biomarker signature for reactive oxidative species. *J. Proteome Res.* **5**, 625-633

79. Fedorova, M., Todorovsky, T., Kuleva, N., and Hoffmann, R. (2010) Quantitative evaluation of tryptophan oxidation in actin and troponin I from skeletal muscles using a rat model of acute oxidative stress. *Proteomics* **10**, 2692-2700

80. Finley, E. L., Dillon, J., Crouch, R. K., and Schey, K. L. (1998) Identification of tryptophan oxidation products in bovine alpha-crystallin. *Protein Sci.* **7**, 2391-2397

81. Ronsein, G. E., Oliveira, M. C. B., Miyamoto, S., Medeiros, M. H. G., and Di Mascio, P. (2008) Tryptophan oxidation by singlet molecular oxygen [O_2 ($^1\Delta_g$)]: mechanistic studies using ^{18}O-labeled hydroperoxides, mass spectrometry, and light emission measurements. *Chem. Res. Toxicol.* **21**, 1271-1283

82. Yang, C.-Y., Gu, Z.-W., Yang, M., Lin, S.-N., Siuzdak, G., and Smith, C. V. (1999) Identification of modified tryptophan residues in apolipoprotein B-100 derived from copper ion-oxidized low-density lipoprotein. *Biochemistry* **38**, 15903-15908

83. Eilstein, J., Giménez-Arnau, E., Duché, D., Rousset, F., and Lepoittevin, J.-P. (2006) Synthesis and reactivity toward nucleophilic amino acids of 2-5-[^{13}C]-dimethyl-*p*-benzoquinonediimine. *Chem. Res. Toxicol.* **19**, 1248-1256

84. Adir, N., Zer, H., Shochat, S., and Ohad, I. (2003) Photoinhibition- a historical perspective. *Photosynth. Res.* **76**, 343-370

85. Krieger-Liszkay, A., Fufezan, C., and Trebst, A. (2008) Singlet oxygen production in photosystem II and related protection mechanism. *Photosynth. Res.* **98**, 551-564

86. Nixon, P. J., Michoux, F., Yu, J., Boehm, M., and Komenda, J. (2010) Recent advances in understanding the assembly and repair of photosystem II. *Ann. Bot.* **106**, 1-16

87. Vass, I., Styring, S., Hundal, T., Koivuniemi, A., Aro, E.-M., and Andersson, B. (1992) Reversible and irreversible intermediates during photoinhibition of photosystem II: stable reduced Q_A species promote chlorophyll triplet formation. *Proc. Natl. Acad. Sci. U. S. A.* **89**, 1408-1412

88. Knox, J. P., and Dodge, A. D. (1985) Singlet oxygen in plants. *Phytochemistry* **24**, 889-896

89. Keren, N., Berg, A., vanKan, P. J. M., Levanon, H., and Ohad, I. (1997) Mechanism of photosystem II photoinactivation and D1 protein degradation at

low light: the role of back electron flow. *Proc. Natl. Acad. Sci. U. S. A.* **94**, 1579-1584

90. Hideg, E., Spetea, C., and Vass, I. (1994) Singlet oxygen and free radical production during acceptor-induced and donor-side photoinhibition: studies with spin-trapping EPR spectroscopy *Biochim. Biophys. Acta* **1186**, 143-152

91. Flors, C., Fryer, M. J., Waring, J., Reeder, B., Bechtold, U., Mullineaux, P. M., Nonell, S., Wilson, M. T., and Baker, N. R. (2006) Imaging the production of singlet oxygen *in vivo* using a new fluorescent sensor, Singlet Oxygen Sensor Green. *J. Exp. Bot.* **57**, 1725-1734

92. Telfer, A., Bishop, S. M., Phillips, D., and Barber, J. (1994) Isolated photosynthetic reaction center of photosystem II as a sensitizer for the formation of singlet oxygen: detection and quantum yield determination using a chemical trapping technique *J. Biol. Chem.* **269**, 13244-13253

93. Mishra, N. P., Francke, C., Vangorkom, H. J., and Ghanotakis, D. F. (1994) Destructive role of singlet oxygen during aerobic illumination of the photosystem II core complex *Biochim. Biophys. Acta* **1186**, 81-90

94. Aro, E. M., Virgin, I., and Andersson, B. (1993) Photoinhibition of photosystem II: inactivation, protein damage, and turnover. *Biochim. Biophys. Acta* **1143**, 113-134

95. Prasil, O., Adir, N., and Ohad, I. (1992) Dynamics of photosystem II: mechanism of photoinhibition and recovery processes. in *The Photosystems: Structure, Function and Molecular Biology* (Barber, J. ed.), Elsevier, Amsterdam. pp 295-348

96. Nishiyama, Y., Allakhverdiev, S. I., Yamamoto, H., Hayashi, H., and Murata, N. (2004) Singlet oxygen inhibits the repair of photosystem II by suppressing the translation elongation of the D1 protein in *Synechocystis* sp PCC 6803. *Biochemistry* **43**, 11321-11330

CHAPTER 3

LIGHT-INDUCED OXIDATIVE STRESS, *N*-FORMYLKYNURENINE, AND OXYGENIC PHOTOSYNTHESIS

by

Tina Michelle Dreaden Kasson[1], Sascha Rexroth[2], and Bridgette A. Barry[1]

[1]School of Chemistry and Biochemistry and the Petit Institute for Bioengineering and Bioscience, Georgia Institute of Technology, Atlanta, GA 30332

[2]Department of Biology, Ruhr-Universität, Bochum, Germany

This research is currently *In Press*.

Tina M. Dreaden Kasson, Sascha Rexroth, and Bridgette A. Barry. Light-induced oxidative stress, *N*-formylkynurenine, and oxygenic photosynthesis. *Plos ONE* 2012.

*****Tandem mass spectrometry experiments in Figure 3.5 were performed by Sascha Rexroth (Department of Biology, Ruhr-Universität, Bochum, Germany).

3.1 Abstract

Light stress in plants results in damage to the water oxidizing reaction center, photosystem II (PSII). Redox signaling, through oxidative modification of amino acid side chains, has been proposed to participate in this process, but the oxidative signals have not yet been identified. Previously, we described an oxidative modification, *N*-formylkynurenine (NFK), of W365 in the CP43 subunit. The yield of this modification increases under light stress conditions, in parallel with the decrease in oxygen evolving activity. In this work, we show that this modification, NFK365-CP43, is present in thylakoid membranes and may be formed by reactive oxygen species produced at the Mn_4CaO_5 cluster in the oxygen- evolving complex. NFK accumulation correlates with the extent of photoinhibition in PSII and thylakoid membranes. A modest increase in ionic strength inhibits NFK365-CP43 formation, and leads to accumulation of a new, light-induced NFK modification (NFK317) in the D1 polypeptide. Western analysis shows that D1 degradation and oligomerization occur under both sets of conditions. The NFK modifications in CP43 and D1 are found 17 and 14 Angstrom from the Mn_4CaO_5 cluster, respectively. Based on these results, we propose that NFK is an oxidative modification that signals for damage and repair in PSII. The data suggest a two pathway model for light stress responses. These pathways involve differential, specific, oxidative modification of the CP43 or D1 polypeptides.

3.2 Introduction

In plants, algae and cyanobacteria, Photosystem II (PSII) catalyzes the photo-oxidation of water to O_2 and protons (1). The electrons derived from water are transferred

sequentially to two quinone molecules, Q_A and Q_B, on the acceptor side of the reaction center (2). The cyanobacterial PSII structure was solved to 1.9 Å resolution (2-7). The membrane-spanning D1 and D2 proteins form the core of the reaction center. These proteins bind the catalytic oxygen evolving complex (OEC), which is a Mn_4CaO_5 cluster, chlorophyll (chl), pheophytin, and the plastoquinones, Q_A and Q_B, (2). The CP43 and CP47 proteins are also found in the core of PSII (reviewed in (8)). CP43 and CP47 span the membrane in the PSII complex, and these subunits contain flexible, hydrophilic loops that protrude into the lumen. Substitutions of amino acids in these loops have demonstrated their importance for complex assembly and protection from photoinhibition (8). Calcium and chloride cofactors are essential for optimal activity under native conditions (9).

Light stress causes protein damage and suboptimal photosynthetic rates in PSII (10,11). A decrease in steady state oxygen evolution, as well as accelerated D1 turnover, is the result. Recovery from photoinhibition involves PSII disassembly, proteolysis of damaged D1, and *de novo* synthesis of a new D1 protein. Re-insertion of a new D1 subunit into the partially disassembled PSII complex and reassembly completes the repair cycle (12). The signaling pathways for complex disassembly and D1 degradation remain unknown. However, post-translational oxidations of amino acids have been proposed to play signaling roles in this process (12).

Post-translational oxidation of Trp to form *N*-formylkynurenine (NFK) (Figure 3.1A) plays a role in oxidative stress responses in some proteins (see for example (13). NFK has been identified in mitochondrial ATP synthase (14), spinach LHCII (15), milk

proteins (16), skeletal muscle proteins (17), apolipoprotein B-100 (13), and *Methylococcus capsulatus*-secreted MopE protein (18).

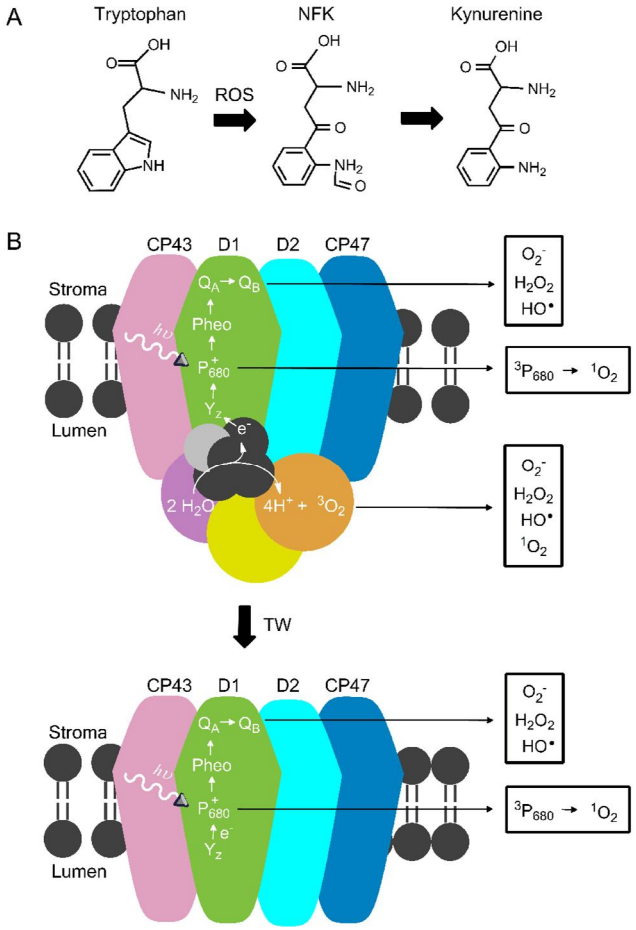

Figure 3.1. Structures of tryptophan, NFK, kynurenine, and PSII. (A) shows the chemical structures of NFK (+32 *m/z*) and kynurenine (+4 *m/z*). (B) shows models of PSII (top) and TW (bottom) PSII. Tris- washing removes the extrinsic subunits and OEC, or Mn_4CaO_5 cluster. The core subunits (CP43, D1, D2 and CP47) and electron transfer cofactors (tyrosine z (Yz), P_{680}, pheophytin (Pheo), plastoquinone A (Q_A), and plastoquinone B (Q_B)) are labeled. The water- splitting reaction at the OEC is shown. The ROS species generated in PSII and TW PSII during photoinhibition are indicated. The subunit colors are the same as in Figure 3.8. CP43 (pink); D1 (green); D2 (light blue); CP47 (dark blue); extrinsic subunits (violet, yellow, and orange).

Recently, we described a light-induced modification, NFK (Figure 3.1A), resulting from the oxidative, post-translational modification (PTM) of W365 in the CP43

subunit (19). A ~two fold increase in the yield of NFK365-CP43 was observed following high light illumination (19). A concomitant two fold decrease in oxygen evolution was detected under the same conditions (19). This result suggests a role for NFK and oxidative stress in plant photoinhibition.

NFK results from the reaction of the Trp side chain with several types of ROS, including singlet oxygen ($^1O_2$) (15,20), ozone (O_3) (21), and hydroxyl radicals ($HO^\bullet$) (22,23). NFK can also result from a metal-catalyzed radical mechanism, followed by reaction with O_2 (13). ROS is produced in PSII, either by recombination reactions producing triplet chlorophyll (^{3}chl) or by reactions at the Mn_4CaO_5 cluster (Figure 3.1B). These are referred to as acceptor side (^{3}chl) and donor side (Mn_4CaO_5) reactions.

In the acceptor side ROS mechanism, double reduction of Q_A results in charge recombination and formation of the excited state ^{3}chl (24). Energy transfer from ^{3}chl to ground state $^3O_2$ results in $^1O_2$ (24). O_2 reduction to $O_2^{\bullet-}$ may also occur under light stress conditions (25). Dismutation to H_2O_2, followed by a single electron reduction, may produce $HO^\bullet$ (25). In the donor side ROS mechanism (Figure 3.1B), release of the extrinsic proteins and OEC during light stress has been reported to stimulate H_2O_2 production (26). The one electron oxidation and reduction of H_2O_2 was proposed to produce $O_2^{\bullet-}$ and $HO^\bullet$, respectively (25).

In this work, we identify a specific, new oxidative modification of tryptophan in the D1 subunit, which is induced by light-stress. We provide evidence that *N*-formylkynurenine modifications in PSII are generated by ROS, which may be derived from the Mn_4CaO_5 cluster. To explain our results, we propose a two-pathway model, in

which NFK functions as a signal for D1 protein turnover, a key step in repair under high light stress.

3.3 Materials and methods

3.3.1 Thylakoid, PSII, and TW PSII membrane preparations

Spinach PSII membranes were isolated as described (27) with modifications (28). Thylakoid membrane (TM) isolation was conducted as described in (27), with a single centrifugation and wash after the initial grinding step. The TM wash buffer was 20 mM 2-(*N*-morpholino)-ethanesulfonic acid (MES)-NaOH (pH 6.0), 150 mM NaCl, 4 mM $MgCl_2 \bullet H_2O$. The final resuspension was in 50 mM MES-NaOH (pH 6.0), 400 mM sucrose, 15 mM NaCl (SMN buffer). Chlorophyll (29) and oxygen assays were conducted as described (30). Oxygen evolution experiments were conducted with red-filtered light from a Dolan-Jenner (Boxborough, MA) Fiber-Lite illuminator at 25 ºC in SMN buffer with 1 mM $K_3Fe(CN)_6$ and recrystallized 1 mM 2,6-dichlorobenzoquinone (DCBQ). Activity rates of PSII membranes and TM were ≥600 and ≥130 μmol O_2 mg chl^{-1} h^{-1}, respectively.

The 18- and 24-kDa extrinsic subunits were removed from PSII membranes with a 2 M NaCl wash (31). PsbO and the Mn_4CaO_5 cluster were removed with a 800 mM tris(hydroxymethyl)aminomethane (Tris)-NaOH, pH 8.0 wash performed for 45 minutes at room temperature in the light (32). Tris-washed (TW) PSII membranes were washed three times with a buffer of 400 mM sucrose, 50 mM 4-(2-hydroxyethyl)-1-

piperazineethanesulfonic acid (HEPES)-NaOH, (pH 7.5) (SH buffer). TW PSII samples were resuspended in the same buffer at a chlorophyll concentration of 2- 4 mg/mL chlorophyll.

3.3.2 Photoinhibition

Photoinhibition experiments were performed on spinach TM, PSII membranes, and TW PSII membranes (19). The final resuspension buffers were used during illumination (see 3.3.1 above). All samples were stirred and kept at 25 ºC with a water bath and dewar, during white light illumination with a Dolan-Jenner (Boxborough, MA) Fiber-Lite illuminator. Illumination of PSII was conducted at a chlorophyll concentration of 1.0 mg/ mL. TM were illuminated at 1.0 or 0.1 mg/ mL chlorophyll. The light intensity used was ~7,000 μmol photons m^{-2} s^{-1} as measured with a Li-Cor (Lincoln, NE) Light Meter (model LI-189 with a ~8 cm diameter sensor). The illumination was performed for two hours. Controls were kept in the dark at room temperature (~25 ºC). Samples were either un-treated or treated with 2 mM NaCl (Fisher Scientific, Fairlawn, NJ), 0.15 mM $ZnCl_2$ (BDH VWR, Radnor, PA), 1 mM disodium-ethylenediaminetetraacetic acid (Na_2EDTA) (JT Baker, Austin, TX), or 2 mM tetra-methylammonium chloride (TMA) (Sigma-Aldrich, St. Louis, MO) by addition just prior to the dark or light incubation. The ionic strength of the SMN buffer alone, prior to the addition of salts, was 34.9 mM. The ionic strength increased to 36.9 mM (2 mM NaCl and 2 mM TMA), 35.4 mM (0.15 mM $ZnCl_2$), and 36.4 mM (1 mM Na_2EDTA) with the additional salts. Oxygen evolution was assayed every 30 minutes.

3.3.3 UV-visible spectrophotometry

Optical spectra of model compounds tryptophan, NFK, and kynurenine were recorded at room temperature from 200-750 nm on a Hitachi (U3000) spectrophotometer (19). The model compounds, 40 μM *L*-tryptophan (Sigma-Aldrich, St. Louis, MO), *L*-kynurenine (Sigma-Aldrich), and NFK (19,33) were suspended in H_2O. The NFK-containing peptide optical spectra were derived from the chromatogram through the use of a Beckman (Brea, CA) System Gold® HPLC, equipped with a 125 solvent module, a 168 photodiode array detector (1 cm path length, 2 nm scan interval), and 32 Karat Software, version 7.0.

3.3.4 Tryptic peptide digestion and high pressure liquid chromatography (HPLC) assay

In-situ trypsin (Life Technologies, Carlsbad, CA) digestion of TM, PSII, and TW PSII was conducted as described (19). HPLC separation, isolation of NFK-containing peptides, and quantitative NFK assay were carried out as previously described (19). Retention times for Fractions A-D were 25, 26, 28, and 34 minutes and were reproducible to $\pm$ 0.6 min (Tables 3.2 and 3.3). The amount of the NFK containing peptide was quantitated by integration of the 350 nm peak by the procedure previously described (19). This area was normalized to the total 220 nm absorption. This normalization corrects for any differences in the yield of tryptic products (Tables 3.2 and 3.3).

3.3.5 Sodium dodecyl sulfate polyacrylamide gel electrophoresis (SDS-PAGE) and D1 protein Western blot

SDS-PAGE of PSII membranes was performed as described (34-36). 24 μg of chl were loaded per lane. Following SDS-PAGE, gels were either stained with 0.05% Brilliant Blue R (Coomassie) (Sigma-Aldrich, St. Louis, MO) or used for D1 Western blot analysis. For the Western blot, an unstained gel was blotted onto a 0.45 μm polyvinylidene fluoride (PVDF) membrane by semi-dry transfer as described (37). A PSII D1 (PsbA) C-terminal antibody (Agrisera, Vannas, Sweden) (1: 10,000 dilution) was used as the primary antibody probe. A secondary anti-chicken- alkaline phosphatase conjugate (Sigma-Aldrich, St. Louis, MO) was the secondary antibody probe (1: 15,000 dilution). A 5-bromo-4-chloro-3-indolyl phosphate/ nitro blue tetrazolium (BCIP/ NBT) liquid substrate system (Sigma-Aldrich, St. Louis, MO) was used for colorimetric detection.

3.3.6 Tandem mass spectrometry (MS/ MS) peptide analysis

PSII tryptic peptides were analyzed as described (19). Representative MS/MS data are shown in 3.5.

3.4 Results

3.4.1 Photoinhibition in PSII and thylakoid membranes (TMs)

A light intensity of 7,000 μmol photons m^{-2} s^{-1} was employed in these studies. This value is typical of conditions used in previous studies of plant light stress (4,000-7,000 μmol photons m^{-2} s^{-1}) (38-40). To evaluate the degree of photoinhibition under these conditions, the steady state rate of oxygen evolution was monitored as a function of illumination time. High light illumination of PSII membranes was conducted at a chlorophyll concentration of 1 mg/ mL, pH 6.0, and 25 °. Compared to the dark control (Figure 3.2A, blue), illumination induced a 3.4 $\pm$ 0.4 fold decrease in oxygen evolution rate in PSII membranes (Figure 3.2A, blue and green). This agrees with our previous report of a 2.4 $\pm$ 0.5 fold decrease under these conditions (19). As expected, a lower light intensity of 500 μmol photons m^{-2} s^{-1} did not significantly decrease oxygen evolution rates (Figure 3.2A, blue and red).

At the same light intensity, thylakoid membrane (TM) samples were not significantly inhibited at a chlorophyll concentration of 1 mg/ mL (Figure 3.2B, black and blue). However, illumination at 0.1 mg/ mL chlorophyll induced a 5.4 ± 0.5 decrease in the steady state oxygen evolution rate (Figure 3.2B, red and green).

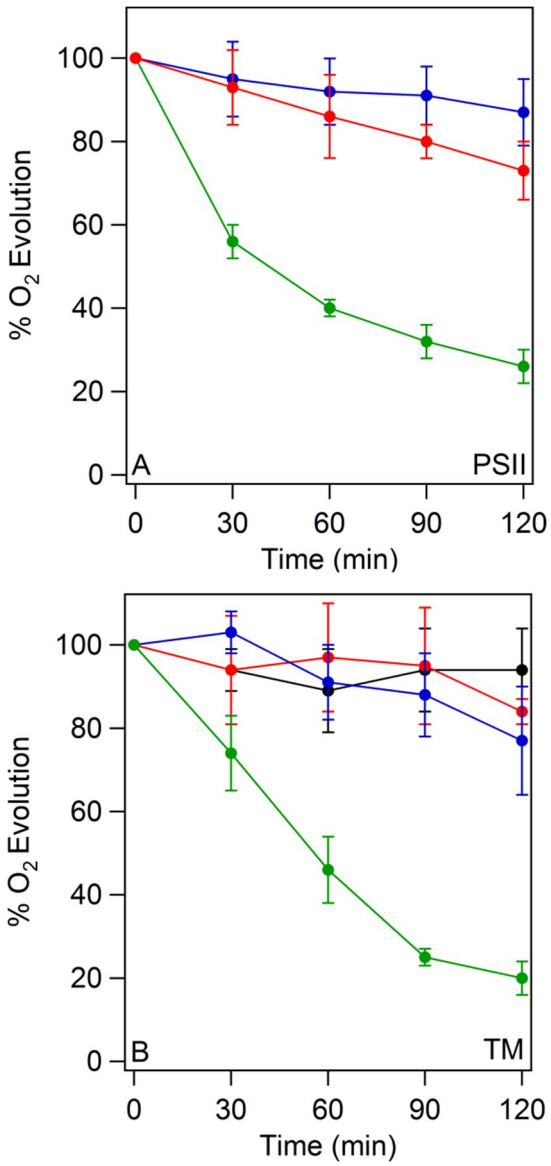

Figure 3.2. Steady state rates of oxygen evolution of PSII membranes (A) and TM (B) during high light illumination and in the dark. In (A), PSII membranes were kept in the dark at 25 °C for two hours (blue). PSII membranes were exposed to a white light intensity of 500 (red) and 7,000 (green) µmol photons m^{-2} s^{-1} for two hours at 25 °C. In (B), TM were kept in the dark (black and red) or exposed to a white light intensity of 7,000 µmol photons m^{-2} s^{-1} at chlorophyll concentrations of 1.0 (blue) or 0.1 mg/ ml (green). Oxygen evolution was assayed every 30 minutes and normalized to time zero. The data shown are an average of three to six experiments. The error bars are plus and minus one standard deviation. See 3.3.2 for experimental conditions.

3.4.2 Purification and MS/MS of NFK- containing peptides in CP43

NFK has a unique absorption at 318 nm (Figure 3.3B, dotted line), when compared to tryptophan (Figure 3.3B, solid line), kynurenine (Figure 3.3B, dashed line), or other modifications of the indole ring (19). This unique absorption spectrum allows the identification and purification of NFK-containing tryptic peptides by HPLC (Figure 3.4). The HPLC chromatogram was monitored at 350 nm during purification of NFK-modified peptides to avoid overlap with the strongly absorbing 280 nm peak. In oxygen-evolving PSII, two different NFK-containing peptides, peptides A and C, were identified (Figure 3.4A and B). Typical absorption spectra, derived from the HPLC chromatograms, are shown in Figure 3.3A.

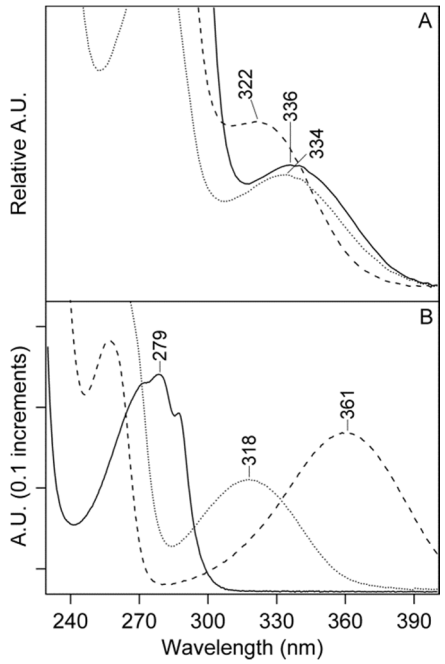

Figure 3.3. Optical absorption of NFK-containing PSII peptides (A) and the model compounds (B), tryptophan, NFK, and kynurenine. (A) shows absorption spectra of NFK-containing peptide fractions A-C. See Table 3.2 for average retention times from 350 nm chromatograms. Fraction A is displayed as a solid line, fraction B as a dashed line, and fraction C as a dotted line. In (B), absorption spectra of 40 μM tryptophan (solid line), 40 μM NFK (dotted line), and 40 μM kynurenine (dashed line) are shown in water. Absorption spectra in A were derived from the HPLC chromatogram and are on an arbitrary y-scale. The spectra in B were measured on a Hitachi spectrophotometer.

Table 3.1. MS/ MS analysis of NFK modifications in fractions A- C

Fraction	PSII subunit	Sequence	Modification	MH^+ (Da)	XCorr
A	CP43	^{363}AP(**W***)LEPLR^{370}	NFK (+32 *m/z*)	1013.5407	2.80
B	D1	^{313}VINT(**W***)ADIINR^{323}	NFK (+32 *m/z*)	1346.7029	3.46
C	CP43	^{363}AP(**W***)LEPLRGPNGLDLSR^{379}	NFK (+32 *m/z*)	1923.0086	2.01

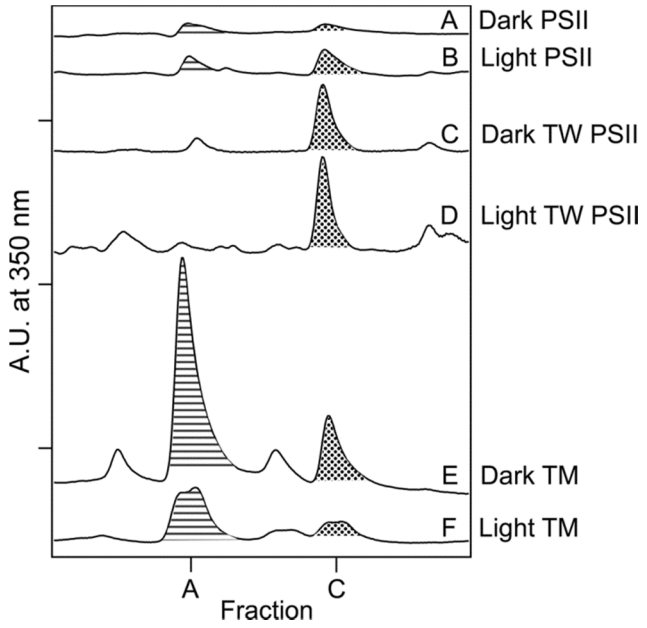

Figure 3.4. Representative 350 nm HPLC chromatograms of tryptic peptides derived from oxygen-evolving PSII (A-B), OEC-removed (TW) PSII (C-D), and TM (E-F). In (A), (C), and (E), samples were incubated in the dark at room temperature for two hours (control). In (B), (D), and (F), samples were illuminated with ~7,000 µmol photons m^{-2} s^{-1} of white light for two hours at 25 ºC. Fraction A is filled with horizontal stripes, and fraction C is filled with dots. The chromatograms are displaced on the y-axis for presentation purposes. The tick increments are 0.085 A.U. See Table 3.2, for average retention times and summary of light-induced changes. Fraction C corresponds to fraction 1 in ref (19)**.**

Using MS/MS (Table 3.1 and Figure 3.5), fraction C (retention time ~28 min.) was identified as NFK-365 in CP43 (^{363}AP(W*)LEPLRGPNGLDLSR^{379}), confirming our earlier result (19). Fraction A contained the same NFK-W365 CP43 modification,

but the peptide was shorter, ^{363}AP(W*)LEPLR^{370} (Table 3.1). Only one NFK peptide was detected in Fractions A and C (Table 3.4). Representative MS/MS data are shown Figure 3.5.

Table 3.2. Average light-induced changes in NFK yield (fold change) and average retention times (ret. time) of HPLC fractions A-D[#]

Fraction	TM		PSII		TW PSII	
	fold change	ret. time	fold change	ret. time	fold change	ret. time
A	0.8 ± 0.6	25.6	0.9 ± 0.2	25.7	NODL	NODL
B	NODL	NODL	NODL	NODL	NODL	NODL
C	0.7 ± 0.2	27.3	2.1 ± 0.5	27.4	1.2 ± 0.3	27.4
D	NODL	NODL	2.4 ± 1.3	34.3	1.4 ± 0.2	34.3

[#]NODL, not observed in dark or light

Table 3.3. Average light-induced changes in NFK yield (fold change) and average retention times (ret. time) of HPLC fractions A-D[#] at increased ionic strength

Fraction	PSII + Na_2EDTA		PSII + $ZnCl_2$		PSII + NaCl		PSII + TMA	
	fold change	ret. time	ret. time	ret. time	fold change	ret. time	fold change	ret. time
A	1.0 ± 0.2	25.3	1.0 ± 0.1	25.3	1.1 ± 0.2	25.7	0.9 ± 0.1	25.3
B	NOD	26.1	NOD	26.1	NOD	26.1	NOD	26.3
C	0.5 ± 0.2	27.6	1.1 ± 0.2	27.6	0.6 ± 0.2	27.6	0.8 ± 0.2	27.2
D	0.6 ± 0.3	34.4	1.1 ± 0.3	34.4	0.8 ± 0.5	34.3	0.9 ± 0.3	33.8

[#]NOD, not observed in dark

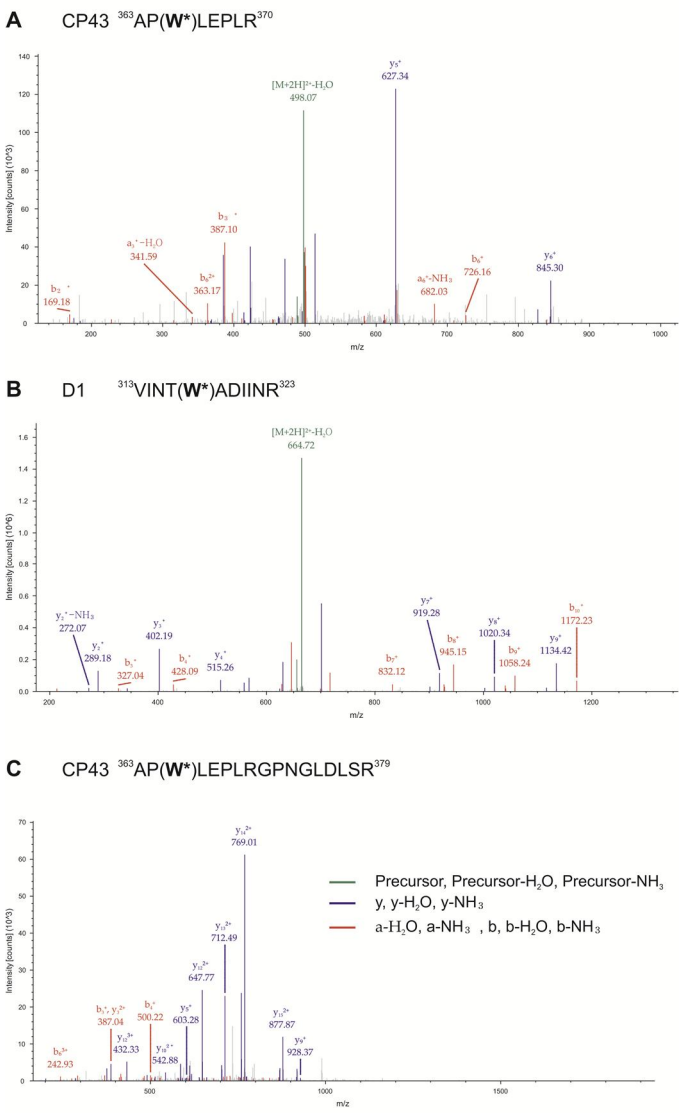

Figure 3.5. Representative MS/MS spectra of NFK modifications in CP43 (A and C) and D1 (B) proteins. The peaks in blue represent the *b*-fragments. The peaks in red represent the *y*-fragments. The NFK modified W is indicated in the corresponding sequences. This residue carries the +32 *m*/*z* masss shift, which was unambiguously assigned to Trp-365 in CP43 (A and C) and Trp-317 in D1 (B). *****Tandem mass spectrometry experiments in were performed by Sascha Rexroth (Department of Biology, Ruhr-Universität, Bochum, Germany).

Table 3.4. Oxidative tryptophan modifications identified by LC-MS-MS in HPLC fractions A-D

Frac.	PSII subunit	Sequence	W mod.	M mod.	MH^+ (Da)	X-Corr
A	CP43	^{363}AP**W**LEPLR^{370}	NFK (+32 *m/z*)		1013.5407	2.80
			Kyn (+4 *m/z*)		985.5459	2.64
			OH-Trp (+16 *m/z*)		997.5453	2.64
	CP43	^{363}AP**W**LEPLRGPNGLDLSR^{379}	Kyn (+4 *m/z*)		1895.0107	2.50
			OH-Trp (+16 *m/z*)		1907.0107	2.83
	CP43	^{358}F**W**DLR^{362}	OH-Trp (+16 *m/z*)		752.3726	1.81
B	D1	^{313}VINT**W**ADIINR^{323}	NFK (+32 *m/z*)		1346.7029	3.46
			Kyn (+4 *m/z*)		1318.7095	4.10
			OH- Trp (+16 *m/z*)		1330.7095	4.01
C	CP43	^{363}AP**W**LEPLRGPNGLDLSR^{379}	NFK (+32 *m/z*)		1923.0086	2.01
			Kyn (+4 *m/z*)		1895.0108	1.94
			OH- Trp (16 *m/z*)		1907.0115	3.18
	CP43	^{383}DIQPWQER^{390}	OH-Trp (+16 *m/z*)		1087.5131	1.54
	CP43	^{358}F**W**DLR^{362}	OH-Trp (+16 *m/z*)		752.3715	1.75
D	D2	^{8}FTKDEKDLFDS**M**DD**W**LR^{24}	NFK (+32 *m/z*)		2192.9786	5.30
			Kyn (+4 *m/z*)		2164.9852	4.24
			OH-Trp (16 *m/z*)		2176.9814	5.74
			OH- Kyn (+20 *m/z*)		2180.9875	4.50
				Met-sulfoxide (+16 *m/z*)	2176.9814	5.93

Table 3.4. Continued

			NFK (+32 *m/z*)	Met-sulfoxide (+16 *m/z*)	2208.9739	5.53
			Kyn (+4 *m/z*)	Met-sulfoxide (+16 *m/z*)	2180.9767	5.61
			OH-Trp (+16 *m/z*)	Met-sulfoxide (+16 *m/z*)	2192.9789	5.38
	D2	^{14}DLFDS**M**DD**W**LR^{24}	NFK (+32 *m/z*)		1444.6027	2.18
			OH-Trp (16 *m/z*)		1428.6091	3.07
			OH- Kyn (+20 *m/z*)		1432.6038	2.39
				Met-sulfoxide (+16 *m/z*)	1428.6100	3.21
			NFK (+32 *m/z*)	Met-sulfoxide (+16 *m/z*)	1460.6058	2.49
			Kyn (+4 *m/z*)	Met-sulfoxide (+16 *m/z*)	1432.6038	3.03
			OH-Trp (+16 *m/z*)	Met-sulfoxide (+16 *m/z*)	1444.6027	2.45

For the identification of peptides filter criteria were set to warrant a false discovery rate of less than 1% on the peptide level. In each of the three independent LC-MS/MS runs of the four fractions, more than 20000 MS/MS spectra were recorded. For fraction A-C. between 3500-5000 spectra were assigned to peptides from 50-80 proteins from *S. oleracea*. In fraction D only, 1200 spectra could be assigned to peptides of about 50 proteins.

3.4.3 CP43 NFK in photoinhibition

To calculate the yield of NFK, the 350 nm peak was integrated, and the value was normalized to the total 220 nm absorption. This corrects for the yield of tryptic peptides

(19). These data are presented in the bar graph shown in Figure 3.6. As shown, formation of NFK-W365 in fraction C is light induced in oxygen- evolving PSII. The yield increases by 2.1 ± 0.6 (Figure 3.6). This increase parallels the 3.4 ± 0.4 fold decrease observed in the steady state oxygen evolution rate (Figure 3.2A, blue and green). However, fraction A (Figure 3.4A and B) does not show a significant light-induced increase (0.9 ± 0.2, Figure 3.6 and Table 3.2).

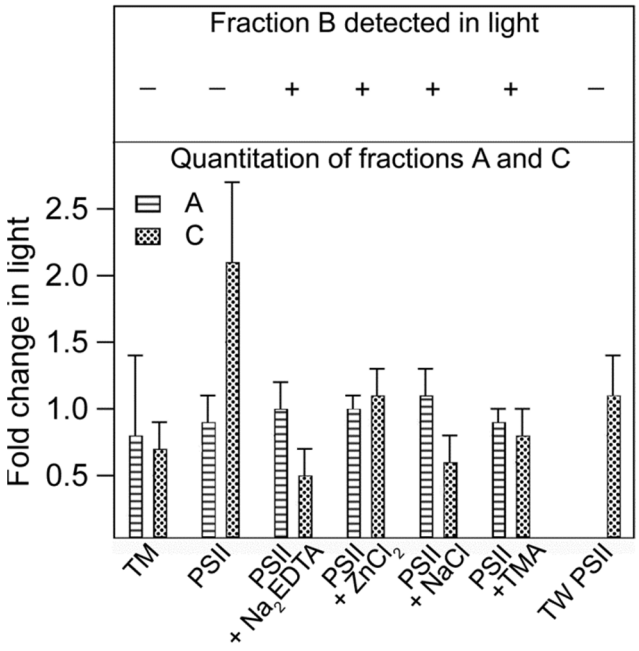

Figure 3.6. Fraction B detection (top) and yield change in fractions A and C (bottom) following high light illumination. The yields were calculated from the average of three-six different experiments. Peaks in the 350 nm chromatogram were integrated, and the area was divided by the area of the 220 nm chromatogram to correct for changes in yield of tryptic peptides. The error bars are one standard deviation. See Tables 3.2 and 3.3 for summary of fold changes and average retention times.

In TW PSII, the Mn_4CaO_5 cluster and extrinsic subunits are removed (32). Under these conditions (Figure 3.1B), without active oxygen evolution, no significant

light induced increase is observed in fraction C (Figures 3.4C and D, Figure 3.6). Fraction A is not observed in TW PSII.

3.4.4 NFK365-CP43 is observed in TM, but does not show a light-induced increase

In TM samples, fractions A and C are observed in the dark and the light (Figures 3.4E and F). Field grown spinach leaves, exposed to unregulated growth conditions, were used for the TM isolation. Thus, NFK modifications may be present in the dark, due to the previous handling of the market spinach. The observation of NFK in TM demonstrates that the modification is not induced by detergent treatment. There is no significant, light- induced increase in these fractions (Figure 3.6 and Table 3.2). This parallels the results of the oxygen evolution assays conducted under the same conditions (1 mg/ mL chlorophyll) in Figure 3.2B (black and red), which showed that the TM preparation was resistant to photoinhibition.

3.4.5 Photoinhibition at increased ionic strength results in a new NFK-containing peptide, peptide B

The photoinhibition experiment was conducted on PSII membranes in SMN buffer to which 2 mM NaCl was added. Compared to PSII in SMN buffer (Figures 3.7A and B), a new peptide, peptide B, was observed in the light (Figures 3.7C and D). Fraction B was not observed in the dark (Figure 3.7C). Under these conditions there was no significant increase in the yield of fractions A or C (Figure 3.6). MS/MS identified peptide B as ^{313}VINT(W*)ADIINR^{323} in D1 (Tables 3.1 and 3.4, Figure 3.5). Only one NFK peptide was detected in this fraction (Table 3.4).

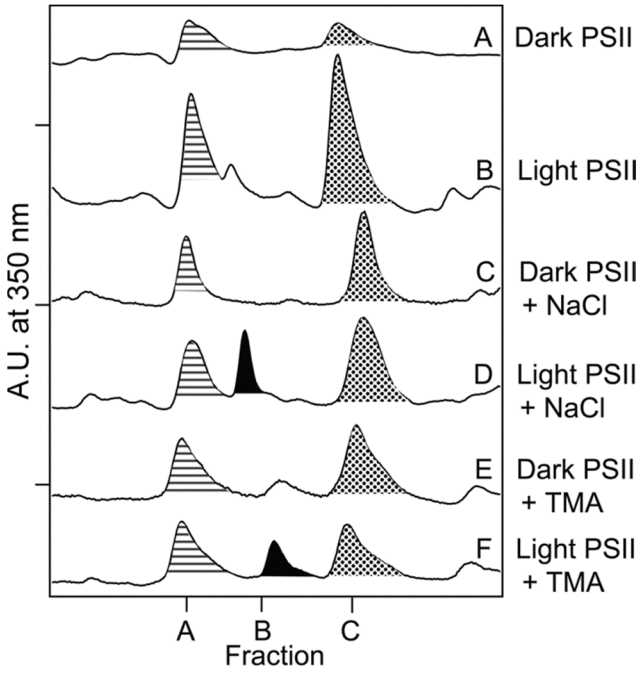

Figure 3.7. Representative 350 nm HPLC chromatograms of oxygen-evolving PSII with and without 2 mM NaCl or TMA. In (A), (C), and (E), samples were incubated in the dark at room temperature for two hours (controls). In (B), (D), and (F), samples were illuminated with ~7,000 μmol photons m^{-2} s^{-1} of white light for two hours at 25 ºC. In (C) and (D), 2 mM NaCl was added just prior to the dark or light incubation. In (E) and (F), 2 mM TMA was added just prior to the dark or light incubation. Fraction A is filled with horizontal stripes, fraction B has solid fill, and fraction C is filled with dots. The chromatograms are displaced on the y-axis for presentation purposes. The tick increments are 0.020 A.U. See Table 3.3 for average retention times and summary of light-induced changes. Fraction C corresponds to fraction 1 in ref (19).

To test if the observation of peptide B depended on the identity of the cation or anion, the experiment was conducted in the presence of $ZnCl_2$ (0.15 mM) and Na_2EDTA (1 mM). Peptide B was observed under both sets of conditions (Figure 3.6). This result is not consistent with a role for a specific mono- or divalent ion.

To rule out the possibility of a non-specific cation-binding site as inducing the fraction B modification, the effect of 2 mM tetra-methyl ammonium chloride (TMA) was assessed. TMA has a nearly three-fold larger ionic radius (2.9 Å) (41) when compared to

Na^+ (1.0 Å) (41) or Zn^{2+} (0.74 Å) (42). TMA could not replace Ca^{2+} (ionic radius = 0.99 Å) (43) in PSII (44) or β-1,4-glucanase (45). In our experiments, we found that 2 mM TMA also induced fraction B in the light (Figure 3.7).

We conclude that the small ionic strength increase underlies the observation of fraction B. The ionic strength of the SMN buffer, prior to the addition of salts, is calculated to be 34.9 mM. The ionic strength increased to 36.9 mM (2 mM NaCl or TMA), 35.4 mM (0.15 mM $ZnCl_2$), and 36.4 mM (1 mM Na_2EDTA) when peptide B was observed in the light.

Approximately 7% of TW PSII reaction centers were reported to contain CP43 NFK-365 (19). Assuming the same extinction coefficients (3750 M^{-1} cm^{-1} at 321 nm (46), the yield of D1 NFK-317 (fraction B) can be estimated. Comparison of HPLC peak intensities indicates that approximately 1% of the PSII centers contain D1 NFK-317 after photoinhibition.

3.4.6 Photoinhibition of PSII membranes is associated with D1 oligomerization and proteolysis

Figure 3.8 shows SDS-PAGE and Western analysis, comparing the reaction of an anti-D1 antibody with PSII membranes. D1 oligomers and proteolytic fragments were observed after illumination. Illumination in the presence of increased NaCl, $ZnCl_2$, and Na_2EDTA gave the same result (Figure 3.8).

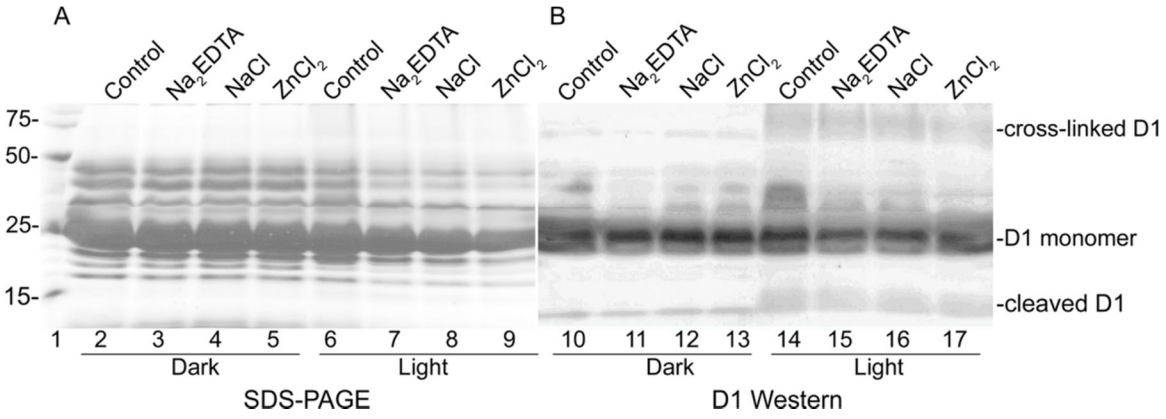

Figure 3.8. SDS-PAGE (A) and Western blot (B) using an antibody specific for the C-terminus of the D1 protein (Agrisera) (B). Control PSII membranes were maintained in the dark (lanes 2-5; lanes 10-13) or exposed to high light (~7,000 µmol photon m^{-2} s^{-1}) for two hours at 25 ºC (lanes 6-9; lanes 14-17). Samples were either untreated (lanes 2, 6, 10, 14) or treated with 1 mM Na_2EDTA (lanes 3, 7, 11 and 15), 2 mM NaCl (lanes 4, 8, 12, and 16), or 0.15 mM $ZnCl_2$ (lanes 5, 9, 13, and 17). Lane 1 displays the molecular weight markers. In both dark and light experiments, 24 µg chl was loaded per lane.

3.4.7 An additional light-induced NFK modification is observed in PSII

An additional NFK peptide was detected with a 34 min retention time (Tables 3.2 and 3.3). This fraction (D) increased in intensity in the light. More than one NFK peptide was detected in this fraction, with one identified as the D2 polypeptide ^{8}FTKDEKDLFDSMDD(W*)LR^{24} and the other identified as the D2 polypeptide ^{14}DLFDSMDD(W*)LR^{24} (Table 3.4). In our previous work, which employed HPLC and affinity purification, an NFK modification of a light-harvesting subunit was detected with a similar retention time. Due to the complexity of this fraction, interpretation of the light induced increase in fraction (D) awaits further experimentation.

3.5 Discussion

3.5.1 Summary

In this work, three NFK containing peptides, originating from the donor side of PSII, are identified. Fraction A, corresponds to ^{363}AP(W*)LEPLR^{370} in CP43 and is observed in oxygen- evolving PSII and TM, but not in TW PSII. Fraction A showed no detectable light-induced increase in any sample that we examined. Fraction C, corresponds to ^{363}AP(W*)LEPLRGPNGLDLSR^{379} in CP43, and is observed in oxygen evolving PSII, TW PSII, and TM. Fraction C showed a light induced increase in only one sample, oxygen- evolving PSII. Fraction B corresponds to ^{313}VINT(W*)ADIINR^{323} in D1. It was observed only in oxygen- evolving PSII, after illumination and under conditions of higher ionic strength.

3.5.2 Location of the NFK modifications

Figure 3.9 shows the position of the NFK modifications in the PSII structure from *T. vulcanus* (2). NFK317-D1 is located ~24 Å away from NFK365-CP43. NFK 365-CP43 is 17 Å from the Mn_4CaO_5 cluster; NFK 317-D1 is 14 Å from the cluster. Figure 3.9 also shows the position of NFK365-CP43 and NFK317-D1 relative to P_{680} and YZ. YZ is an electron transfer intermediate during the water oxidizing reaction (Figure 3.1B) (47). YZ is oxidized by the primary chlorophyll donor, P_{680}, and in its radical form, YZ is a strong oxidant (48). However, NFK365-CP43 is 19 Å from YZ and 30 Å from P_{680}. NFK317-D1 is 27 Å from YZ and 19 Å from P_{680}. Thus, a YZ or P_{680} radical-based mechanism for the formation of the NFK modifications seems unlikely.

Sequence conservation across photosynthetic organisms supports an important evolutionary role for both NFK- modified tryptophans. Although these core subunits are consistent in plants and cyanobacteria, some distinct structural differences remain. These differences mainly lie in the extrinsic (49) and light harvesting antennae (50) polypeptides. Thus, the location and role of NFK in cyanobacteria remains to be determined.

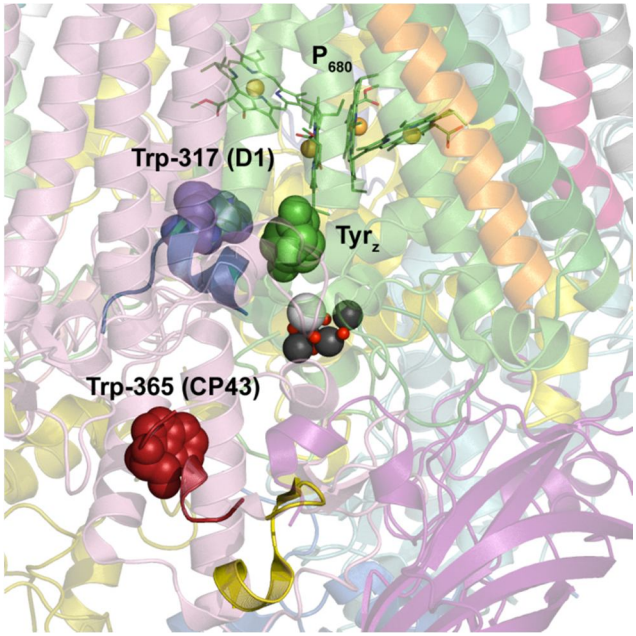

Figure 3.9. Predicted locations of NFK modifications, NFK365-CP43 and NFK317-D1, in the *T. vulcanus* PSII structure (2). The OEC is shown in black, grey, and red. P_{680} and YZ (green spacefill) are shown above the OEC. The CP43 and D1 backbones are displayed in pink and green, respectively. The side chain of Trp-365 in CP43 is in red spacefill. The side chain of Trp-317 in D1 is in blue spacefill. MS/MS detected tryptic peptides corresponding to fraction A (red and yellow combined), B (blue), and C (red) are highlighted. The image was rendered with the Pymol Molecular Grapics System (www.pymol.org).

3.5.3 ROS and specificity of NFK modifications in PSII and other proteins

In our experiments, we attribute the formation of NFK to the reaction of the Trp side chain with ROS (51). Studies in mitochondrial proteins have concluded that the NFK modification is a ROS-targeted mechanism (14,52,53). In mitochondrial ATP synthase, the NFK modification was channeled to a single Trp residue (Trp-503) (14). In the mitochondrial aconitase-2 protein, site-specific oxidation of Trp-373 was also observed (52). The specificity of the post-translational NFK modification in PSII and other proteins suggests a selective physiological role for the modification.

We demonstrate here that removal of the Mn_4CaO_5 cluster and extrinsic subunits prevents light-induced accumulation of NFK in the CP43 subunit. Previously, EPR spin trapping experiments have suggested that photoinhibited oxygen evolving PSII produces both $^1O_2$ and $HO^{\bullet}$ (54). However, only $HO^{\bullet}$ was detected in Mn-depleted PSII (54). Coupled with our data, this previous result is supportive of the conclusion that $^1O_2$ (15), and not $HO^{\bullet}$ (22), reacts with Trp to form NFK. Our results suggest a Mn_4CaO_5 origin for the reactive oxygen species, which oxidizes the Trp side chain. However, we cannot rule out the possibility that extrinsic subunit removal or acceptor side alterations are contributing factors.

3.5.4 NFK in D1 turnover and photoinhibition

Photoinhibition is known to induce D1 protein damage and a high rate of D1 turnover (10,12,55). Previous studies have identified intermolecular cross-links of D1 with D2, cytochrome b_{559}, and CP43 (56,57). In intact leaves and chloroplasts, D1 damage and turnover also occurred by D1 fragmentation and cross-linking (56).These

cross-links were proposed to participate in pathways for complete degradation of damaged D1 *in vivo* (56,57). NFK can bind covalently to primary amine- containing side chains (19), such as arginine and lysine, and may participate in this proteolysis pathway. The Western blot analysis of PSII membranes, presented here, confirmed that D1 cleavage and oligomerization occurred when NFK accumulated either in CP43 or in D1. The 3.4 ± 0.4 decrease in oxygen evolution rate of PSII membranes under the same conditions is further support for a correlation of photoinhibitory effects with NFK formation.

Reversible, light induced structural changes in the degree of spinach TM stacking (grana) have been observed by electron microscopy (58). These dynamic alterations in structural organization may be involved in protection from light stress (59) and would not occur in isolated PSII membrane fractions. In future work, we will explore the impact of these topological changes. In these experiments, we compared TM with PSII for two reasons. First, we wished to examine the possibility that the NFK modification is induced by detergent treatment. Observation of the NFK modification in TM in the dark eliminates this possibility. The residual level of oxidative modification in the dark may be due to the use of market, field grown spinach, which is transported and harvested under uncontrolled conditions. Second, TM samples do not photoinhibit at the high chl concentrations necessary for the HPLC assay. Therefore, TM preparations provide an important negative control for the PSII experiments. We report that illumination of TM did not accumulate NFK, supporting the conclusion that the increase in NFK yield is caused by light stress. We attribute the resistance to photoinhibition in the TM to a

shading effect (60), because illumination of TM with the same light intensity at a lower chlorophyll concentration (0.1 mg/ mL) significantly decreased activity.

3.5.5 Effects of ionic strength on oxidative modifications

In this work, we found the interesting result that small ionic strength increases had a dramatic effect on the pattern of NFK modifications. However, this change did not alter the degradation pattern of D1 as assessed with a C-terminal antibody. Although the D1 degradation pattern was not changed, the alternative D1-NFK modification to Trp-317 was induced by increasing ionic strength. The ionic strength effect may cause conformational changes in the extrinsic loops. Lowering of the thylakoid lumen pH during excess light involves protein conformational changes that may be necessary in non-photochemical quenching (61).

Concomitant Mg^{2+} efflux into the stroma occurs during the transition from dark to light conditions (62,63). Thus, ionic strength induced events are essential in regulatory pathways in TM and PSII. Further evidence for loop dynamics is provided by the inefficient tryptic cleavage of CP43 in TW PSII, noted here. For example, both the ^{363}AP(W*)LEPLR^{370} peptide (fraction A) and the ^{363}AP(W*)LEPLRGPNGLDLSR^{379} (fraction C) peptide were observed in intact PSII and TM. However, in TW PSII, the shorter CP43 peptide ^{363}AP(W*)LEPLR^{370} was not detected. These results can be attributed to different conformations of the CP43 loop region. These conformational changes may be important in control of photoinhibitory responses in the chloroplast, where changes in the proton motive force can occur during illumination.

3.5.6 NFK in PSII signaling and repair

The signaling pathways for induction and control of D1 turnover are not known. Oxidative PTMs of aromatic amino acids have been proposed to participate in signaling. The NFK modifications identified here may function as these signals. We showed previously that substitutions at Trp-365 (Trp-352 in *Synechocystis* 6803) did not affect the steady-state rate of oxygen evolution under normal light-saturated conditions (30). This result indicated that mutations at Trp-365 do not alter the structure of PSII or change the overall rates of electron transfer. However, the mutants displayed an increased rate of photoinhibition at higher light intensities (5,000 μmol photons m^{-2} s^{-1}) (64). Thus, the inability to form NFK in the mutants resulted in reduced repair during high light stress. Because the light-induced increases in NFK in CP43 and D1 appear to be mutually exclusive, we propose that these modifications occur on two different damage/repair pathways. Inhibition of the CP43 pathway promotes the D1 oxidative pathway.

The primary proposed protease involved in D1 turnover, FtsH (65,66), has been proposed to recognize partially unfolded proteins (67). Oxidation of Trp to NFK may promote partial protein or unfolding required for signal recognition by the protease (65). Replacement of NFK with unmodified Trp requires *de novo* protein synthesis (68). Multiple NFK modifications may be required for continuous D1 turnover. Interestingly, an increase in CP43 degradation and cross-linking was observed during photoinhibition and donor side inactivation (40).

3.6 Conclusions

Our data provide evidence for specific oxidative modifications of PSII subunits. These PTMs are induced by high light stress and are under differential control of ionic strength. We propose that NFK plays a role in signaling for repair during D1 turnover. In a two-pathway signaling model for repair, inhibition of one NFK signaling pathway (the "CP43" pathway) stimulates repair by the alternative pathway (the "D1" pathway). These results provide new insight into redox signaling in oxygenic photosynthesis.

3.7 Acknowledgments

We wish to thank Dr. Adam Offenbacher for helpful discussions.

3.8 References

1. Nelson, N., and Yocum, C. F. (2006) Structure and function of photosystems I and II. *Annu. Rev. Plant Biol.* **57**, 521-565

2. Umena, Y., Kawakami, K., Shen, J.-R., and Kamiya, N. (2011) Crystal structure of oxygen-evolving photosystem II at a resolution of 1.9 Å. *Nature* **473**, 55-60

3. Ferreira, K. N., Iverson, T. M., Maghlaoui, K., Barber, J., and Iwata, S. (2004) Architecture of the photosynthetic oxygen-evolving center. *Science* **303**, 1831-1838

4. Guskov, A., Kern, J., Gabdulkhakov, A., Broser, M., Zouni, A., and Saenger, W. (2009) Cyanobacterial photosystem II at 2.9 Å resolution and the role of quinones, lipids, channels and chloride. *Nat. Struct. Mol. Biol.* **16**, 334- 342

5. Kamiya, N., and Shen, J.-R. (2003) Crystal structure of oxygen-evolving photosystem II from *Thermosynechococcus vulcanus* at 3.7 Å resolution. *Proc. Natl. Acad. Sci. U. S. A.* **100**, 98-103

6. Loll, B., Kern, J., Saenger, W., Zouni, A., and Biesiadka, J. (2005) Towards complete cofactor arrangement in the 3.0 Å resolution structure of photosystem II. *Nature* **438**, 1040-1044

7. Zouni, A., Witt, H.-T., Kern, J., Fromme, P., Krauß, N., Saenger, W., and Orth, P. (2001) Crystal structure of photosystem II from *Synechococcus elongatus* at 3.8 Å resolution. *Nature* **409**, 739-743

8. Bricker, T. M., and Frankel, L. K. (2002) The structure and function of CP47 and CP43 in photosystem II. *Photosynth. Res.* **72**, 131-146

9. Yocum, C. F. (2008) The calcium and chloride requirements of the O_2 evolving complex. *Coord. Chem. Rev.* **252**, 296-305

10. Tyystjärvi, E. (2008) Photoinhibition of photosystem II and photodamage of the oxygen evolving manganese cluster. *Coord. Chem. Rev.* **252**, 361-376

11. Yamamoto, Y., Aminaka, R., Yoshioka, M., Khatoon, M., Komayama, K., Takenaka, D., Yamashita, A., Nijo, N., Inagawa, K., Morita, N., Sasaki, T., and

Yamamoto, Y. (2008) Quality control of photosystem II: impact of light and heat stresses. *Photosynth. Res.* **98**, 589-608

12. Nixon, P. J., Michoux, F., Yu, J., Boehm, M., and Komenda, J. (2010) Recent advances in understanding the assembly and repair of photosystem II. *Ann. Bot.* **106**, 1-16

13. Gießauf, A., van Wickern, B., Simat, T., Steinhart, H., and Esterbauer, H. (1996) Formation of *N*-formylkynurenine suggests the involvement of apolipoprotein B-100 centered tryptophan radicals in the initiation of LDL lipid peroxidation. *FEBS Lett.* **389**, 136- 140

14. Rexroth, S., Poetsch, A., Rögner, M., Hamann, A., Werner, A., Osiewacz, H. D., Schäfer, E. R., Seelert, H., and Dencher, N. A. (2012) Reactive oxygen species target specific tryptophan site in the mitochondrial ATP Synthase. *Biochim. Biophys. Acta* **1817**, 381-387

15. Rinalducci, S., Campostrini, N., Antonioli, P., Righetti, P. G., Roepstorff, P., and Zolla, L. (2005) Formation of truncated proteins and high-molecular-mass aggregates upon soft illumination of photosynthetic proteins. *J. Proteome Res.* **4**, 2327-2337

16. Ehrenshaft, M., Silva, S. d. O., Perdivara, I., Bilski, P., Sik, R. H., Chignell, C. F., Tomer, K. B., and Mason, R. P. (2009) Immunological detection of *N*-formylkynurenine in oxidized proteins. *Free Radic. Biol. Med.* **46**, 1260-1266

17. Fedorova, M., Todorovsky, T., Kuleva, N., and Hoffmann, R. (2010) Quantitative evaluation of tryptophan oxidation in actin and troponin I from skeletal muscles using a rat model of acute oxidative stress. *Proteomics* **10**, 2692-2700

18. Helland, R., Fjellbirkeland, A., Karlsen, O. A., Ve, T., Lillehaug, J. R., and Jensen, H. B. (2008) An oxidized tryptophan facilitates copper binding in *Methylococcus capsulatus*-secreted protein MopE. *J. Biol. Chem.* **283**, 13897-13904

19. Dreaden, T. M., Chen, J., Rexroth, S., and Barry, B. A. (2011) *N*-formylkynurenine as a marker of high light stress in photosynthesis. *J. Biol. Chem.* **286**, 22632-22641

20. Gracanin, M., Hawkins, C. L., Pattison, D. I., and Davies, M. J. (2009) Singlet-oxygen-mediated amino acid and protein oxidation: formation of tryptophan peroxides and decomposition products. *Free Radic. Biol. Med.* **47**, 92-102

21. Previero, A., Coletti-Previero, M.-A., and Jollès, P. (1967) Localization of non-essential tryptophan residues for biological activity of lysozyme. *J. Mol. Biol.* **24**, 261-268

22. Guptasarma, P., Balasubramanian, D., Matsugo, S., and Saito, I. (1992) Hydroxyl radical mediated damage to proteins, with special reference to the crystallins. *Biochemistry* **31**, 4296-4303

23. Finley, E. L., Dillon, J., Crouch, R. K., and Schey, K. L. (1998) Identification of tryptophan oxidation products in bovine alpha-crystallin. *Protein Sci.* **7**, 2391-2397

24. Krieger-Liszkay, A., Fufezan, C., and Trebst, A. (2008) Singlet oxygen production in photosystem II and related protection mechanism. *Photosynth. Res.* **98**, 551-564

25. Pospíšil, P. (2009) Production of reactive oxygen species by photosystem II. *Biochim. Biophys. Acta* **1787**, 1151-1160

26. Hillier, W., and Wydrzynski, T. (1993) Increases in peroxide formation by the photosystem II oxygen-evolving reactions upon removal of the extrinsic 16, 22, and 33 kDa proteins are reversed by $CaCl_2$ addition. *Photosynth. Res.* **38**, 417-423

27. Berthold, D. A., Babcock, G. T., and Yocum, C. F. (1981) A highly resolved, oxygen-evolving photosystem II preparation from spinach thylakoid membranes. *FEBS Lett.* **134**, 231-234

28. Anderson, L. B., Ouellette, A. J. A., and Barry, B. A. (2000) Probing the structure of photosystem II with amines and phenylhydrazine. *J. Biol. Chem.* **275**, 4920-4927

29. Lichtenthaler, H. K. (1987) Chlorophylls and carotenoids- pigments of photosynthetic biomembranes. *Methods Enzymol.* **148**, 350-382

30. Barry, B. A. (1995) Tyrosyl radicals in photosystem II. *Methods Enzymol.* **258**, 303-319

31. Ghanotakis, D. F., Babcock, G. T., and Yocum, C. F. (1984) Calcium reconstitutes high rates of oxygen evolution in polypeptide depleted photosystem II preparations. *FEBS Lett.* **167**, 127-130

32. Yamamoto, Y., Doi, M., Tamura, N., and Nishimura, M. (1981) Release of polypeptides from highly active O_2-evolving photosystem II preparations by tris treatment. *FEBS Lett.* **133**, 265-268

33. Simat, T., Meyer, K., and Steinhart, H. (1994) Synthesis and analysis of oxidation of carbonyl condensation compounds of tryptophan. *J. Chromatogr. A* **661**, 93-99

34. Piccioni, R., Bellemare, G., and Chua, N. (1982). in *Methods in Chloroplast Molecular Biology* (Edelman, H., Hallick, R. B., and Chua, N.-H. eds.), Elsevier, Amsterdam. pp 985-1014

35. Bollag, D. M., and Edelstein, S. J. (1991) *Protein Methods*, Wiley-Liss, New York

36. Ouellette, A. J. A., Anderson, L. B., and Barry, B. A. (1998) Amine binding and oxidation at the catalytic site for photosynthetic water oxidation. *Proc. Natl. Acad. Sci. U. S. A.* **95**, 2204-2209

37. Towbin, H., Staehelin, T., and Gordon, J. (1979) Electrophoretic transfer of proteins from polyacrylamide gels to nitrocellulose sheets: procedure and some applications. *Proc. Natl. Acad. Sci. U. S. A.* **76**, 4350-4354

38. Henmi, T., Miyao, M., and Yamamoto, Y. (2004) Release and reactive-oxygen-mediated damage of the oxygen-evolving complex subunits of PSII during photoinhibition. *Plant Cell Physiol.* **45**, 243-250

39. Virgin, I., Styring, S., and Andersson, B. (1988) Photosystem II disorganization and manganese release after photoinhibition of isolated spinach thylakoid membranes. *FEBS Lett.* **233**, 408-412

40. Yamamoto, Y., and Akasada, T. (1995) Degradation of antenna chlorophyll-binding protein CP43 during photoinhibition of photosystem II. *Biochemistry* **34**, 9038-9045

41. McKinnon, N. K., Reeves, D. C., and Akabas, M. H. (2011) 5-HT3 receptor ion size selectivity is a property of the transmembrane channel, not the cytoplasmic vestibule portals. *J. Gen. Physiol.* **138**, 453-466

42. Rochu, D., Viguié, N., Renault, F., Crouzier, D., Froment, M.-T., and Masson, P. (2004) Contribution of the active-site metal cation to the catalytic activity and to the conformational stability of phosphotriesterase: temperature- and pH-dependence. *Biochem. J.* **380**, 627-633

43. Boda, D., Nonner, W., Valiskó, M., Henderson, D., Eisenberg, B., and Gillespie, D. (2007) Steric selectivity in Na channels arising from protein polarization and mobile side chains. *Biophys. J.* **93**, 1960-1980

44. Waggoner, C. M., Pecoraro, V., and Yocum, C. F. (1989) Monovalent cations (Na^+, K^+, Cs^+) inhibit calcium activation of photosynthetic oxygen evolution. *FEBS Lett.* **244**, 237-240

45. Johnson, P. E., Creagh, A. L., Brun, E., Joe, K., Tomme, P., Haynes, C. A., and McIntosh, L. P. (1998) Calcium binding by the N-terminal cellulose-binding domain from *Cellulomonas fimi* β-1,4-glucanase CenC. *Biochemistry* **37**, 12772-12781

46. Mehler, A. H., and Knox, W. E. (1950) The conversion of tryptophan to kynurenine in the liver II. The enzymatic hydrolysis of formylkynurenine. *J. Biol. Chem.* **187**, 431-438

47. Barry, B. A. (2011) Proton coupled electron transfer and redox active tyrosines in photosystem II. *J. Photochem. Photobiol. B-Biol.* **104**, 60-71

48. Macdonald, G. M., Steenhuis, J. J., and Barry, B. A. (1995) A difference fourier-transform infrared spectroscopic study of chlorophyll oxidation in hydroxylamine- treated photosystem II. *J. Biol. Chem.* **270**, 8420-8428

49. Roose, J. L., Wegener, K. M., and Pakrasi, H. B. (2007) The extrinsic proteins of photosystem II. *Photosynth. Res.* **92**, 369-387

50. Grossman, A. R., Bhaya, D., Apt, K. E., and Kehoe, D. M. (1995) Light-harvesting complexes in oxygenic photosynthesis: diversity, control, and evolution. *Annu. Rev. Genet.* **29**, 231-288

51. Berlett, B. S., and Stadtman, E. R. (1997) Protein oxidation in aging, disease, and oxidative stress. *J. Biol. Chem.* **272**, 20313-20316

52. Hunzinger, C., Wozny, W., Schwall, G. P., Poznanović, S., Stegmann, W., Zengerling, H., Schoepf, R., Groebe, K., Cahill, M. A., Osiewacz, H. D., Jägemann, N., Bloch, M., Dencher, N. A., Krause, F., and Schrattenholz, A. (2006) Comparative profiling of the mammalian mitochondrial proteome: multiple aconitase-2 isoforms including *N*-formylkynurenine modifications as part of a protein biomarker signature for reactive oxidative species. *J. Proteome Res.* **5**, 625-633

53. Møller, I. M., and Kristensen, B. K. (2006) Protein oxidation in plant mitochondria detected as oxidized tryptophan. *Free Radic. Biol. Med.* **40**, 430-435

54. Krieger, A., Rutherford, A. W., Vass, I., and Hideg, E. (1998) Relationship between activity, D1 loss, and Mn binding in photoinhibition of photosystem II. *Biochemistry* **37**, 16262-16269

55. Adir, N., Zer, H., Shochat, S., and Ohad, I. (2003) Photoinhibition- a historical perspective. *Photosynth. Res.* **76**, 343-370

56. Mizusawa, N., Tomo, T., Satoh, K., and Miyao, M. (2003) Degradation of the D1 protein of photosystem II under illumination *in vivo*: two different pathways involving cleavage or intermolecular cross-linking. *Biochemistry* **42**, 10034-10044

57. Mori, H., Yamashita, Y., Akasaka, T., and Yamamoto, Y. (1995) Further characterization of the loss of antenna chlorophyll- binding protein CP43 from photosystem II during donor- side photoinhibition. *Biochim. Biophys. Acta* **1228**, 37-42

58. Rozak, P. R., Seiser, R. M., Wacholtz, W. F., and Wise, R. R. (2002) Rapid, reversible alterations in spinach thylakoid appression upon changes in light intensity. *Plant Cell Environ.* **25**, 421-429

59. Anderson, J. M., and Aro, E.-M. (1994) Grana stackig and protection of photosystem II in thylakoid membranes of higher plant leaves under sustained high irradiance: an hypothesis. *Photosynth. Res.* **41**, 315-326

60. Pätsikkä, E., Kairavuo, M., Šeršen, F., Aro, E.-M., and Tyystjärvi, E. (2002) Excess copper predisposes photosystem II to photoinhibition in vivo by outcompeting iron and causing decrease in leaf chlorophyll. *Plant Physiol.* **129**, 1359-1367

61. Müller, P., Li, X.-P., and Niyogi, K. K. (2001) Non-photochemical quenching. A response to excess light energy. *Plant Physiol.* **125**, 1558-1566

62. Hind, G., Nakatani, H. Y., and Izawa, S. (1974) Light- dependent redistribution of ions in suspensions of chloroplast thylakoid membranes. *Proc. Natl. Acad. Sci. U. S. A.* **71**, 1484-1488

63. Ishijima, S., Uchibori, A., Takagi, H., Maki, R., and Ohnishi, M. (2003) Light-induced increase in free Mg^{2+} concentration in spinach chloroplasts: measurement of free Mg^{2+} by using a fluorescent probe and necessity of stromal alkalinization. *Arch. Biochem. Biophys.* **412**, 126-132

64. Anderson, L. B., Maderia, M., Ouellette, A. J. A., Putnam-Evans, C., Higgins, L., Krick, T., MacCoss, M. J., Lim, H., Yates, J. R., III, and Barry, B. A. (2002) Posttranslational modifications in the CP43 subunit of photosystem II. *Proc. Natl. Acad. Sci. U. S. A.* **99**, 14676-14681

65. Nixon, P. J., Barker, M., Boehm, M., de Vries, R., and Komenda, J. (2005) FtsH-mediated repair of the photosystem II complex in response to light stress. *J. Exp. Bot.* **56**, 357-363

66. Huesgen, P. F., Schuhmann, H., and Adamska, I. (2006) Photodamaged D1 protein is degraded in *Arabidopsis* mutants lacking the Deg2 protease. *FEBS Lett.* **580**, 6929-6932

67. Herman, C., Prakash, S., Lu, C. Z., Matouschek, A., and Gross, C. A. (2003) Lack of a robust unfoldase activity confers a unique level of substrate specificity to the universal AAA protease FtsH. *Mol. Cell* **11**, 659-669

68. Shacter, E. (2000) Quantification and significance of protein oxidation in biological samples. *Drug Metab. Rev.* **32**, 307-326

CHAPTER 4

PHOTOSYNTHETIC OXYGEN EVOLUTION: SIGNALING ROLE FOR *N*-FORMYLKYNURENINE IN LIGHT-INDUCED REPAIR

by

Tina Michelle Dreaden Kasson[1] and Bridgette A. Barry[1]

School of Chemistry and Biochemistry and the Petit Institute for Bioengineering and Bioscience, Georgia Institute of Technology, Atlanta, GA 30332

4.1 Abstract

Knowledge of how photosynthetic organisms adapt to altered environmental conditions has become critical due to increased global warming. Exposure to high light stress in the PSII enzyme results in protein damage and activity inhibition, called photoinhibition. In this work, we provide *in vivo* evidence in support of a protective role for the post translational modification CP43-NFK-365. Site-directed mutation of Trp-365 in the CP43 subunit to alanine, cysteine, and leucine in the cyanobacterium *Synechocystis* sp. PCC 6803 induced an increased rate of photoinhibition at light intensities of 3,000 and 8,000 μmol photons m^{-2} s^{-1}. The $t_{1/2}$ for photoinhibition in *wildtype* and CP43 W365 mutant cell lines were undistinguishable at a light intensity of 10,000 μmol photons m^{-2} s^{-1}, suggesting an additional damage or repair pathway dominates at extreme light intensities. Trp-365 is conserved and oxidatively modified to *N*-formylkynurenine (NFK) in plant PSII (Dreaden *et al.* (2011) *J. Biol. Chem.* 286, 22632-22641). We demonstrate here that NFK and post-translational carbonyl modifications accumulate during illumination in both plant PSII membranes and *Synechocystis* thylakoid membranes. These data provide support for a NFK protective role. NFK may function as a signal in repair. A modified repair cycle with NFK as a signal is proposed.

4.2 Introduction

Increasing CO_2 emissions and the dire energy market have shifted research towards alternative clean energy sources. Studies of photosynthetic organisms have progressed to the forefront of these efforts because they possess the capability to cleanly and efficiently harness solar energy for conversion of CO_2 to carbon-based energy

sources. Recent research has been heavily focused on studies of photosynthetic cyanobacteria and algae as model systems for clean energy production (1). Cultivation of cyanobacterial and algal species for H_2 production is currently a growing field (1). Thus, an in-depth understanding of the biochemistry involved in these light-driven reactions is essential.

Projected trends and effects of global warming have further promoted studies of how photosynthetic organisms adapt to changing environmental stresses. These organisms are sensitive to direct effects of global warming and ozone depletion, including increased temperature and UV light stress. Stress from excess high intensity light results in protein damage and activity inhibition, called photoinhibition (2). To protect from long-term damage, photosynthetic species initiate a repair cycle (3). Many unanswered questions remain regarding signaling pathways in repair. Further understanding of the repair process will be required for cultivation of resilient crops in the future.

The photosynthetic reactions occur in specialized membranes, thylakoid membranes, of plants, algae, and cyanobacteria. A series of large protein complexes catalyze the reactions. PSII participates in the oxidation of water to O_2 and protons. The cyanobacterial PSII structure was solved to 1.9 Å resolution (4-9). The Mn_4CaO_5 cluster, or oxygen evolving complex (OEC), active site is located close to the lumenal surface of the membrane complex (4). Calcium and chloride ions are required for maximal activity (4,10). Electrons derived from water at the active site are transferred through a series of cofactors, including a pheophytin molecule and two plastoquinone molecules, Q_A and Q_B, on the stromal or acceptor side of the membrane (4).

The D1 and D2 polypeptides span the membrane at the central core of the PSII reaction center and bind the electron transfer cofactors (4). The CP43 and CP47 chlorophyll binding proteins surround the D1/ D2 core (4). Substitutions and deletions in the flexible lumenal loops of CP43 and CP47 have demonstrated their importance in PSII complex assembly and protection from light-induced stress (11). Three extrinsic polypeptides, psbO, the 12 kDa, and cyt. c_{550}, bind to the lumenal surface opposing the active site cluster in cyanobacteria (4).

The D1 protein is the primary site of damage from light stress in PSII. D1 consequently exhibits a high rate of turnover under these conditions (3). Light-induced reactive oxygen species (ROS) are inevitable and are known to play a role in photoinhibition (12). Initiation of the repair cycle for replacement of damaged D1 involves partial PSII complex disassembly, D1 proteolysis and removal, new D1 synthesis and re-insertion, and finally PSII complex reassembly (3). Although signals for initiation of proteolysis and repair are unclear, post translational oxidation of amino acids has been proposed to play signaling roles for degradation of damaged components (13).

We previously reported that Trp side chains in CP43 (Trp-365) and D1 (Trp-317) react with ROS during photoinhibition to form *N*-formylkynurenine (NFK) (Figure 4.1) in plant PSII (14,15). Site-directed mutation of CP43 Trp-365 in *Synechocystis* sp. PCC 6803 resulted in an increased rate of photoinhibition (16). Steady state rates of oxygen evolution were unaffected, which supported a protective role for the conserved Trp during light stress with 5,000 µmol photons m^{-2} s^{-1} (16). In this work, we investigate the light intensity dependence on the protective effect of Trp-365 (CP43) *in vivo*. Using a small molecule that binds NFK and activated carbonyls, we also show illumination

induces NFK and/ or carbonyl modifications in plant PSII and *Synechocystis* 6803 thylakoid membranes. The data suggest that NFK modifications during photoinhibition function as signals in repair from light induced stress.

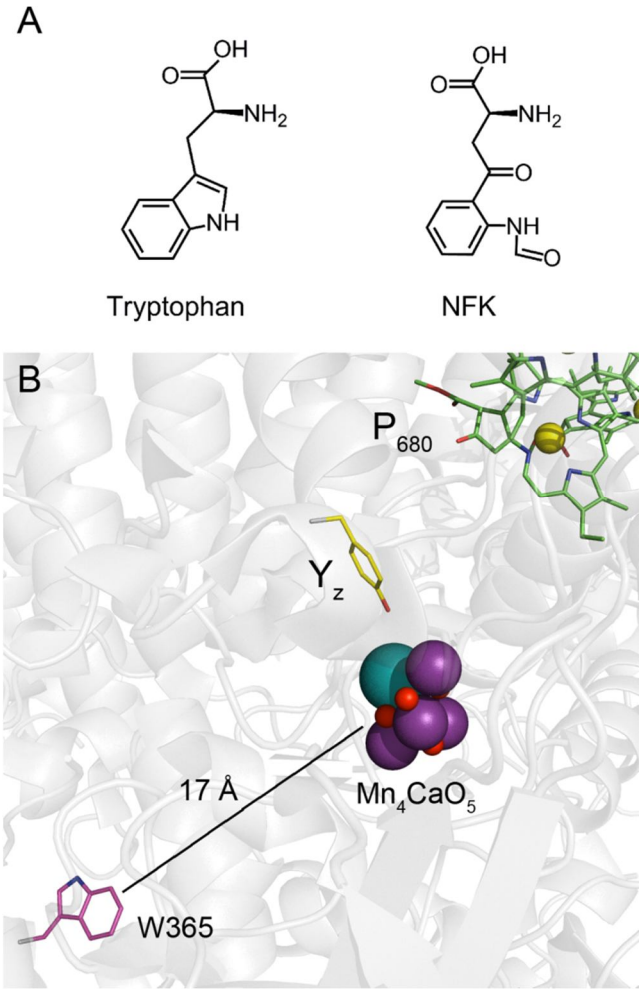

Figure 4.1. Tryptophan, NFK, and Trp-365 in the 1.9 Å resolution cyanobacterial structure. (A) shows the chemical structures of tryptophan and NFK. (B) shows the location of Trp-365 in the 1.9 Å crystal structure from *T. vulcanus* (4). The Trp-365 side chain is displayed shown in magenta. The Mn_4CaO_5 cluster (OEC) is displayed in violet and teal. Yz and P_{680} are labeled.

4.3 Materials and methods

4.3.1 *Synechocystis* 6803 cells and PSII membranes

Three site-directed mutations at Trp-365 in CP43 (Trp-352 in *Synechocystis sp.* PCC 6803) were constructed (Table 4.1) (16). The Trp was mutated to a cysteine (W352C), alanine (W352A), or leucine (W352L). Cyanobacterial strains were maintained on solid media containing BG-11 (17), 5 mM glucose, 10 µM 3-(3,4-dichlorophenyl)-1,1-dimethylurea (DCMU), and 10 µg/ mL kanamycin. Liquid media contained BG-11 only. Liquid cultures were grown to an $O.D._{730}$ of ~1.5- 2 with a light intensity of ~150 µmol photons m^{-2} s^{-1}. The cells were grown at 30 ºC, bubbled with sterile air, and harvested by centrifugation.

Table 4.1. Nomenclature for *Synechocystis* 6803 cell lines

	Wt	**CP43 W365A mutant**	**CP43 W365C mutant**	**CP43 W365L mutant**
name	*Synechocystis* 6803 *wt*	*Synechocystis* 6803 W365A	*Synechocystis* 6803 W365C	*Synechocystis* 6803 W365L

PSII membranes were isolated from market spinach (18) with modifications (19). Chlorophyll (20) and oxygen assays were conducted as described (21).

4.3.2 Photoinhibition

Photoinhibition experiments on *Synechocystis* cells were conducted as previously described (16,22,23). The cells were resuspended in BG-11 (17) and assayed the same day. A 10 mL aliquot of cells (20 μg/ mL chlorophyll concentration) was illuminated with white light from a Dolan-Jenner (Boxborough, MA) Fiber-Lite illuminator at light intensities of ~3,000, 8,000, and 10,000 μmol photons m^{-2} s^{-1} and at 25 ºC. The light intensity was measured with a Li-Cor (Lincoln, NE) Light Meter (model LI-189 with a ~8 cm diameter sensor). At the indicated time, a 20 μg sample of chlorophyll was extracted for oxygen evolution measurements (21). The assays were performed at 25 ºC in BG-11 media with 1 mM $K_3Fe(CN)_6$ and recrystallized 1 mM DCBQ. Red-filtered light from a Dolan-Jenner illuminator was used in the oxygen evolution assays. Rate constants for photoinhibitory decay were calculated by using $\lambda=\ln[N_0/N]/t$ (16). The corresponding half-time was calculated by $t_{1/2}= \ln 2/ \lambda$.

Photoinhibition in PSII membranes was conducted as described (15). Inhibition with white light intensities of 500, 3,000, and 7,000 μmol photons m^{-2} s^{-1} at 25 °C was compared to PSII membranes maintained in the dark at room temperature.

4.3.3 D1 Protein Western Blot

Harvested *Synechocystis* cells were washed with 25% glycerol, 20 mM 2-(*N*-morpholino)ethanesulfonic acid (MES)-HCl, pH 6.0, 20 mM $CaCl_2$, and 20 mM $MgCl_2$. The cells were resuspended to 1 mg/ ml chlorophyll in BG-11 and kept in the dark at

room temperature or illuminated with white light (3,000 µmol photons m^{-2} s^{-1}) at 25 °C for two hours. Thylakoid membranes were isolated (24) and analyzed by SDS-PAGE (25,26). Five µg of chlorophyll was loaded per lane. Gels were blotted onto a 0.45 µm polyvinylidene fluoride (PVDF) membrane by semi-dry transfer (27). A C-terminal D1 (PsbA) antibody (Agrisera, Vannas, Sweden) (1: 10,000) was used. Anti-chicken-alkaline phosphatase (Sigma-Aldrick, St. Louis, MO) (1: 15,000) and 5-bromo-4-chloro-3-indolyl phosphate/ nitro blue tetrazolium (BCIP/ NBT) liquid substrate (Sigma-Aldrich, St. Louis, MO) were used for colorimetric development.

4.3.4 NFK Western blot with B5A

Synechocystis thylakoid membranes were isolated by sonication. Cell lysis was induced by 30-second cycles of sonication (50W) in the presence of 100 µg/ml phenylmethanesulfonylfluoride (Sigma Aldrich, St. Louis, MO), 30 µg/ml tosyl phenylalanyl chloromethyl ketone (Sigma Aldrich, St. Louis, MO), and 5 µg/ml pepstatin (Sigma Aldrich, St. Louis, MO). Eight cycles of sonication, with four minutes of rest were performed on ice. Centrifugation at 2,300 x *g* for 2 minutes separated unbroken cells from membranes. The resultant supernatant was centrifuged at 16,000 x *g* for 20 minutes. The isolated thylakoid membranes were dark-maintained or illuminated with white light for two hours (see 4.3.2).

Following dark or high light incubation, *Synechocystis* thylakoids or spinach PSII membranes were analyzed by SDS-PAGE (25,26) and Western blot as described for the D1 antibody (see 4.3.3). Labeling with 4 mM 5-(biotinamido)-pentylamine (B5A) (Life

Technologies, Carlsbad, CA) was performed during protein denaturation in 5.4 M urea, 4% SDS, 125 mM dithiothreitol, 104 mM Na_2CO_3. Twelve micrograms chlorophyll was loaded per lane for spinach PSII, and 1 μg per lane for *Synechocystis* thylakoid membranes. B5A binding sites were probed with avidin- alkaline phosphatase (Sigma Aldrich, St. Louis, MO) (1:500 dilution) and BCIP/ NBT (Sigma-Aldrich)

4.4 Results

4.4.1 Trp-365 protects from photoinhibition *in vivo*

We examined the protective effect of Trp-365 in CP43 at three different light intensities. Trp-365 was mutated to an alanine (W365A), cysteine (W365C), or leucine (W365L) (16). At light intensities of 3,000 and 8,000 μmol photons m^{-2} s^{-1}, *wildtype* (*wt*) *Synechocystis* 6803 cells maintained higher rates of oxygen evolution compared to the cells containing site-directed mutations of CP43 (Figures 4.2A-B). At 3,000 μmol photons m^{-2} s^{-1}, *wt* cells had a 10- 12 fold longer half time ($t_{1/2}$) compared to the mutants (Table 4.2). The Synechocystis *wt* cells had a 2- 3 fold longer $t_{1/2}$ than the CP43 mutant cell lines at 8,000 μmol photons m^{-2} s^{-1} (Table 4.2). The $t_{1/2}$ values for *wt* and mutants at 10,000 μmol photons m^{-2} s^{-1} did not significantly differ (Figure 4.2C and Table 4.2).

Table 4.2. Half-lives ($t_{1/2}$) for photoinhibition in *Synechocystis* 6803

Light intensity	*Wt*	W365A	W365C	W365L
3,000	171	17	17	14
8,000	16	7	6	6
10,000	5	6	4	5

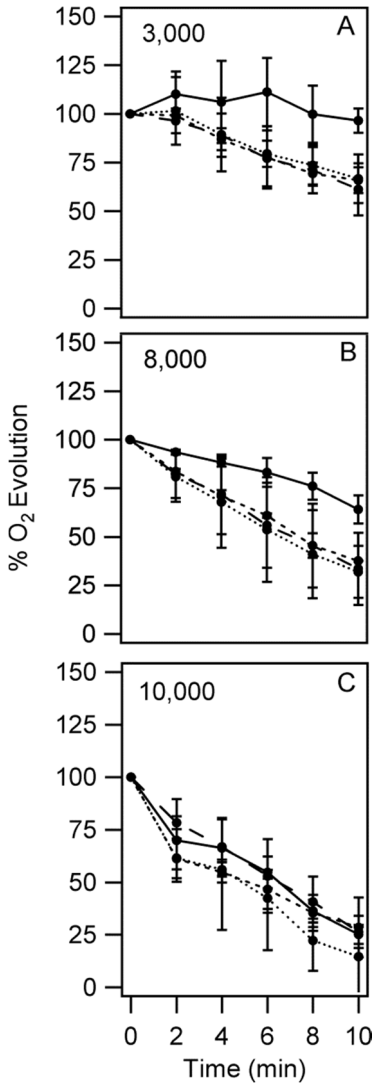

Figure 4.2. Photoinhibition of *Synechocystis* 6803 CP43 *wt* and W365 mutant cell lines. Rates of photoinhibition in the three site-directed *Synechocystis* 6803 mutants, W365A (fine dashed line), W365C (dotted line), and W365L (course dashed line) were compared to *wt* (solid line). Oxygen evolution rates were normalized to the starting rate at time = 0. In panels A-C, light intensities of 3,000 (A), 8,000 (B), and 10,000 (C) µmol photons m^{-2} s^{-1} were used. Each point represents the average of three independent experiments with different cell cultures. The error bars are ± standard deviation of the three experiments.

4.4.2 Total D1 content is unaltered in W365 mutants

Synechocystis 6803 cells were dark- maintained or illuminated with a white light intensity of 3,000 µmol photons m^{-2} s^{-1} for two hours at 25 °C. Thylakoid membranes

were isolated from the cells after the dark or light incubation period. Although *Synechocystis* CP43 W365 mutants exhibited an increased rate of photoinhibition at this light intensity (Figure 4.2A), the total D1 protein yield is unaffected as assessed by our C-terminal antibody (Figure 4.3). This result supports that the W365 mutations do not affect normal PSII assembly or completely inhibit repair during whole cell illumination.

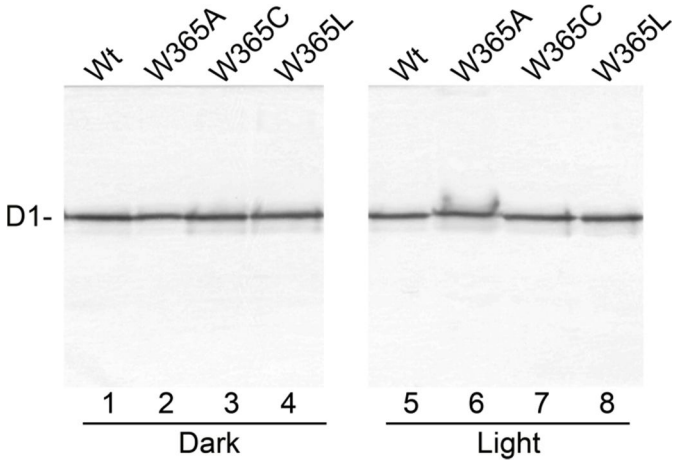

Figure 4.3. D1 protein content in *Synechocystis* 6803 thylakoid membranes. D1 protein content was compared in *wt* and CP43 W365 mutants. Cells were either kept in the dark at room temperature or illuminated with 3,000 μmol photons m^{-2} s^{-1} at 25 °C for two hours. Thylakoid membranes were isolated after the dark (lanes 1-4) or light (lanes 5-8) incubation. ~5 μg of chlorophyll was loaded per lane. A D1 C-terminal antibody (Agrisera) was used to probe for D1 protein.

4.4.3 NFK and/ or carbonyl modifications accumulate in plant PSII and *Synechocystis* thylakoid membranes upon illumination

To further probe NFK localization and formation during photoinhibition *in vitro*, Western blot analysis with a small molecule that binds NFK, 5-(biotinamido)-pentylamine (B5A), was employed (Figure 4.4). B5A, a biotin-amine conjugate, was shown to form a covalent amidine-like complex with NFK by UVRR spectroscopic analysis (14). B5A can also bind to other post-translationally modified carbonyls (28).

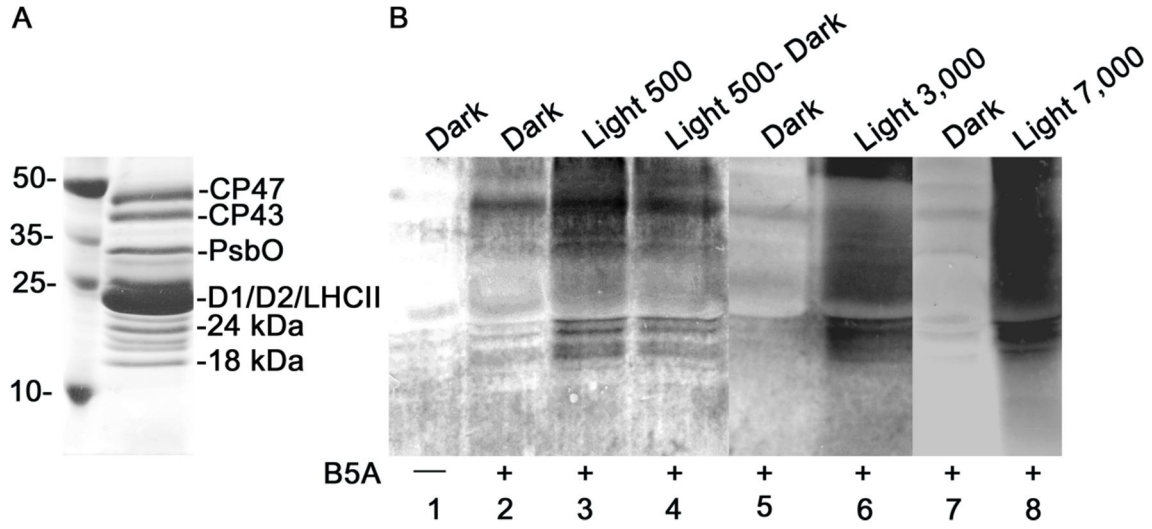

Figure 4.4. B5A Western detection of NFK and activated carbonyl in spinach PSII membranes. (A) Coomassie stained SDS-PAGE analysis of spinach PSII membranes. The core subunits are labeled. (B) B5A Western blot of dark control and illuminated PSII. Control PSII membranes were kept in the dark for two hours at room temperature (lanes 1, 2, 5, and 7). Light stress was induced by illumination with white light intensities of 500 (lane 3), 3,000 (lane 6), or 7,000 (lane 7) µmol photons m^{-2} s^{-1} for two hours at 25 °C. Lane 4 shows a 2 hour illumination with 500 µmol photons m^{-2} s^{-1}, followed by a 1 hour dark incubation. B5A (4 mM) was added to PSII samples during denaturation (lanes 2-7), prior to gel loading. As a control, B5A was not added to lane 1. B5A binding sites were probed with avidin- alkaline phosphatase. 12 µg chlorophyll was loaded per lane.

Compared to a control without B5A (Figure 4.4B, lane 1), B5A binding occurred specifically in plant PSII membranes in CP43 (~43 kDa) and D1/ LHCII (~25 kDa) (Figure 4.4B, lanes 2, 5, and 7). An increase in NFK and/ or carbonylation occurred following two hour illumination with 500, 3,000, and 7,000 µmol photons m^{-2} s^{-1} (Figure 4.4B, lanes 3, 6, and 8). A 1 hour dark incubation after illumination did not reverse the B5A binding (Figure 4.4B, lane 4). This result is expected because repair cannot occur in isolated PSII membranes *in vitro*. Illumination with 3,000 µmol photons m^{-2} s^{-1} also induced an increase in NFK and/or carbonyl modifications in *Synechocystis wt* and W365 mutant thylakoid membranes (Figure 4.5). An increased B5A-binding was observed in

the CP43 protein of *Synechocystis wt* dark-maintained membranes, compared to the W365 mutants (Figure 4.5, lanes 3-6).

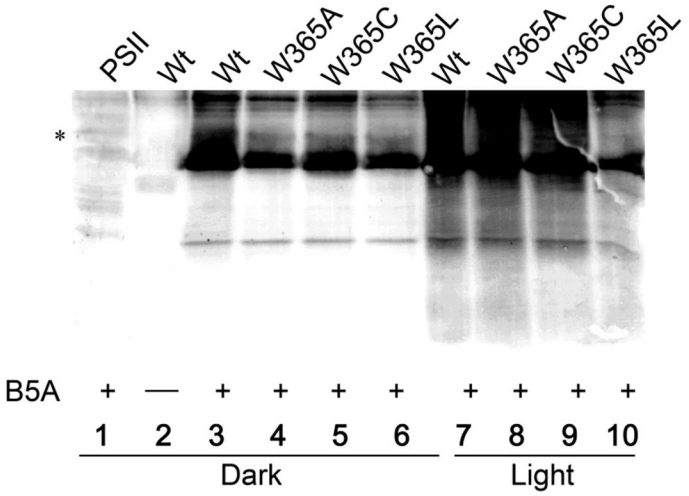

Figure 4.5. B5A Western detection of NFK and activated carbonyls in *Synechocystis* 6803 thylakoid membranes. Thylakoid membranes were isolated from *wt* and CP43 W365 site-directed mutants. The membranes were kept in the dark at room temperature (lanes 2-6) or illuminated with 3,000 µmol photons m^{-2} s^{-1} (lanes 7-10) for two hours at 25 °C. For comparison, lane 1 shows spinach PSII membranes that were maintained in the dark for two hours. B5A (4 mM) was added during denaturation (lanes 2-7), prior to gel loading. 12 µg (spinach PSII membranes) and 1 µg (*Synechocystis* thylakoid membranes) chlorophyll was loaded per lane. B5A binding sites were probed with avidin- alkaline phosphatase. The CP43 band is labeled with a "*".

4.5 Discussion

4.5.1 Summary

In this work we show that Trp-365 in the CP43 protein plays a relevant protective role *in vivo*. Trp oxidations to NFK and carbonyl modifications accumulate during light stress in plant PSII membranes and *Synehcocystis* 6803 thylakoid membranes. CP43 W365 site-directed mutants exhibit a significantly shorter $t_{1/2}$ for photoinhibition,

compared to *Synechocystis wt* that can oxidize Trp to NFK. These results indicate that inhibition of a key step in repair occurs under these conditions. We propose that the NFK-365 modification functions as a signal for disassembly or proteolysis in repair.

4.5.2 W365 substitution does not affect PSII reaction center assembly

Site-directed mutation of Trp-365 did not have a detectable effect on PSII structure, function, or assembly under normal physiological conditions. Even though the chemical properties of the substitutions (alanine, cysteine, leucine) varied significantly from the hydrophobic tryptophan, steady state rates of oxygen evolution were maintained. Maintenance of activity under light-saturated conditions supports that Trp-365 is not playing a specific structural role in protein-protein contacts or assembly. Examination of the location in the 1.9 Å resolution crystal structure (4) demonstrates that the Trp side chain is located in a loop region on the lumenal surface (Figure 4.1). Unless involved in a protein contact, substitutions in flexible loops are not expected to induce significant effects on protein structure or assembly.

Western blot analysis with a C-terminal D1 antibody supports that the monomeric D1 protein contents are unaffected by the substitutions. The D1 protein is located in the PSII core and binds the oxygen-evolving complex and electron transfer cofactors (4). The *Synechocystis* 6803 W365 mutants may contain a larger proportion of unassembled or damaged D1 compared to *wt*, which would not be distinguishable by the SDS-PAGE analysis.

4.5.3 NFK in repair from photoinhibition

In vivo photoinhibition studies in *Synechocystis* are advantageous because repair mechanisms remain intact. In the work presented here, *Synechocystis* 6803 W365 mutants are only impaired during stress from high light illumination. Thus, the natural Trp must play a role in repair under those conditions.

Trp-365 is highly conserved across photosynthetic organisms (16). We previously reported that Trp-365 is oxidized to NFK in plant PSII during photoinhibition (14,15). NFK formed from reaction with ROS generated at the OEC 17 Å away (15). Here, we show that post translational NFK and carbonyl modifications accumulate following illumination in both plant PSII membranes and *Synechocystis* thylakoid membranes. The data suggest that the protective effect is attributed to the ability of the *wt* to oxidize the Trp to NFK.

Basic steps involved in D1 turnover are partial PSII disassembly, damaged D1 degradation, new D1 synthesis, insertion into a partially disassembled complex, and finally PSII re-assembly (Figure 4.5) (3). The filamentation temperature-sensitive (FtsH) protease is the proposed protease involved in D1 degradation (29). Signaling processes in repair, however, remain unknown. Post translational side chain oxidations have been proposed to function as signals for the FtsH protease (3,13). NFK-365 may participate in this signaling role (Figure 4.5, step 1).

In one proposed model for repair in *Synechocystis*, induction of a conformational change may signal for removal of the damaged subunit (13). Based on this model, slower rates of D1 degradation would result from an enhanced stabilization induced by

decreased post-translational oxidations (13). Decreased proteolysis in the Trp-365 mutants, which cannot be oxidized, would explain the increased rate of photoinhibition.

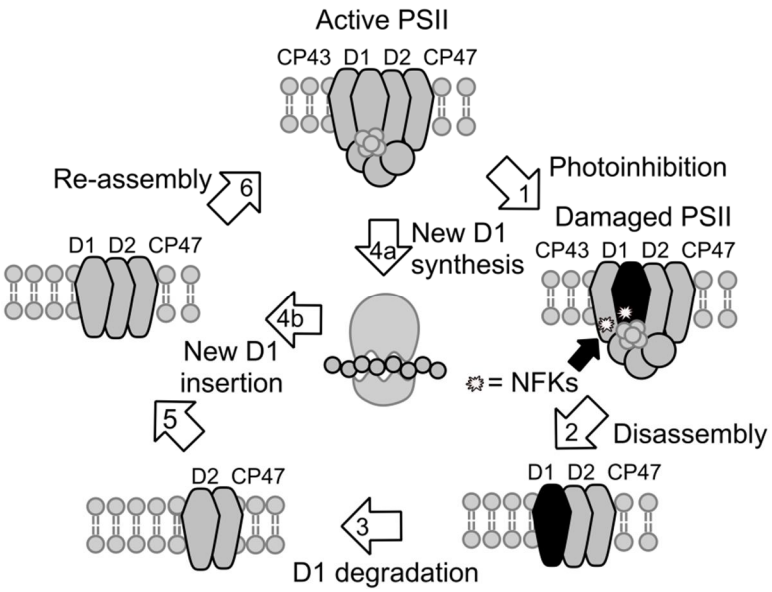

Figure 4.6. Role of NFK in the D1 repair cycle. In step 1, the D1 polypeptide is damaged by exposure to high light illumination, or photoinhibition, and NFK formation occurs. The damaged PSII complex is partially disassembled in step 2. CP43, the OEC, and the extrinsic subunits are removed to enable access to the damaged D1 protein. Damaged D1 is degraded and removed in step 3. In steps 4 and 5, a new D1 polypeptide is synthesized and inserted into the partial D2-CP47 complex. Re-assembly of the complex in step 6 re-activates photosynthetic activity. NFK modifications at Trp-365 (CP43) and/or Trp-315 (D1) may function as signals for disassembly (step 2) or D1 degradation (step 3).

4.5.4 Light intensity dependence

The protective effect of the natural CP43 W365 in *Synechocystis wt* cells demonstrates a light intensity dependence. This result indicates that additional pathways of damage or repair come into play at extreme light intensities. The Synechocystis 6803 W365 mutants may accumulate alternative NFK modifications, such as NFK-317 (D1)

(15). Release and damage of polypeptides under extreme light conditions could also explain the outcome (30,31).

4.6 Conclusions

The data presented here support a modified description for a repair model involving NFK. During light stress, NFK forms at W365 from reaction with ROS generated at the Mn_4CaO_5 cluster active site (Figure 5, step 1). The oxidation may trigger a conformational change to enable disassembly (Figure 5, step 2) or function as a signal for D1 proteolysis (Figure 5, step 3). Damaged D1 removal enables synthesis (Figure 5, steps 4a-b) and insertion of a new D1 protein into the partial D2-CP47 complex (Figure 5, step 5). Re-assembly completes the repair cycle and re-activates photosynthetic oxygen evolution.

4.7 Acknowledgments

We would like to thank Professor Cindy Putnam-Evans for the gift of the Synechocystis 6803 *wt* and W365 mutant cell lines, as well as for helpful discussions regarding the photoinhibition experiments.

4.8 References

1. Kruse, O., Rupprecht, J., Mussgnug, J. H., Dismukes, G. C., and Hankamer, B. (2005) Photosynthesis: A blueprint for solar energy capture and biohydrogen production technologies. *Photochem. Photobiol. Sci.* **4**, 957-970

2. Adir, N., Zer, H., Shochat, S., and Ohad, I. (2003) Photoinhibition- a historical perspective. *Photosynth. Res.* **76**, 343-370

3. Nixon, P. J., Michoux, F., Yu, J., Boehm, M., and Komenda, J. (2010) Recent advances in understanding the assembly and repair of photosystem II. *Ann. Bot.* **106**, 1-16

4. Umena, Y., Kawakami, K., Shen, J.-R., and Kamiya, N. (2011) Crystal structure of oxygen-evolving photosystem II at a resolution of 1.9 Å. *Nature* **473**, 55-60

5. Guskov, A., Kern, J., Gabdulkhakov, A., Broser, M., Zouni, A., and Saenger, W. (2009) Cyanobacterial photosystem II at 2.9 Å resolution and the role of quinones, lipids, channels and chloride. *Nat. Struct. Mol. Biol.* **16**, 334- 342

6. Ferreira, K. N., Iverson, T. M., Maghlaoui, K., Barber, J., and Iwata, S. (2004) Architecture of the photosynthetic oxygen-evolving center. *Science* **303**, 1831-1838

7. Zouni, A., Witt, H.-T., Kern, J., Fromme, P., Krauß, N., Saenger, W., and Orth, P. (2001) Crystal structure of photosystem II from *Synechococcus elongatus* at 3.8 Å resolution. *Nature* **409**, 739-743

8. Kamiya, N., and Shen, J.-R. (2003) Crystal structure of oxygen-evolving photosystem II from *Thermosynechococcus vulcanus* at 3.7 Å resolution. *Proc. Natl. Acad. Sci. U. S. A.* **100**, 98-103

9. Loll, B., Kern, J., Saenger, W., Zouni, A., and Biesiadka, J. (2005) Towards complete cofactor arrangement in the 3.0 Å resolution structure of photosystem II. *Nature* **438**, 1040-1044

10. Yocum, C. F. (2008) The calcium and chloride requirements of the O_2 evolving complex. *Coord. Chem. Rev.* **252**, 296-305

11. Bricker, T. M., and Frankel, L. K. (2002) The structure and function of CP47 and CP43 in photosystem II. *Photosynth. Res.* **72**, 131-146

12. Hideg, E., Spetea, C., and Vass, I. (1994) Singlet oxygen and free radical production during acceptor-induced and donor-side photoinhibition: studies with spin-trapping EPR spectroscopy *Biochim. Biophys. Acta* **1186**, 143-152

13. Nixon, P. J., Barker, M., Boehm, M., de Vries, R., and Komenda, J. (2005) FtsH-mediated repair of the photosystem II complex in response to light stress. *J. Exp. Bot.* **56**, 357-363

14. Dreaden, T. M., Chen, J., Rexroth, S., and Barry, B. A. (2011) *N*-formylkynurenine as a marker of high light stress in photosynthesis. *J. Biol. Chem.* **286**, 22632-22641

15. Dreaden Kasson, T. M., and Barry, B. A. (2012) Light-induced oxidative Stress, *N*-formylkynurenine, and oxygenic photosynthesis *Plos ONE* **Accepted**

16. Anderson, L. B., Maderia, M., Ouellette, A. J. A., Putnam-Evans, C., Higgins, L., Krick, T., MacCoss, M. J., Lim, H., Yates, J. R., III, and Barry, B. A. (2002) Posttranslational modifications in the CP43 subunit of photosystem II. *Proc. Natl. Acad. Sci. U. S. A.* **99**, 14676-14681

17. Rippka, R., Deruelles, J., Waterbury, J. B., Herdman, M., and Stanier, R. Y. (1979) Generic assignments, strain histories and properties of pure cultures of cyanobacteria. *J. Gen. Microbiol.* **111**, 1-61

18. Berthold, D. A., Babcock, G. T., and Yocum, C. F. (1981) A highly resolved, oxygen-evolving photosystem II preparation from spinach thylakoid membranes. *FEBS Lett.* **134**, 231-234

19. Anderson, L. B., Ouellette, A. J. A., and Barry, B. A. (2000) Probing the structure of photosystem II with amines and phenylhydrazine. *J. Biol. Chem.* **275**, 4920-4927

20. Lichtenthaler, H. K. (1987) Chlorophylls and carotenoids- pigments of photosynthetic biomembranes. *Methods Enzymol.* **148**, 350-382

21. Barry, B. A. (1995) Tyrosyl radicals in photosystem II. *Methods Enzymol.* **258**, 303-319

22. Rosenberg, C., Christian, J., Bricker, T. M., and Putnam-Evans, C. (1999) Site-directed mutagenesis of glutamate residues in the large extrinsic loop of the photosystem II protein CP43 affects oxygen-evolving activity and PSII assembly. *Biochemistry* **38**, 15994-16000

23. Knoepfle, N., Bricker, T. M., and Putnam-Evans, C. (1999) Site-directed mutagenesis of basic arginine residues 305 and 342 in the CP43 protein of photosystem II affects oxygen-evolving activity in *Synechocystis* 6803. *Biochemistry* **38**, 1582-1588

24. Komenda, J., Lupínková, L., and Kopecký, J. (2002) Absence of the psbH gene product destabilizes photosystem II complex and bicarbonate binding on its acceptor side in Synechocystis PCC 6803. *Eur. J. Biochem.* **269**, 610-619

25. Piccioni, R., Bellemare, G., and Chua, N. (1982). in *Methods in Chloroplast Molecular Biology* (Edelman, H., Hallick, R. B., and Chua, N.-H. eds.), Elsevier, Amsterdam. pp 985-1014

26. Bollag, D. M., and Edelstein, S. J. (1991) *Protein Methods*, Wiley-Liss, New York

27. Towbin, H., Staehelin, T., and Gordon, J. (1979) Electrophoretic transfer of proteins from polyacrylamide gels to nitrocellulose sheets: procedure and some applications. *Proc. Natl. Acad. Sci. U. S. A.* **76**, 4350-4354

28. Rexroth, S., Wong, C. C. L., Park, J. H., Yates, J. R., III, and Barry, B. A. (2007) An activated glutamate residue identified in photosystem II at the interface between the manganese-stabilizing subunit and the D2 polypeptide. *J. Biol. Chem.* **282**, 27802-27809

29. Adam, Z., Zaltsman, A., Sinvany-Villalobo, G., and Sakamoto, W. (2005) FtsH proteases in chloroplasts and cyanobacteria. *Physiol. Plant.* **123**, 386-390

30. Henmi, T., Miyao, M., and Yamamoto, Y. (2004) Release and reactive-oxygen-mediated damage of the oxygen-evolving complex subunits of PSII during photoinhibition. *Plant Cell Physiol.* **45**, 243-250

31. Yamamoto, Y., and Akasada, T. (1995) Degradation of antenna chlorophyll-binding protein CP43 during photoinhibition of photosystem II. *Biochemistry* **34**, 9038-9045

CHAPTER 5

2D CRYSTALLIZATION AND ELECTRON MICROSCOPY OF SPINACH PHOTOSYSTEM II

by

Tina Michelle Dreaden Kasson[1], Ingeborg Schmidt-Krey[1,2], and Bridgette A. Barry[1]

[1]School of Chemistry and Biochemistry and the Petit Institute for Bioengineering and Bioscience, Georgia Institute of Technology, Atlanta, GA 30332

[2]School of Biology, Georgia Institute of Technology, Atlanta, GA 30332

5.1 Abstract

In oxygenic photosynthesis, plants convert sunlight energy into chemical energy. Photosystem II (PSII) catalyzes the oxidation of water to oxygen released into the atmosphere. This process maintains Earth's aerobic environment. The catalytic efficiency of PSII is compromised by environmental stress, such as increased light intensity and temperature. Accelerating global climate changes underscore the significance of understanding the function and mechanism of photosynthetic water oxidation. Biophysical changes associated with PSII damage and repair cycles are unknown. PSII structure determination under physiological and light stressed conditions would afford considerable insight into this process. Currently, only low resolution data of partial and inactive plant PSII enzyme is available. In the work described here, proteoliposomes containing spinach PSII cores were generated by dialysis with exogenous DMPC lipids. At lipid-to-proteins (LPRs) of 1.5- 2.0, all of the proteoliposomes examined contained multiple, closely spaced areas of PSII order within the artificial membrane. The PSII core complexes maintained their structural integrity, a relevant aspect for functional studies. Minimal improvement of dialysis conditions should lead to uniform 2D crystals. Optimization of 2D crystals is the bottleneck in protein structure determination by electron crystallography.

5.2 Introduction

Oxygenic photosynthesis is the enzyme-catalyzed conversion of light energy to biochemical energy. This process occurs in the thylakoid membranes of plants, algae, and cyanobacteria. Photosystem II (PSII) catalyzes the photo-induced oxidation of water and

reduction of plastoquinone. Each monomer is composed of more than 20 protein subunits, chlorophylls, carotenoids, and redox-active cofactors (1,2). The active site of water oxidation is a Mn_4CaO_5 metallocluster, or oxygen-evolving complex (OEC), located on the lumenal side of the membrane complex (1).

PSII is composed of membrane-spanning intrinsic and hydrophilic extrinsic polypeptides (Figure 5.1) (1). The intrinsic membrane-spanning proteins contain flexible loops that protrude into lumenal interior of the thylakoid membrane (1). The D1, D2, CP43, and CP47 polypeptides form the intrinsic core complex of PSII. The D1 protein binds the electron transfer cofactors and Mn_4CaO_5 active site (Figure 5.1) (3). The D1/ D2 core is flanked by the CP43 and CP47 proteins (Figure 5.1), which bind light-harvesting antennae chlorophyll molecules (4).

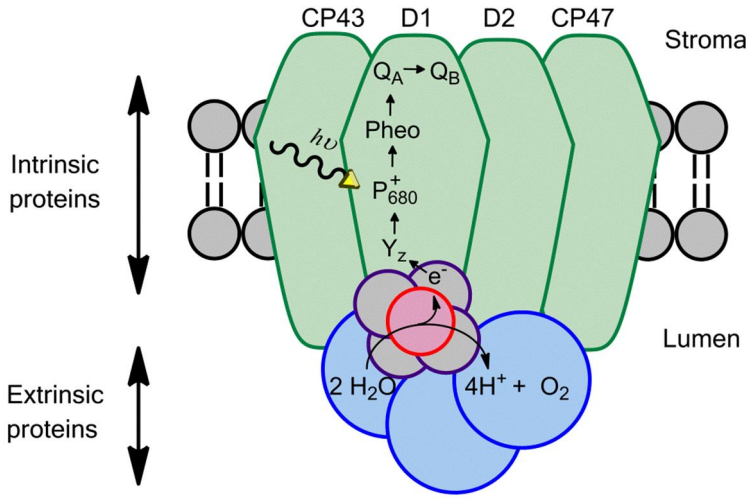

Figure 5.1. PSII core complex structure in the thylakoid membrane. The intrinsic (green) and extrinsic (blue) polypeptides are labeled. The active site Mn_4CaO_5 cluster is displayed in violet and red. The redox active cofactors (Yz, P_{680}^+, Pheo, Q_A, and Q_B) are labeled.

The Mn_4CaO_5 active site protected by three extrinsic polypeptides (5). In plants, these extrinsic proteins, the 18-kDa, 24-kDa, and psbO (or the 33-kDa, manganese stabilizing protein, MSP), are essential for maximal oxygen evolution under physiological conditions (5). PsbO is the only extrinsic protein that is conserved in both cyanobacteria and plants (6). In addition to psbO, cyanobacteria also contain cyt. c_{550} and the 12-kDa protein (1).

Plant and cyanobacterial PSII also utilize different light-harvesting systems (7). These protein systems bind light energy absorbing chlorophyll and other pigments at orientations that enable efficient transfer into the reaction center. Plants contain the trimeric light harvesting complex II (LHCII) (8), which flanks PSII in the membrane. Hydrophilic phycobilisome proteins bind to the membrane surface in cyanobacteria (9).

The cyanobacterial PSII structure has been solved to 1.9 Å resolution (1,2,10-13). In contrast, the resolution of a plant PSII structure remains at 8 Å resolution (14). This intermediate resolution structure was missing the essential extrinsic polypeptides, LHCII, and the Mn_4CaO_5 active site, which rendered the enzyme inactive (14). Although the PSII core reaction center is similar in all types of photosynthetic organisms, the differences in subunit composition suggest that fundamental functional and/ or mechanistic variability exists between prokaryotes and eukaryotes. A functionally competent or more complete PSII plant enzyme structure at higher resolution will aid in clarification of these differences.

A thorough grasp of the function of any protein requires a high resolution structural model. Crystallography is an approach commonly utilized for this purpose.

These methods, however, are not trivial. Specifically, intricacies involved in large-scale isolation and high yield purification of these flexible biomolecules, which are required for preparation of 3-dimensional (3D) crystals for traditional X-ray crystallography, are inherently involved tasks. Additional complications are involved for hydrophobic membrane-bound proteins. These difficulties, such as disruption of the native phospholipid membrane and replacement with non-native detergent molecules without denaturation, structural changes, or aggregation, have notably impeded efforts to reveal high resolution structures of many membrane proteins. Finally, the substantial size of the PSII dimer, with a molecular weight of ~700 kDa and at least 20 subunits per monomer (1), provides yet another impediment to crystallization (see Appendix A for an overview of 2D crystallization methods for membrane protein complexes) .

Electron crystallography is an alternative approach for membrane proteins that requires smaller 2-dimensional (2D) crystals of approximately 1 μm^2 in size (15). Like X-ray methods, electron crystallography can provide 3D structural information of proteins at atomic resolution (16). However, it has some advantages over traditional X-ray methods in the case of plant PSII. First, membrane proteins more easily form 2D crystals in lipid bilayers (17), in contrast to larger 3D crystals outside of a membrane. Second, the effects of radiation damage to the protein itself, as well as reduction of the Mn_4CaO_5 active site, can be minimized by using very low electron doses when recording images and diffraction patterns (18). Reduction of the metal center, as well as structural changes in the local environment, is known to occur during X-ray diffraction (19).

With the long-term aim of high resolution structure determination of plant PSII by electron crystallography, we have demonstrated progress in acquisition of 2D crystals of

an intact PSII complex. The experimental methodology involves PSII membrane purification from spinach leaves (20), detergent solubilization, and chromatographic PSII enrichment (21). Addition of exogenous lipids and dialysis removes detergent and induces PSII reconstitution into a lipid bilayer. Structural integrity and activity are assessed before and after 2D crystallization trials (Figure 5.2). Optimization of dialysis conditions lead to increased order within the proteoliposome, demonstrating progress towards 2D crystal formation. These types of 2D crystals, upon minor optimization, will be used for 3D structure determination of plant PSII by electron crystallography. PSII structures under normal and high light stressed conditions can be compared. Structural differences under the different conditions will provide novel insight into the PSII damage and repair cycle (22).

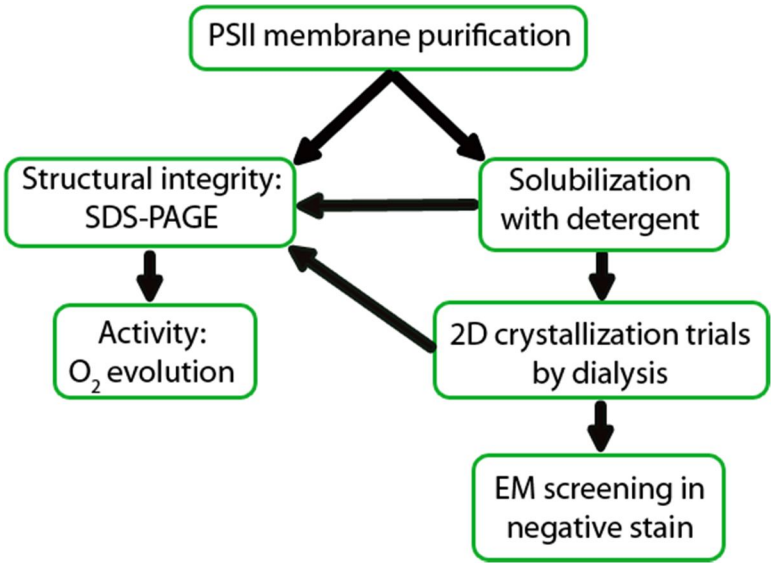

Figure 5.2. Experimental overview of steps involved in PSII purification, 2D crystallization, and EM screening. Structural integrity and activity of PSII are assessed before and after 2D crystallization trials.

5.3 Materials and methods

5.3.1 PSII membrane purification and partial solubilization

PSII membranes were isolated from market spinach as described (20) with modifications (23). PSII membranes were resuspended in 400 mM sucrose, 20 mM 2-(*N*-morpholino)-ethanesulfonic acid (MES)- NaOH (pH 6.0), 15 mM NaCl (SMN buffer).

0.01- 0.50 % (w/v) *n*-dodecyl-β-D-maltoside (DDM) (Affymetrix, Santa Clara, CA) was added to PSII membranes just prior to dialysis (see 5.3.6 for dialysis conditions).

5.3.2 PSII core complex purification

PSII core complexes were isolated from PSII membranes as described (21). 1 mg/ mL chlorophyll was solubilized with 1% (DDM) in a buffer of 50 mM MES-NaOH (pH 6.0), 15 mM NaCl, 25% glycerol. Samples were shaken on ice in the dark for 20 minutes. A single centrifugation at 120,000 x g for 30 minutes (4 °C) separated unsolubilized material. The supernatant was filtered with a 0.45 μm syringe filter and loaded onto a MonoQ HR5/5 column (Amersham Biosciences, Uppsala, Sweden). The column was equilibrated with 50 mM MES-NaOH (pH 6.0), 7.5 mM $CaCl_2$, 25% glycerol, 0.05% DDM. Elution was performed with an 11 mL gradient of 0- 360 mM NaCl.

5.3.3 SDS-PAGE analysis

SDS-PAGE of PSII, before and after 2D crystallization by dialysis, was performed as described (24-26). 6 μg chlorophyll was loaded per lane. Gels were stained with 0.05% Brillant Blue R (Coomassie) (Sigma-Aldrich, St. Louis, MO).

5.3.4 Oxygen evolution assays

Chlorophyll (27) and oxygen evolution (28) assays were conducted as described. Oxygen evolution assays were conducted at 25 °C in SMN buffer with red-filtered light from a Dolan-Jenner (Boxborough, MA) Fiber-Lite illuminator, recrystallized 1 mM 2,6-dichlorobenzoquinone (DCBQ), and 1 mM $Fe(III)(CN)_6$. PSII membrane rates of oxygen evolution were ≥ 600 μmol photons m^{-2} s^{-1}.

5.3.5 2D crystallization trials by dialysis

All sample preparation, dialysis, and EM were performed in the dark under dim green light illumination. For dialysis experiments, 10 mm tubing with a 12-14,000 MWCO (Spectrum Laboratories, Inc., Rancho Dominguez, CA) and a 250 mL detergent free buffer was used. Following dialysis, proteoliposomes were transferred to 1.5 mL eppendorf tubes. EM grids were prepared immediately. Remaining samples were flash frozen in liquid N_2 and stored at -70 °C.

Partially solubilized PSII (5.3.2 Partial solubilization of PSII membranes) was dialyzed against a buffer of 50 mM MES- NaOH (pH 6.0), 5 mM $MgCl_2$, 400 mM sucrose, 15 mM NaCl for 7 days at 8 °C. For each 2D crystallization trial, 100 μL chl (50 μg) was used.

PSII core complexes were combined with solubilized dimyristoylphosphatidylcholine (DMPC) (Avanti Polar Lipids, Alabaster, AL) at lipid-to-protein ratios (LPRs) of 0- 2.5. For an LPR of 1.0, 50 µg chl was combined with 50 µg DMPC. Solubilized PSII- DMPC mixtures were dialyzed against a buffer of 50 mM MES- NaOH (pH 6.0), 15 mM NaCl, 7.5 mM $CaCl_2$, 25 % glycerol. Dialysis was performed for 7 days at 4-20 °C.

5.3.6 Negative stain and screening by electron microscopy

Following dialysis, 2 µL dialysate were applied to 3 mm carbon- coated 400 mesh copper grids (SPI Supplies, West Chester, PA). The grids were washed with 2 µL of sucrose free buffer (50 mM MES- NaOH (pH 6.0), 15 mM NaCl, 7.5 mM $CaCl_2$) to decrease sample thickness and to wash away any excess viscous sucrose. The grids were stained with 2 µL 1% uranyl acetate (Ted Pella, Redding, CA). EM screening was performed with a 120 kV JEM-1400 transmission electron microscope (TEM) (JEOL Ltd., Peabody, MA), equipped with Gatan, Inc. (Warrendale, PA) Orius SC1000 and Ultrascan 1000 charge-coupled device (CCD) cameras. Fourier transform (FT) and fast Fourier transform (FFT) analysis of high magnification images using Digital Micrograph imaging software (Gatan, Inc., Warrendale, PA) was used to screen for areas of crystal order.

5.4 Results

5.4.1 PSII partial solubilization and dialysis promotes order in small areas of the thylakoid membrane

PSII- enriched membranes isolated from spinach are ~0.6- 0.8 μm in diameter (Figure 5.3A). PSII is arranged in pseudo-crystalline arrays within the native thylakoid membrane (29). To increase the order of PSII units within the native membrane, a "partial" solubilization of the membranes with low concentrations of DDM, a non-ionic detergent, was performed. Dialysis of PSII in the presence of minimal detergent could induce a re-ordering in the membrane (Figure 5.4A). Prior to dialysis, DDM was added at concentrations from 0.01-1.00 %. Samples were then dialyzed in the dark for 7 days at 8 ºC (Table 5.1). The largest membranes were obtained with 0.03- 0.07% DDM (Table 5.1). Membranes were not observed following addition of 0.5 % DDM (Table 5.1).

Table 5.1 2D crystallization trials of partially solubilized PSII

% DDM (*w/v*)	Temperature	Membranes[a]	Average size[b]
0.00 %	8 °C	+	0.7 μm
0.01 %	8 °C	+	0.7 μm
0.03 %	8 °C	+	1.0 μm
0.05 %	8 °C	+	3.5 μm
0.07 %	8 °C	+	1.0 μm
0.10 %	8 °C	+	0.5 μm
0.50 %	8 °C	—	—

[a]membranes (proteoliposomes) were observed (+) or not observed (—) following dialysis; [b]average representative membrane size

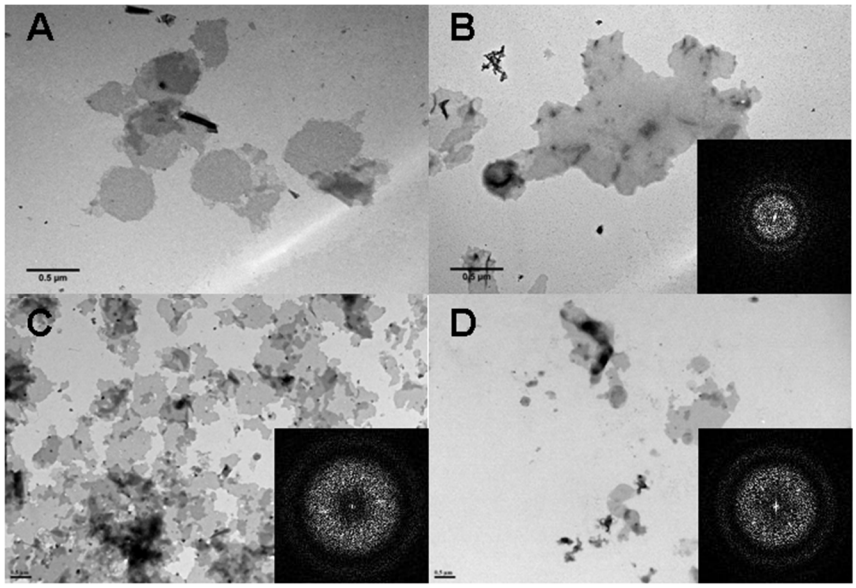

Figure 5.3 EM images of PSII membranes after dialysis for 7 days. All images are shown in negative stain with 1% uranyl acetate. (A) shows native PSII membranes (no additional lipids). (B) shows PSII membranes following partial solubilizaton with 0.05% DDM (no additional lipids). (C) shows completely solubilized PSII cores from peak 2 (Figure 5.5) following reconstitution with DMPC at a LPR of 1.8. Membranes in (D) are the same as C, except the LPR was 2.0. The insets of B-D display corresponding FFTs. In the FFTs, the 6 (B) or 4 (C and D) distinct white spots within the first order ring indicate crystalline order. The scale bars shown are 0.5 μm.

Figure 5.3B-C shows representative EM images of partially solubilized PSII, following dialysis. No additional lipids were added. The images were acquired of samples negatively stained in a 1% uranyl acetate negative stain. 0.03-0.05% DDM induced formation of proteoliposome sheets with the strongest spots in an online FFT (insets of Figure 5.3B-C). FFT analysis of EM images acquired with a CCD camera enabled immediate assessment of crystallinity (15). Regular spots, above the level of noise, in an online FFT indicate crystalline order within small areas of the membrane (insets of Figure 5.3B-C).

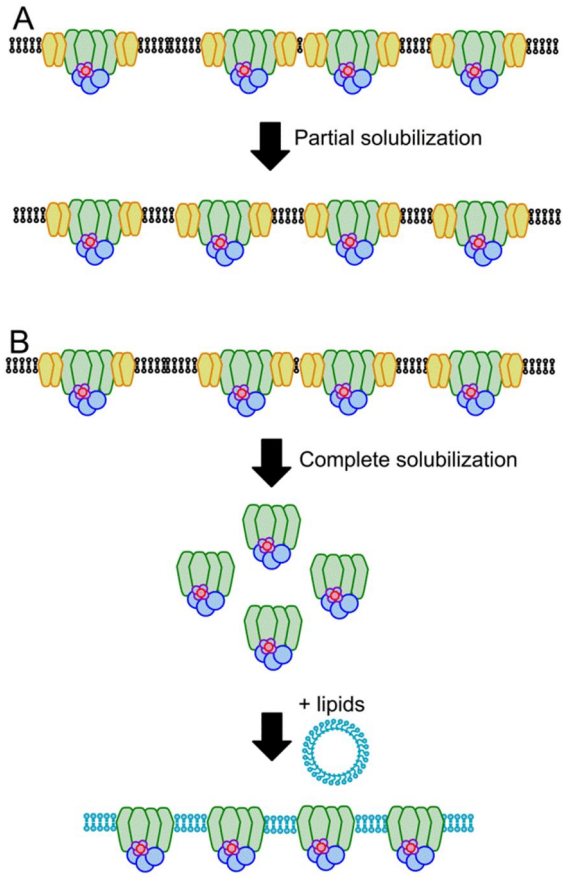

Figure 5.4. Overview of 2D crystallization approaches. Spinach PSII membranes (20) are the starting material in both methods. In A, addition of 0.01-0.5% DDM induces a re-ordering of PSII in the chloroplast thylakoid membrane. In B, complete solubilization with 1% DDM (21) removes PSII from the native membrane, and reconstitution with exogenous lipids results in ordered proteoliposomes. The LHCII complexes shown in orange are also removed during detergent solubilization.

5.4.2 Complete solubilization to increase PSII homogeneity

The PSII membrane preparation used for 2D crystallization (20,23) contains minor amounts of PSI, cytochrome b_6f, and ATP Synthase (30). A high degree of protein purity is an essential parameter in 2D crystallization (15). To increase the PSII homogeneity, the PSII membranes were completely solubilized with 1% DDM (21).

Solubilized PSII were separated from other thylakoid membrane complexes and the light harvesting complex II (LHCII) protein by anion exchange chromatography (21) (Figure 5.4B).

For chromatographic purification, an 11 mL gradient of 0-360 mM NaCl was used on a MonoQ HR 5/5 column (21). LHCII proteins elute at ~140 mM NaCl (5 mL) (Figure 5.5, peak 1). PSII cores elute with ~260 mM NaCl (9 mL) (Figure, 5.5, peak 2). Other minor amounts of membrane protein complexes originally present were also separated from PSII cores (21). PSII cores in peak 2 were collected and used for 2D crystallization trials.

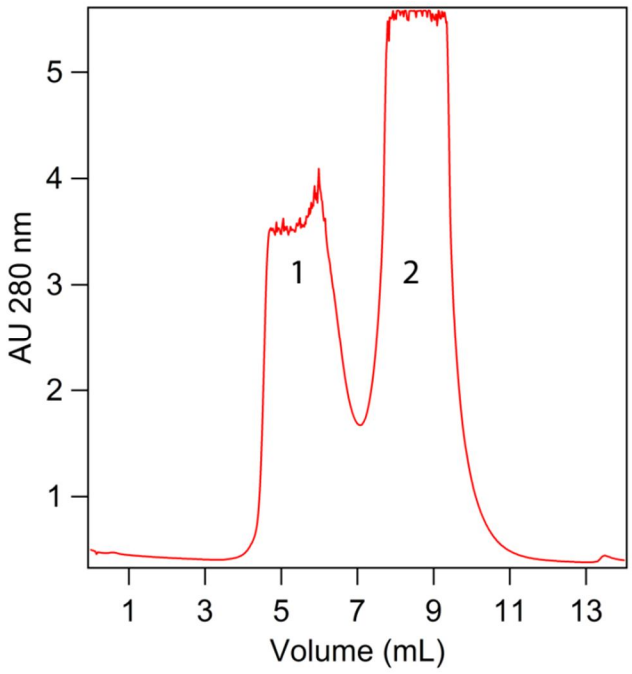

Figure 5.5. 280 nm elution profile of solubilized PSII by FPLC. The y-axis shows absorbance at 280 nm (AU). The x-axis shows volume of the NaCl gradient. PSII was solubilized with 1% DDM and eluted with an 11 mL gradient of 0-360 mM NaCl (21). The flow rate was 0.5 mL/ min and 0.5 mL fractions were collected. Peak 1 eluted with ~140 mM NaCl (5 mL) and contained LHCII proteins (21). Peak 2 contained PSII complexes and eluted with ~260 mM (9 mL) NaCl (21).

5.4.3. The structural integrity of PSII core complexes are maintained

SDS-PAGE analysis confirms that peak 1 (Figure 5.5) contains the 25 kDa LHCII monomer (Figure 5.6, lane 3). Peak 2 contains intact PSII core complexes (Figure 5.6, lane 4). PSII core complexes contain the main protein subunits capable of optimal oxygen evolution activity (21). These proteins are the membrane-spanning D1, D2, CP43, and CP47 proteins, as well as the three extrinsic proteins, PsbO, 18-kDa, and 24-kDa (Figure 5.1). For comparison, lane 2 of Figure 5.6 shows PSII membranes before solubilization and chromatogrpahy.

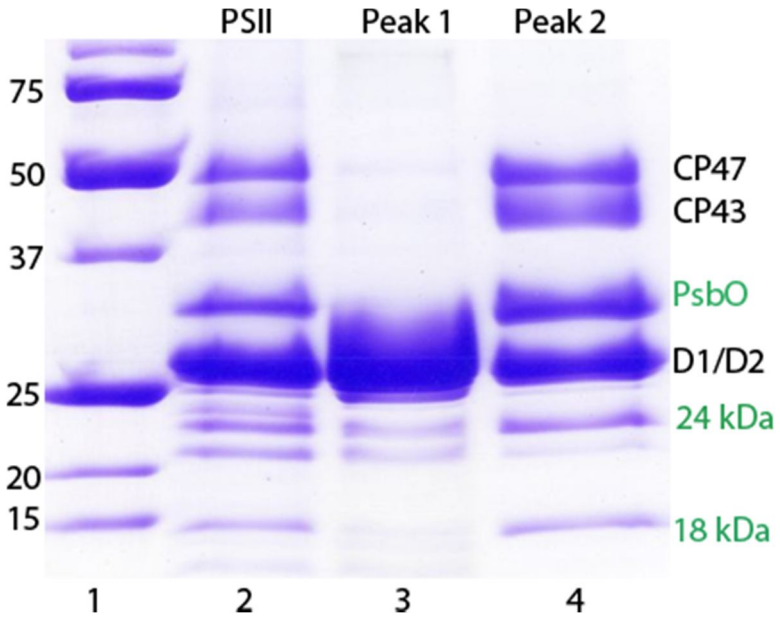

Figure 5.6. SDS-PAGE composition analyses of PSII membranes before and after solubilization. Lane 1 contains a molecular weight marker. Lane 2 shows PSII before solubilization. Peaks 1 and 2 (Figure 5.5) are shown in lanes 3 and 4, respectively. PSII core proteins are labeled on the right side of the gel, and the extrinsic subunits are displayed in green (Figure 5.1).

5.4.4 Oxygen evolution of purified PSII cores

MacDonald and coworkers (21) previously showed that PSII cores have a two-fold higher rate of oxygen evolution compared to PSII membranes (21). Under the experimental conditions here, however, PSII cores demonstrated a 55% decrease in activity after dialysis for 7 days at 8 °C (Table 5.2). The decreased activity may be explained by PSII's sensitivity to detergents. Minor experimental modifications to the time of detergent exposure prior to column loading should lead to increased activity. PSII inactivation before dialysis explains the complete loss in activity at the end of the dialysis time (Table 5.2).

Table 5.2. Oxygen evolution rates of PSII samples before and after dialysis

Before/ After Dialysis	Sample	O_2 evolution*
Before	PSII membranes	100 %
After	"	70 %
Before	PSII cores	55 %
After	PSII cores	0 %

*Rate of O_2 evolution was measured in units of μmol O_2 mg chl^{-1} hr^{-1}. The rates shown were normalized to the PSII membrane rate before dialysis (~800 O_2 mg chl^{-1} hr^{-1}).

5.4.5 2D crystallization trials with PSII cores

PSII cores (Figure 5.5, peak 2) were mixed with exogenous DMPC lipids at lipid-to-protein ratios (LPRs) of 1.0- 2.5 and dialyzed for 7 days at 20 ºC (Figure 5.4). All LPRs tested generated membrane sheets with diameters of ~0.5-1.5 μm (Table 5.4). LPRs

between 1.5 and 2.0 produced membranes with the highest degree of order, demonstrated by rather strong spots in FFTs (Figure 5.4C and D). In contrast to previous experiments, these membranes contained closely spaced areas of order within most membranes. The majority of membranes screened contained at least one area of order. Small adjustments in LPR, dialysis time, or temperature are hopeful to afford increased order within the membranes.

Table 5.3. 2D crystallization trials of PSII cores reconstituted with DMPC lipids

LPR	Temperature	Membranes[a]	Average size[b]
0.0	20 °C	—	—
1.0	20 °C	+	1.0 μm
1.3	20 °C	+	1.5 μm
1.5	20 °C	+	1.5 μm
1.8	20 °C	+	1.0 μm
2.0	20 °C	+	1.0 μm
2.5	20 °C	+	—

[a]membranes (proteoliposomes) were observed (+) or not observed (—) following dialysis; [b]average representative membrane size

5.5 Discussion

5.5.1 Summary

Spinach PSII cores formed 2D membranes with exogenous DMPC following dialysis. At LPRs of 1.5- 2.0, all of the membranes examined contained multiple, closely spaced areas of order. PSII cores remained intact following dialysis. Optimization of the detergent addition step before chromatographic purification should preserve O_2 evolution activity before dialysis. Additional minor adjustments to the LPR, dialysis time, or temperature may lead to larger continuous areas of order in a 2D crystal.

5.5.2 Partial solubilization increases PSII membrane size and order

A plant PSII structure embedded in a native lipid bilayer would provide the most relevant information regarding *in vivo* function. PSII is arranged in a pseudo-crystalline organization in isolated membranes with an average diameter of 0.7 μm (29). However, order in the native membranes is limited to small areas. A uniform area (at least 1 μm^2) of sufficient order is the minimum requirement for structure determination by electron crystallography (15). Thus, the initial experimental approach focused on ordering PSII into 2D crystalline arrays within the native thylakoid membranes.

Partial solubilization with 0.01- 0.05% DDM and lipid removal by dialysis increased PSII order within the membranes, as indicated by spots in online FFTs of EM images in negative stain. DDM is a mild, non-ionic detergent, frequently used for membrane protein purification (21). DDM has a critical micelle concentration (CMC) of 0.0087% (0.17 mM) (31). A temperature of 8 °C was used to promote slow detergent removal during dialysis. Prolonged exposure to higher temperatures may have also induced PSII degradation and inactivation. PSII order was limited to small areas of ~50 nm in a small proportion of the membranes screened.

Membranes also increased in size, up to ~3.5 μm. Because the conditions only mildly disrupt the membrane, PSII complexes already embedded provide a nucleation point for crystal formation. As detergent molecules are replaced by lipids, the membranes increase in size.

5.5.3 PSII core purification increases sample homogeneity

Protein purity is an essential consideration in formation of well-ordered 2D crystals (15). The PSII membrane preparation used in the partial solubilization approach (20,23) contains minor amounts of PSI, cytochrome b_6f, and ATP Synthase (30). A similar partial solubilization approach also observed that PSII enriched membranes also contain PSII supercomplexes with varying amounts of light harvesting antennae proteins (32). Mixtures of PSII supercomplexes and other membrane proteins will likely inhibit regular PSII packing within a 2D crystal.

PSII core complex purification increased the homogeneity and decreased the size of the PSII complex (21). The enrichment was reported to increase the rate of oxygen evolution by two fold (21). However, core complexes purified by the same procedure here exhibited a 55% decrease in activity immediately following purification. The loss in activity observed may be attributed to differences in experimental technique. Detergent addition is a critical step in solubilization of membrane proteins. Modification of this step by slower, drop-wise addition, or decreasing the incubation time before column loading is expected to optimize the purification to maintain high activity rates.

5.5.4 PSII cores form proteoliposomes with DMPC

Without the addition of exogenous lipids, detergent removal from the PSII cores by dialysis induced aggregation (data not shown). This result is expected, given the hydrophobic nature of the PSII proteins. Although some lipids may have been co-purified during the chromatographic step, PSII could not form observable proteoliposomes.

Upon mixture with exogenous DMPC and dialysis, PSII cores reconstituted into membranes at all of the LPRs tested. Interestingly, membranes were formed at 20 °C, below the DMPC phase transition temperature of 23 °C. This phenomenon was previously observed for 2D crystals of human vitamin K- dependent γ- glutamyl carboxylase (33). Typically, 2D crystallization is performed above the lipid phase transition temperature. Because PSII is sensitive to temperature (34), 20 °C was chosen as a starting point for crystallization trials. Lower temperatures may also enable membrane formation.

DMPC is not a native lipid present in thylakoid membranes (35). However, it has been used successfully in 2D crystallization of many membrane proteins (33,36). In most cases the identity of the lipid is not a limiting factor in successful crystallization (15).

Proteoliposomes formed with LPRs between 1.5 and 2.0 exhibited the most significant order, as assessed by spots in online FFTs. Most of the membranes examined contained multiple closely spaced areas of order. Optimization of the LPR, dialysis temperature, or dialysis time should lead to more uniform PSII order within the membrane. The membranes are already sufficient in diameter (≥ 1 μm) for high resolution 3D structure (15).

5.5.6 2D crystallization parameters

Numerous parameters are important in 2D crystallization of membrane proteins by dialysis. Sample purity, detergent, buffer composition, dialysis time, and temperature are all influential parameters in obtaining well-ordered crystals (15). Typically, 2D crystallization trials involve varying one or two parameters at a time. In the experiments

presented here, dialysis buffer conditions were chosen to promote PSII stability and activity. Multiple types of conditions may be tested before optimal conditions are obtained.

Most frequently, however, the LPR is the determining factor in successful 2D crystallization (15,37). Given the promising results for PSII 2D crystals with LPRs between 1.5 and 2.0, testing of LPRs less than 1.5 should be the next step. Lower LPRs may encourage tighter, more highly ordered, crystal packing within the membrane.

5.6 Conclusions

In 2D crystallization trials, PSII cores formed 1.0- 3.5 μm membranes with DMPC lipids. The membranes formed at 20 °C, below the phase transition temperature of DMPC. PSII core complexes remained intact following 2D crystallization trials, retaining the extrinsic polypeptides and the Mn_4CaO_5 active site cluster. The membranes contained multiple, closely spaced areas of order. Optimization of crystallization conditions, including the LPR, crystallization temperature, or time, should promote PSII order into continuous, uniform, crystalline lattice. These 2D crystals, containing an intact PSII complex, will present considerable information regarding photosynthetic PSII function.

5.7 Acknowledgments

This work was supported by the Integrative BioSystems Institute (IBSI) at the Georgia Institute of Technology. The authors wish to acknowledge Matthew Johnson, Laura Kim, Maureen Metcalfe, and Gengxiang Zhao for helpful discussions.

5.8 References

1. Umena, Y., Kawakami, K., Shen, J.-R., and Kamiya, N. (2011) Crystal structure of oxygen-evolving photosystem II at a resolution of 1.9 Å. *Nature* **473**, 55-60

2. Guskov, A., Kern, J., Gabdulkhakov, A., Broser, M., Zouni, A., and Saenger, W. (2009) Cyanobacterial photosystem II at 2.9 Å resolution and the role of quinones, lipids, channels and chloride. *Nat. Struct. Mol. Biol.* **16**, 334- 342

3. Nanba, O., and Satoh, K. (1987) Isolation of a photosystem II reaction center consisting of D-1 and D-2 polypeptides and cytochrome *b*-559. *Proc. Natl. Acad. Sci. U. S. A.* **84**, 109-112

4. Bricker, T. M., and Frankel, L. K. (2002) The structure and function of CP47 and CP43 in photosystem II. *Photosynth. Res.* **72**, 131-146

5. Miyao, M., and Murata, N. (1989) The mode of binding of 3 extrinsic proteins of 33-kDa, 23-kDa, and 18-kDa in the photosystem II complex of spinach. *Biochim. Biophys. Acta* **977**, 315- 321

6. De Las Rivas, J., and Barber, J. (2004) Analysis of the structure of the PsbO protein and its implications. *Photosynth. Res.* **81**, 329-343

7. Grossman, A. R., Bhaya, D., Apt, K. E., and Kehoe, D. M. (1995) Light-harvesting complexes in oxygenic photosynthesis: diversity, control, and evolution. *Annu. Rev. Genet.* **29**, 231-288

8. Kühlbrandt, W., Wang, D. N., and Fujiyoshi, Y. (1994) Atomic model of plant light- harvesting complex by electron crystallography. *Nature* **367**, 614-621

9. Grossman, A. R., Schaefer, M. R., Chiang, G. G., and Collier, J. L. (1993) The phycobilisome, a light-harvesting complex responsive to environmental conditions. *Microbiol. Rev.* **57**, 725-749

10. Ferreira, K. N., Iverson, T. M., Maghlaoui, K., Barber, J., and Iwata, S. (2004) Architecture of the photosynthetic oxygen-evolving center. *Science* **303**, 1831-1838

11. Zouni, A., Witt, H.-T., Kern, J., Fromme, P., Krauß, N., Saenger, W., and Orth, P. (2001) Crystal structure of photosystem II from *Synechococcus elongatus* at 3.8 Å resolution. *Nature* **409**, 739-743

12. Kamiya, N., and Shen, J.-R. (2003) Crystal structure of oxygen-evolving photosystem II from *Thermosynechococcus vulcanus* at 3.7 Å resolution. *Proc. Natl. Acad. Sci. U. S. A.* **100**, 98-103

13. Loll, B., Kern, J., Saenger, W., Zouni, A., and Biesiadka, J. (2005) Towards complete cofactor arrangement in the 3.0 Å resolution structure of photosystem II. *Nature* **438**, 1040-1044

14. Rhee, K.-H., Morris, E. P., Barber, J., and Kühlbrandt, W. (1998) Three-dimensional structure of the plant photosystem II reaction center at 8 Å resolution. *Nature* **396**, 283-286

15. Schmidt-Krey, I. (2007) Electron crystallography of membrane proteins: two-dimensional crystallization and screening by electron microscopy. *Methods* **41**, 417-426

16. Fujiyoshi, Y. (2011) Electron crystallography for structural and functional studies of membrane proteins. *J. Electron Microsc.* **60**, S149-S159

17. Rigaud, J. L., Chami, M., Lambert, O., Levy, D., and Ranck, J.-L. (2000) Use of detergents in two-dimensional crystallization of membrane proteins. *Biochim. Biophys. Acta-Biomembr.* **1508**, 112-128

18. Massover, W. H. (2007) Radiation damage to protein specimens from electron beam imaging and diffraction: a mini-review of anti-damage approaches, with special reference to synchrotron X-ray crystallography. *J. Synchrot. Radiat.* **14**, 116-127

19. Yano, J., Kern, J., Irrgang, K.-D., Latimer, M. J., Bergmann, U., Glatzel, P., Pushkar, U., Biesiadka, J., Loll, B., Sauer, K., Messinger, J., Zouni, A., and Yachandra, V. K. (2005) X-ray damage to the Mn_4Ca complex in single crystals of photosystem II: a case study for metalloprotein crystallography. *Proceedings of the National Academy of Sciences* **102**, 12047-12052

20. Berthold, D. A., Babcock, G. T., and Yocum, C. F. (1981) A highly resolved, oxygen-evolving photosystem II preparation from spinach thylakoid membranes. *FEBS Lett.* **134**, 231-234

21. Macdonald, G. M., and Barry, B. A. (1992) Difference FT-IR study of a novel biochemical preparation of photosystem II. *Biochemistry* **31**, 9848-9856

22. Nixon, P. J., Michoux, F., Yu, J., Boehm, M., and Komenda, J. (2010) Recent advances in understanding the assembly and repair of photosystem II. *Ann. Bot.* **106**, 1-16

23. Anderson, L. B., Ouellette, A. J. A., and Barry, B. A. (2000) Probing the structure of photosystem II with amines and phenylhydrazine. *J. Biol. Chem.* **275**, 4920-4927

24. Piccioni, R., Bellemare, G., and Chua, N. (1982). in *Methods in Chloroplast Molecular Biology* (Edelman, H., Hallick, R. B., and Chua, N.-H. eds.), Elsevier, Amsterdam. pp 985-1014

25. Bollag, D. M., and Edelstein, S. J. (1991) *Protein Methods*, Wiley-Liss, New York

26. Ouellette, A. J. A., Anderson, L. B., and Barry, B. A. (1998) Amine binding and oxidation at the catalytic site for photosynthetic water oxidation. *Proc. Natl. Acad. Sci. U. S. A.* **95**, 2204-2209

27. Lichtenthaler, H. K. (1987) Chlorophylls and carotenoids- pigments of photosynthetic biomembranes. *Methods Enzymol.* **148**, 350-382

28. Barry, B. A. (1995) Tyrosyl radicals in photosystem II. *Methods Enzymol.* **258**, 303-319

29. Seibert, M., DeWit, M., and Staehelin, L. A. (1987) Structural localization of the O_2- evolving apparatus to multimeric (tetrameric) particles on the lumenal surface of freeze- etched photosynthetic membranes. *J. Cell Biol.* **105**, 2257-2265

30. Rexroth, S., Wong, C. C. L., Park, J. H., Yates, J. R., III, and Barry, B. A. (2007) An activated glutamate residue identified in photosystem II at the interface

between the manganese-stabilizing subunit and the D2 polypeptide. *J. Biol. Chem.* **282**, 27802-27809

31. Vanaken, T., Foxallvanaken, S., Castleman, S., and Fergusonmiller, S. (1986) Alkyl glycoside detergents- Synthesis and applications to the study of membrane proteins. *Methods Enzymol.* **125**, 27-35

32. Boekema, E. J., van Roon, H., Calkoen, F., Bassi, R., and Dekker, J. P. (1999) Multiple types of association of photosystem II and its light-harvesting antenna in partially solubilized photosystem II membranes. *Biochemistry* **38**, 2233-2239

33. Schmidt-Krey, I., Haase, W., Mutucumarana, V., Stafford, D. W., and Kühlbrandt, W. (2007) Two-dimensional crystallization of human vitamin K-dependent γ-glutamyl carboxylase. *J. Struct. Biol.* **157**, 437-442

34. Yamamoto, Y., Aminaka, R., Yoshioka, M., Khatoon, M., Komayama, K., Takenaka, D., Yamashita, A., Nijo, N., Inagawa, K., Morita, N., and Sasaki, T. (2008) Quality control of photosystem II: impact of light and heat stresses. *Photosynth. Res.* **98**, 589-608

35. Bruce, B. D. (1998) The role of lipids in plastid protein transport. *Plant Mol. Biol.* **38**, 223-246

36. Zhao, G., Johnson, M. C., Schnell, J. R., Kanaoka, Y., Haase, W., Irikura, D., Lam, B. K., and Schmidt-Krey, I. (2010) Two-dimensional crystallization conditions of human leukotriene C_4 synthase requiring adjustment of a particularly large combination of specific parameters. *J. Struct. Biol.* **169**, 450-454

37. Kühlbrandt, W. (2003). in *Membrane protein purificaiton and crystallization: A practical approach* (Schägger, H., and Hunte, C. eds.), Academic Press, San Diego. pp 253-284

CHAPTER 6

6.1 Conclusions

Exposure to high light intensity in photosynthetic plants and cyanobacteria results in the phenomenon of photoinhibition. In Photosystem II (PSII), oxygen evolution activity is inhibited and the D1 protein is damaged. Reactive oxygen species (ROS) produced during light stress react specifically with tryptophan side chains in the PSII core complex. *N*-formylkynurenine (NFK), a UV absorbing chromophore, results from reaction of tryptophans with ROS in the CP43 (NFK-365) and D1 (NFK-317) subunits. In plant PSII, NFK-365 accumulation correlates with a decrease in oxygen evolution during high light illumination. These results support a role for NFK in oxidative stress and photoinhibition.

NFK accumulation correlates with the extent of photoinhibition in PSII and thylakoid membranes. These modifications may be formed by reaction with ROS produced at the Mn_4CaO_5 cluster in the oxygen- evolving complex. Supporting this interpretation, the NFK modifications in CP43 and D1 are found 17 and 14 Angstrom from the Mn_4CaO_5 cluster, respectively. D1 degradation and oligomerization, key events in D1 repair, also occur under both sets of conditions. The PTMs are under differential control of ionic strength, suggesting a two pathway model for light stress responses. Based on these results, a role for NFK in signaling for repair during D1 turnover is proposed. In a two-pathway signaling model for repair, inhibition of one NFK signaling pathway (the "CP43" pathway) stimulates repair by the alternative pathway (the "D1"

pathway). These results provide new insight into redox signaling in oxygenic photosynthesisis.

As demonstrated in *Synechocystis* 6803, the inability to form NFK-365-CP43 protects from photoinhibition *in vivo*. The protective effect was dependent on light intensity, suggesting that a second pathway of damage and or repair becomes dominant at extreme light intensities. The "D1" pathway described above may participate at higher light intensity. Further modification of a repair model involving NFK can be described. During light stress, NFK forms from reaction with ROS (via W365-CP43 or W317-D1) generated at the Mn_4CaO_5 cluster active site. The oxidation and indole ring cleavage reaction triggers a conformational change that acts as a signal for D1 turnover. NFK may promote removal of the extrinsic subunits and CP43, which is required for degradation and turnover of D1. Mutation of W365 to a residue that cannot be oxidized prevents the probable conformational change and signal. In mutants unable to form NFK in CP43, the damaged D1 is stabilized in the complex. The result is an inefficient repair cycle and increased photoinhibition. The experiments presented here provide novel insight into photoinhibition and repair in oxygenic photosynthesis.

6.2 Future Directions

NFK can be formed from tryptophan reaction with $^1O_2$ or $HO^{\bullet}$. Investigation of the type of ROS involved in NFK formation during photoinhibition would be valuable. Detection and quantitiation can be done with ROS specific electron paramagnetic resonance (EPR) spin traps. Thylakoid or PSII membrane isolation from *Arabidopsis* plants grown under controlled conditions, as opposed to field grown spinach, would provide reproducible results. The type and yield of ROS produced in *Arabidopsis* could be compared in plants grown under control and high light conditions. Because NFK accumulates during light stress, a corresponding increase in a particular species would provide support for involvement in NFK formation.

The fate of NFK- modified proteins *in vivo* could be investigated in *Arabidopsis* chloroplasts. A NFK- specific label, such as the amine-biotin (B5A), would allow electron microscopic tracking with an avidin-gold nanoparticle conjugate. Changes in PSII sub-complexes may be relevant during light stress and repair *in vivo*. NFK could be tracked in chloroplasts isolated from control and high light stressed *Arabidopsis* leaves. Localization and tracking of NFK modifications in PSII sub-complexes would provide relevant information on the role of oxidative modifications in the repair cycle.

APPENDIX A

TWO-DIMENSIONAL CRYSTALLIZATION OF MEMBRANE PROTEIN COMPLEXES FOR STRUCTURE-FUNCTION STUDIES BY ELECTRON CRYSTALLOGRAPHY

by

Tina Michelle Dreaden Kasson[1,4], Matt C. Johnson[2], Blanca Barquera[3], Bridgette A. Barry[1,4], and Ingeborg Schmidt-Krey[1,2]

[1]School of Chemistry and Biochemistry, Georgia Institute of Technology, Atlanta, GA 30332

[2]School of Biology, Georgia Institute of Technology, Atlanta, GA 30332

[3]Department of Biology, Rensselaer Polytechnic Institute, Troy, NY 12180

[4]Petit Institute for Bioengineering and Bioscience, Georgia Institute of Technology, Atlanta, GA 30332

This research was originally published in *Microscopy: Science, Technology, Applications and Education*.

Tina M. Dreaden, Matthew C. Johnson, Blanca Barquera, Bridgette A. Barry, Ingeborg Schmidt-Krey. (2010) "Two-dimensional crystallization of membrane protein complexes for structure-function atudies by electron crystallography." In *Microscopy: Science, Technology, Applications and Education.* Eds. Méndez-Vilas, A. and Díaz, J.. 337- 346.

A.1 Abstract

Membrane proteins comprise one of the major challenges in structural biology. Membrane protein complexes pose particular difficulties because they not only require careful solubilization, but additionally the structural, as well as functional integrity, of the entire complex needs to be maintained. Electron crystallography of two-dimensional (2D) crystals is an important emerging approach in the study of the structure and function of membrane protein complexes.

The most common method used for 2D crystallization of membrane proteins is reconstitution into a phospholipid bilayer by dialysis. Reconstitution is especially suitable for membrane protein complexes because the membrane protein is in a close-to-native phospholipid bilayer during crystallization, storage, and data collection by electron cryo-microscopy (cryo-EM).

Membrane protein complexes require additional experimental methods and precautions compared to monomeric or homooligomeric membrane proteins. Overviews of 2D crystallization and cryo-EM, with an emphasis on critical points for ensuring functional and structural integrity of the membrane protein complexes, are described here.

A.2 Introduction

Since the first breakthrough in the structure determination of a membrane protein with the help of two-dimensional (2D) crystals and transmission electron cryo-microscopy (cryo-EM) in 1975 (1), electron crystallography has become an indispensable biophysical technique for the study of structure-function relationships in membrane proteins. Progressive advances in the field have promoted increased interest in the study

of large membrane protein complexes composed of multiple subunits and oligomeric states. Despite difficulties in achieving high purity and yield during isolation and 2D crystallization of fragile membrane complexes, even low resolution structural information can provide substantial insight into the oligomeric state, overall dimensions, and subunit organization. Electron crystallography is complementary to X-ray crystallography. However, a noteworthy advantage of 2D crystals and cryo-EM is the use of either native or artificial lipids to mimic a native membrane environment, in contrast to most 3D crystals used in traditional X-ray techniques.

Similar to monomeric or homooligomeric proteins, the determination of conditions to induce 2D crystallization is the bottleneck in structure determination of large, multi-subunit membrane protein complexes. In addition to the inherent intricacies in terms of purity and functional integrity, as well as the number of parameters tested in formation of large, well-ordered 2D crystals, protein complexes involve yet another dimension of intricacy. Specifically, structural integrity of the complex must be evaluated at each successive experimental step, from the initial purification to every crystallization trial. As the chemical forces between individual protein subunits typically involve relatively labile non-covalent interactions, such as electrostatic interactions, successful purification and 2D crystallization of intact and active complexes are not trivial.

Impressive and intensive efforts by X-ray crystallography have resulted in a few structures of membrane protein complexes (2). These structures are even more impressive considering the larger amounts of protein required, the need to carefully stabilize the complexes in detergents amenable to three-dimensional (3D) crystallization, and the considerable time frames invested in determining these structures. Relatively

little is known about the structure of membrane protein complexes compared to monomeric or homooligomeric membrane proteins. However, electron crystallography, combined with single particle analysis, has provided the largest range of information on membrane protein complexes. A substantial breadth of work has been focused on the Photosystem II (PSII) complex in higher plants (Table A.1), which catalyzes water oxidation in the thylakoid membranes of chloroplasts (3). The highest resolution partial PSII structure remains at 8 Å resolution (4); although, lower resolution structures with additional subunits have provided valuable information (Table A.1). More recently, the hetero-trimeric SecYEG membrane assembly structure was also solved at 8 Å resolution by electron crystallography, and the structure showed a dimer fully capable of the native function in protein translocation activity (5). Considerable work has also been done on the structure of the photosynthetic reaction-center-light-harvesting complex I (RC-LHI), isolated from the purple membrane archeabacteria *Rhodospirillum rubrum*, with projection maps obtained to resolutions as high as 8.5 Å (6-8).

Electron crystallography of two-dimensional crystals holds tremendous promise for structure determination of membrane proteins, but the delicate nature of multi-subunit complexes requires additional precautions (Figure A.1). A variety of supplemental experimental techniques to ensure the maintenance of structural integrity are required for success. Here, various methods specific for 2D crystallization of membrane protein complexes will be outlined. These techniques are applied from initial purification to each crystallization trial to verify the structural and functional integrity of the membrane protein complex structure to be solved by cryo-EM of 2D crystals.

Table A.1 Overview of membrane protein structures, purification, and 2D crystallization conditions.

Complex	Species	Res [a] (Å)	Olig [b]	2D/ 3D [c]	Subunits	2D morph [d]	Time (days)	Temp (ºC)	Purification	Lipids	Misc [e]
PSII (9)	*S.oleracea* (spinach)	20	M[1]	2D	CP47, D1, D2, *cytb*559	T[3]	4	20	PSII membranes (TX-100[8]), HTG[9]	none	≥15 ºC, Zn^{2+} ions
" (10)	"	8	D[2]	2D	"	"	"	"	"	"	30% glycerol
" (4)	"	8	M[1]	3D	"	"	"	"	"	"	"
" (11)	"	29	D[2]	3D	"	V[4], S[5]	several	RT[7]	PSII membranes (TX-100[8]), OG[10], sucrose gradient	PTL[14]	LPR[19] critical
" (12)	"	9	D[2]	2D	CP47, D1, D2, *cytb*559, CP43, MSP	"	1 (BB[6])	19	"	"	"
" (13)	"	10	D[2]	3D	CP47, D1, D2, *cytb*559	T[3]	"	"	"	"	"
" (14)	"	20	M[1]	2D	CP47, CP43, D1, D2, MSP	T[3]	1-5	6-22	PSII membranes (TX-100[8]), OTG[11]	DMPC[15]	LPR 0.1-1
" (15)	*S. elongatus*	16	M[1]	2D	CP47, CP43, D1, D2, MSP	S[5]	2 (BB[6])	20	TM[12] prep, ion exchange, sucrose gradient	PTL[14]	5 mM $ZnSO_4$, 5 mM $MgCl_2$
SecYEG (5)	*E. coli*	8	D[2]	3D	Sec Y, Sec E, Sec G	V[4]	several weeks	23	*E. coli* expression, OG[10], $C_{12}E_9$[13], gel filtration, ion exchange	PE[16]	LPR 0.2, "several weeks", 23 ºC
RC-LH1 (8)	*R. rubrum*	8.5	M[1]	2D	RC, LH1	V[4], S[5]	2.7	20-35	sucrose gradient, ion exchange, size exclusion	DOPC[17], DHPC[18]	LPR 1.0-1.2 (w/w)

Abbreviations: [a]resolution; [b]oligomer; [c]2D/3D structure; [d]morphology; [e]miscellaneous factors noted important for 2D crystallization; [1]monomer; [2]dimer; [3]tubes; [4]vesicles; [5]sheets; [6]BioBeads; [7]room temperature; [8]Triton X-100; [9]*n*-heptyl-β-D-thioglucoside; [10]*n*-octyl β-D-glucopyranoside; [11]*n*-octyl β-D-thioglucopyranoside; [12]thylakoid membrane; [13]nonaethylene glycol monododecyl ether; [14]purified thylakoid lipids; [15]dimyristoylphosphatidylcholine; [16]phosphatidylethanolamine; [17]1,2-dioleoyl-sn-glycero-3-phosphocholine; [18]1,2-diheptanoyl-sn-glycero-3-phosphocholine; [19]lipid-to-protein ratio

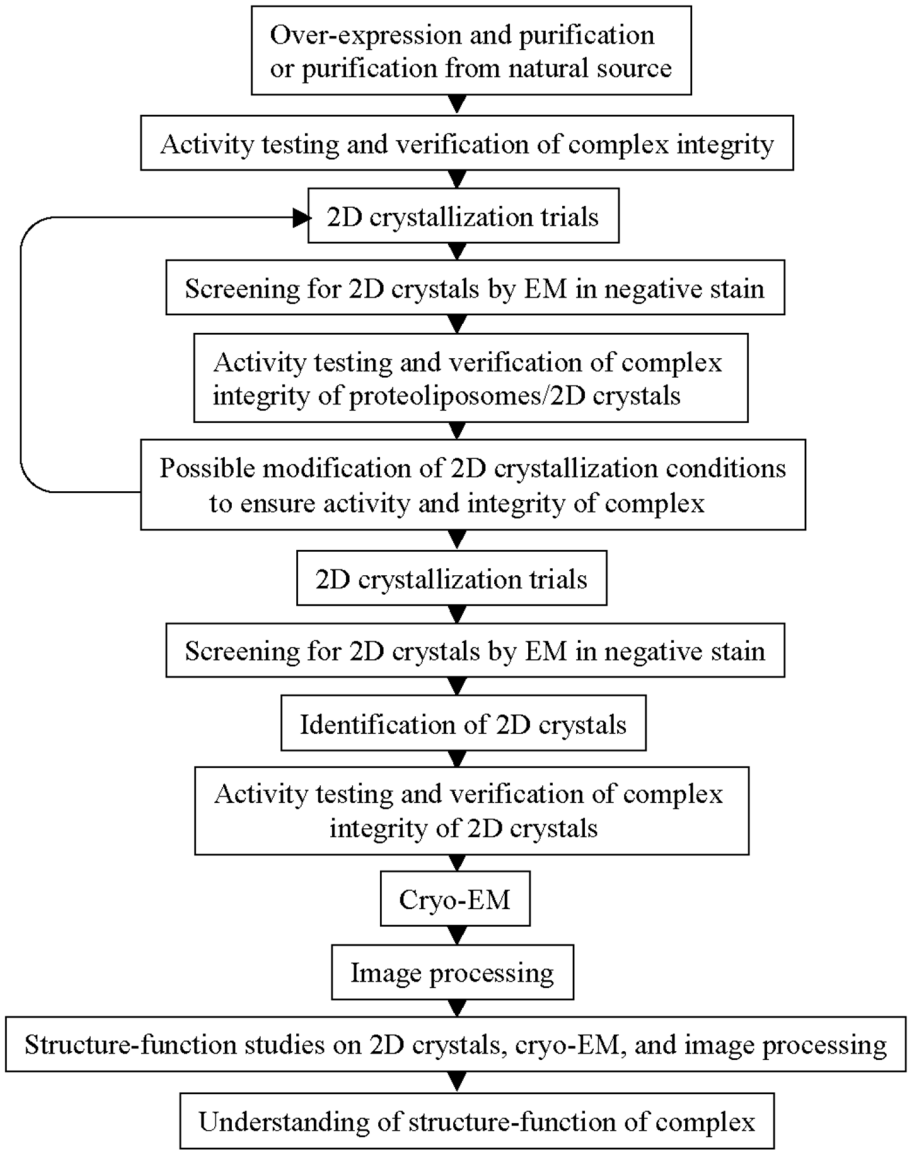

Figure A.1 2D crystallization of membrane protein complexes involves additional steps of verification of the complex integrity.

A.3 Methods in electron crystallography of membrane protein complexes

A.3.1 Overview of 2D crystallization and cryo-electron microscopy

Electron crystallography entails 2D crystallization, data collection by electron cryo-microscopy (cryo-EM), and finally image processing to solve the 3D structure of a

membrane protein. In contrast to traditional X-ray crystallography that utilizes large 3D crystals, 2D crystals consist of single layers of proteins embedded in a lipid bilayer reminiscent of the native lipid environment. The most commonly utilized process to obtain 2D crystals is reconstitution into proteoliposomes (proteins embedded in a lipid bilayer) by means of slow detergent removal by dialysis. In this approach, purified, detergent-solubilized proteins, with the detergent-protein mixture containing ideally no or minimal amounts of essential lipid, are mixed with native or exogenous lipids and placed inside a dialysis membrane or device. The combined mixture is dialyzed against a detergent-free buffer under optimal parameters for 2D crystallization. Under favorable conditions, the solubilized protein is reconstituted with lipids into a membrane ordered in two dimensions. Alternative 2D crystallization techniques for membrane proteins involve lipid monolayer 2D crystallization (16), the batch method via incubation (17), or dialysis of purified membrane proteins containing small amounts of co-purified lipids (9; unpublished observations). Screening for 2D crystals occurs by negative stain of the dialysate and evaluation by EM. Once the 2D crystals are optimized in size (to ideally ≥ 1 μm) and order, cryo-EM image acquisition and image processing results in the projection (2D) and/or 3D structure.

At present, the tangible limiting factor in structure determination by electron crystallography is 2D crystallization, which is characterized by a protein-specific, multi-dimensional phase diagram of important parameters for obtaining membrane crystals. Multi-subunit membrane protein complexes add even further complications. First, high purity and yield of the proteins of interest are often difficult to establish, especially for hydrophobic membrane proteins. Second, the detergent used for isolation is important, as

the detergent identity can affect the amount of co-purified lipids, as well as alter the structural integrity of membrane protein complexes. Third, the type and quantity of lipids added for reconstitution into membranes, or lipid-to-protein (LPR) ratio, is possibly the most important factor. Both native lipids and exogenous lipids have been used in 2D crystallization of membrane proteins, with dimyristoyl phosphatidylcholine (DMPC) identified as the most successfully used phospholipid in 2D crystallization (18). Fourth, the dialysis conditions, including the dialysis buffer composition, dialysis temperature, and dialysis time, are all important factors. Significant parameters of the dialysis buffer are the pH, salt types, salt concentrations, and glycerol concentrations, which can all affect successful crystal formation. Typically, variation in only one or more of these parameters can lead to 2D crystallization, and careful screening for crystals is also critical step.

When working with membrane protein complexes, additional caution in variation of the above-mentioned parameters during crystallization trials must be taken to ensure maintenance of structural integrity and retention of subunits (Figure A.1). In particular, unfavorable increases in salt concentration or temperature can easily disrupt weak electrostatic interactions between subunits in complexes. Homogeneity in subunit composition during purification is another concern in crystallization of proteins with multiple subunits. In general, 2D crystallization approaches to membrane complexes parallel those of single subunit or homooligomeric proteins, but additional complications require precautions and biochemical insight into the complex.

A.3.2 Gel electrophoresis

Sodium dodecyl sulfate polyacrylamide gel electrophoresis (SDS-PAGE) is a commonly used technique for the separation of non-identical proteins in a complex based on size. SDS-PAGE is a valuable method for the assessment of membrane protein complexes before and after 2D crystallization. Protein subunits can become easily detached during experimental manipulations, dialysis, and various conditions. The gel can also indicate possible cleavage or degradation of proteins that may occur during the dialysis time.

In SDS-PAGE, an anionic detergent, SDS, is used to solubilize and denature proteins. Molecules of SDS bind to proteins in a fixed mass ratio of ~1.4 grams SDS per gram of protein, and as a result, the native intrinsic charges of the proteins become negligible in the presence of the large negative charge imparted by the SDS. Proteins treated with SDS will assume rod-like shapes with equivalent mass-to-charge ratios. Consequently, the mobility through a polyacrylamide gel matrix will depend linearly based on the logarithm of molecular mass. Typically, gels for most proteins can be prepared according to the Laemmli method (19) with concentrations of ~0.1% SDS in the gel and ~2- 4% SDS in the sample buffer. Urea is a non-ionic chaotropic agent that can also be used to increase the solubility of some difficult to denature hydrophobic membrane proteins and can enhance the acuity of bands in a gel. Urea concentrations of ~4 M urea in the gel and ~5 M in the sample buffer should suffice. While SDS and urea disrupt non-covalent interactions between protein subunits in a complex, they do not break disulfide bonds. Thus, addition of reducing agents to the sample buffer, such as dithiothreitol (DTT) or β-mercaptoethanol, will ensure that these bonds are cleaved.

Gel electrophoresis analysis should first be performed following protein purification to ensure purity, to verify composition, and to establish a baseline for the 2D crystallization trials. A standard molecular weight marker is also run with every gel. Although many protein gel methods indicate heating or boiling the protein sample during or following denaturation, this approach is not compatible for membrane proteins because high temperatures can induce aggregation of the hydrophobic proteins.

To ensure that membrane protein complexes remain intact following crystallization, the 2D crystal composition needs to be analyzed on a gel and compared to the native assembly before crystallization. Ideally, PAGE is performed after introduction of each new dialysis condition. After dialysis, the 2D crystals are pelleted by centrifugation, and the supernatant is removed, which will contain any unbound proteins. The crystals are washed in dialysis buffer and centrifuged one to two times to ensure elimination of non-complexed proteins. Following a final resuspension in buffer, the crystals are solubilized and denatured in a sample buffer containing SDS, a reducing agent (DTT or β-mercaptoethanol), urea (if needed), and a color marker (such as Bromophenol Blue). At least one hour at room temperature is usually required for thorough denaturation. The solubilized 2D crystals are pelleted again to separate any unsolubilized membrane material or aggregates, the samples are loaded in the gel, and an electric potential is applied to the gel until the color marker reaches the bottom of the gel. A Coomassie Brilliant Blue R-250 (19) or silver stain (20) can be used to visualize the protein bands.

Comparison of 2D crystals before and after crystallization will indicate if loss of protein subunits occurs during dialysis (Figure A.2). Unfavorable conditions, such as

high temperatures, pH, or salt concentrations, can result in loss of structural integrity of a complex. Degradation of some protein subunits can also occur in the presence of proteases. The appearance of small molecular weight bands on the gel can be diagnostic for proteolytic cleavage. In the event that subunits are lost or degraded during dialysis, modifications to crystallization conditions can be initiated. Although SDS-PAGE is a very effective technique for evaluation of membrane protein complexes, one should be cautioned that incomplete or inconsistent occupancy of a particular protein in 2D crystals can result in contradictory results. While a gel can indicate the presence of a subunit in the complex in solution, a density map may not support a clear assignment. An example of this scenario involved the absence of density for the MSP (manganese stabilizing protein) subunit of PSII; however, MSP was identified in a gel of the crystals (13).

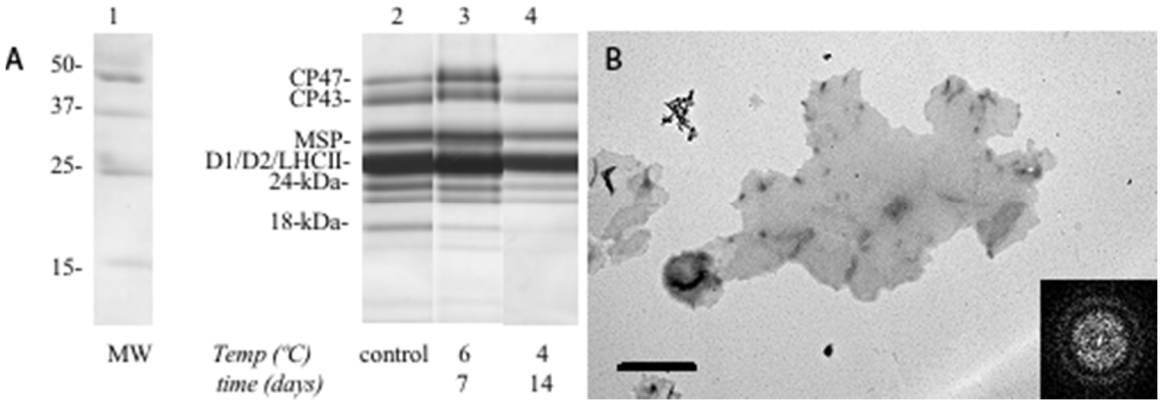

Figure A.2 Photosystem II (PSII) 2D crystals and subunit composition. In A, SDS-PAGE evaluates the structural integrity of PSII crystalline complexes following dialysis. In the gel, lane 1 contains the molecular weight (MW) marker, and lane 2 contains control PSII before dialysis for comparison; the major subunit bands are assigned. Lane 3 contains 2D crystals of PSII after dialysis for 7 days at 6 ºC, and lane 4 also contains 2D crystals subsequent to dialysis for 14 days at 4 ºC. Under the indicated crystallization conditions, PSII complexes in lane 3 appear mostly intact, compared to the control in lane 2, while the PSII complexes in lane 4 lack the 18-kDa protein. B shows an example of a PSII crystal following solubilization with 0.05% n-dodecyl α-D-maltoside (DDM-α) and dialysis for 7 days at 8 ºC. An FFT of the 2D crystal is shown in the inset of B. The scale bar in B is 0.5 μm. PSII was isolated by the method of (21) with modifications (22).

A.3.3 Western blots

When an antibody is available for a protein of interest, a Western blot, or immunoblot, is useful in unambiguous assignment of protein bands. In PSII, the psbI protein in 2D crystals was confirmed by immunoblotting analysis (9). Sometimes the apparent molecular weight of a protein on a gel can differ from the actual or predicted molecular weight based on the known sequence. In this case, a Western blot can aid in the assignment. Also, degraded proteins can sometimes be assigned from this type of experiment. However, binding ability depends on the location of the epitope, and the antibody may or may not bind to a degradation product. Two identical gels should always be prepared when doing a Western blot because one will be used for the actual blot, and the other gel will be used for comparison after the blot.

The general procedure of a Western blot involves transfer of proteins from an unstained gel onto a sheet of nitrocellulose or polyvinylidine difluoride (PVDF) membrane, which non-specifically binds proteins. Transfer is followed by specific binding with antibodies and development with a colorimetric reaction. The Towbin method is a common technique for many applications (23). Proteins are transferred onto the membrane support by application of an electric current with a semi-dry transfer apparatus. Unoccupied binding sites on the blot are blocked with a non-specific protein solution, such as casein or non-fat milk. The blot is incubated in the blocking protein solution for at least 24 hours because failure to fully block non-specific sites will result in a darkened background from non-specific antibody binding. The blot is incubated with a solution of the primary antibody, specific for the protein of interest, for a sufficient amount of time, and the unbound antibody is washed away. Finally, the blot is incubated

with a secondary antibody, targeting the species-specific primary antibody. The secondary antibody is covalently liked to a reporter enzyme that produces a colorimetric reaction when incubated with a substrate; the unbound secondary antibody conjugate is washed away. Alkaline phosphatase (AP) is a commonly used reporter enzyme because it produces a dark purple precipitate when incubated with a mixture of 5-Bromo-4-Chloro-3'-Indolyphosphate (BCIP) and Nitro-Blue Tetrazolium (NBT) (24). Mixtures of BCIP and NBT are commercially available.

Once the blot is developed, the specifically-stained bands are compared to the bands in the SDS gel to confirm uncertain protein identities. As cautioned with the SDS-PAGE, assignment of a protein in a Western blot does not necessarily indicate homogeneous binding to complexes derived from the 2D crystals. However, it is still a very useful method for identification of proteins with unusual apparent molecular weights, degradation products, or proteins with overlapping bands due to molecular weight similarities.

A.3.4 Size exclusion chromatography

Size exclusion chromatography (SEC), which separates suspended particles by hydrodynamic volume, can be a valuable tool in analyzing characteristics of detergent-solubilized membrane protein complexes. A SEC column consists of packed spherical gel particles of distinct dimensions and pore size. As protein particles move through this matrix with buffer flow, smaller particles are free to diffuse through the gel particles while larger particles are excluded from the gel particles and must move around them. The end result is that the smaller particles must flow through a greater volume of buffer

before being eluted, and the larger particles will elute first. Control of particle size and pore size enables the user to easily separate protein particles of arbitrary size from a heterogenous solution, or to observe the range of particle sizes present. Assuming that the solubilized sample is of sufficient purity, it is possible to observe the self-associated oligomeric state and the degree of detergent binding (25). A bound detergent micelle can make a substantial additional contribution to the hydrodynamic volume. However, chromatograms of a protein solubilized with a number of detergents of varying alkyl chain lengths can be compared. In this case, the volume excluded by the micelle is variable, while that of the protein is not. Size exclusion chromatography reflects additional qualities that are of particular interest to membrane protein 2D crystallization, such as the protein radius in the center of the membrane bilayer, the Stokes radius, the average radius, and the molecular mass (26).

A.3.5 Optical spectroscopy

UltraViolet-Visible (UV-Vis) absorption spectroscopy can be used before and after 2D crystallization to evaluate changes in cofactor or pigment composition. Proteins absorb light in the UV region (100-400 nm) due to aromatic side chains and peptide bonds. Visible light absorption (400-700 nm) occurs with conjugated molecules and heavy metals, such as cofactors, pigments, and active site complexes. Most molecules that absorb light in the visible portion of the spectrum are not covalently bound to the protein; thus, loss of protein subunits during crystallization may result in loss of these types of non-covalently bound molecules. Comparison of the optical absorption before and after crystallization is advantageous and an uncomplicated experiment for some

proteins with one or more types of visible light absorbing molecules. Redox state changes in some cofactors or metal centers may also be seen in an absorption spectrum. However, analogous spectra before and after 2D crystallization may not always provide helpful information regarding structural integrity. In PSII, the compositions of complexes prior to and following 2D crystallization were significantly different; although, the absorption spectra were comparable (14).

A.3.6 Immuno-gold labeling

An immunochemical technique for specific labeling of protein subunits with colloidal gold particle-antibody conjugates enables complex orientation determination within the membrane of a 2D crystal by EM. The high electron density of the gold particles enables straightforward visualization on the surface of a membrane after negative stain. For direct detection and localization, gold particles (~1-40 nm) can be conjugated to primary antibodies for a particular protein of interest within the complex, such as one that binds to a defined surface-exposed region on one side of the membrane. For indirect detection in a wider array of applications, secondary antibodies conjugated to gold particles can also be used. Under some circumstances, membrane orientation can vary between types of crystal morphologies, and immuno-gold labeling can aid in such a distinction. Immuno-gold labeling in both PSII (14) and SecYEG (5) has established protein complex orientation within membranes.

Briefly, the method involves binding the gold-antibody conjugates to the crystals by simple incubation, followed by assessment under the electron microscope. The labeled complexes are washed thoroughly to remove any non-specifically bound particles. In the

case of indirect detection with secondary antibody conjugates, the washing should follow both incubation with the primary antibody and the secondary antibody-gold conjugate. Finally, the 2D crystals are fixed with a negative stain, such as 1% uranyl acetate, and screened by EM. Immuno-gold labeling can be useful for subunits of both known and unknown binding locations within a protein complex.

A.3.7 Activity assays

Because 2D crystallization of membrane proteins requires the reconstitution (or native isolation) of the membrane proteins in a lipid bilayer, the conformation of the crystallized protein more closely resembles the native formation than that of the detergent-solubilized protein. For membrane protein complexes in particular, reconstitution into the membrane may also coax different subunits into binding that may not bind to the complex in a detergent-solubilized state, particularly those that include significant subunit-subunit interactions within the hydrophobic interior of the membrane. In addition, for single layer (non-stacking) 2D crystals, both sides of the crystal may be exposed to solvent, negating problems in substrate access for studies of enzymatic membrane proteins. Activity testing of 2D crystals is of special interest because the assays may be performed directly on the samples that will be used for gathering structural data, lending significant support for any functional conclusions drawn from these data.

A.3.8 Storage of 2D crystals

Storage requirements for 2D crystals are somewhat variable; crystals have been known to remain stable at room temperature for months and even years. Common

temperatures for storage are room temperature, 4°C, -80°C, or in liquid nitrogen. Because the stability of 2D crytals over longer periods of time can vary significantly from protein to protein, it is important to carefully observe and verify the long term stability of each sample (18). For storage at lower temperatures, smaller aliquots of 3-10 µl are plunge-frozen in liquid nitrogen and kept in a -80°C freezer or in a liquid nitrogen dewar. Membrane protein complexes with soluble subunits might require additional testing to ensure integrity of the complex after storage. Two-dimensional crystals of PSII undergo rapid degradation unless they are flash-frozen in liquid nitrogen and stored at -80°C (unpublished observations).

A.3.9 Screening for 2D crystals and electron cryo-microscopy

One of the most critical steps in identifying 2D crystals is careful screening of the crystallization trials for ordered arrays within membranes (18). Initial identification of even low percentages of poorly ordered 2D crystals can provide important guidelines to quickly optimize the formation of large and well-ordered arrays. A eukaryotic membrane protein, where one experiment revealed only 2% of proteoliposomes contained small crystal arrays, was induced to grow 2D crystals of several microns in diameter in 100% of the membranes with three further steps of optimization (27). This example illustrates the importance of investments of time and effort to identify optimal conditions and prevent the dismissal of a specific condition that in fact provides key information. The care involved in screening of negatively stained samples by EM is on the same level as for any type of 2D crystals, whether the sample consists of monomers, smaller homooligomers, or soluble proteins. For membrane protein complexes, individual

screening trials and conditions will often require the additional step of verifying both the protein activity as well as the integrity of the entire complex as outlined above (Figure A. 1). Both projection and 3D structures should confirm these findings.

Cryo-EM sample preparation follows the same protocols for membrane protein complexes as for ordered arrays of other membrane proteins. These could involve vitrification of the sample on the grid by back-injection (17), the carbon-sandwich (28,29), or plunging (30). While in conventional back-injection and plunging the sample is applied to one layer of carbon film followed by vitrification, the carbon-sandwich technique follows the same protocol as back-injection with an additional step of a second carbon film placed onto the 2D crystal solution. Thus, a sandwich of two carbon films is formed with the sample in the middle. The carbon-sandwich might provide a particular advantage for complexes with larger soluble domains or subunits since the second carbon film prevents contact of the samples with the air-water interface (31). Addition of a sugar or tannic acid to stabilize either the back-injection or the carbon sandwich grid preparation will again require testing of the mixture for integrity. A possible issue in the sample preparation could be the thickness of a very large membrane protein complex, but since large complexes of both membrane and soluble proteins have successfully been studied by cryo-EM single particle analysis (32), issues with cryo-EM grid preparation will more likely be due to incompatibility with buffer conditions or suboptimal ice thickness.

A.3.10 Automation of 2D crystallization and EM for membrane protein complexes

Two-dimensional crystallization of membrane proteins through detergent removal by dialysis and screening for 2D crystals by EM can often be a labor-intensive procedure. Data acquisition is also labor intensive once crystals of suitable quality are produced. In general, many different dialysis buffers, lipids, protein concentrations, lipid-to-protein ratios and other factors must be tested before a suitable combination for 2D crystallization is found, and each trial may require up to a week or more of dialysis. Evaluating samples for crystal order and size can also be a major time investment. The grids must be prepared, loaded into the electron microscope, and screened visually by experienced personnel. Once a suitable location in high-dimensional crystallization space has been found that reliably produces 2D crystals of high enough quality, the ordered proteoliposomes are ready for the cryo-EM data collection stage, which can also be a major time investment. There is considerable benefit, then, in automating these processes in order to increase the number of parallel trials that may be performed. This approach greatly reduces the time required to obtain two-dimensional crystals suitable for high-resolution data collection, as well as the time required to then collect that data. A number of groups are currently pursuing promising automation projects, among them modified fluid-handling systems to remove detergent via continuous flow dialysis with or without the use of BioBeads (33-35) and addition of cyclodextrin (36). Screening of samples via EM can be accelerated via automation of EM grid preparation and handling (33,35,37). Of particular interest are programs such as Leginon and PASyS, which can be used in conjunction with the electron microscope to systematically scan grids for areas of interest, and procure images, with varying levels of user interaction (38-41). Such

systems are currently of limited availability, but it is expected that in the future this may not be the case. Despite the advantages in terms of time saved, however, the greater number of simultaneous trials that can be performed requires an equally greater amount of purified protein. An unavoidable limit to crystallization trials remains the amount of protein available, which is usually a more severe obstacle for membrane protein complexes. On the other hand, automation of dialysis, requiring smaller amounts of protein than currently used, would be of tremendous benefit for the study of membrane protein complexes.

A.4 Summary of membrane protein complex structures

A.4.1 Photosystem II (PSII)

Although a vast array of work has concentrated on structure determination of PSII in higher plants by electron crystallography methods, a composition of more than 25 subunits and a temperature, detergent, and salt sensitivity constitute the chief experimental impediments. A variety of approaches have yielded assorted structural results and details. Although the reconstitution of solubilized membrane proteins into 2D crystals generally relies on addition of exogenous lipids, some PSII structures have been solved without the addition of lipids. N-heptyl-β-D-thioglucoside solubilization of PSII membrane fragments resulted in co-purification of a sufficient amount of endogenous lipids to enable 2D crystallization (4,9,10). In fact, the highest resolution structure of spinach PSII at 8 Å resolution was crystallized without supplementary lipids (4); however, this structure only contained the D1, D2, CP47, and cytb-559 proteins (4). A

dialysis temperature above 15 ºC and the presence of 0.5- 1 mM zinc ions was also observed to be essential for formation of large, well-ordered 2D crystals (9). Alternatively, reconstitution of n-octyl-β-D-glucopyranoside solubilized PSII with various ratios of additional purified thylakoid lipids also enabled induction of 2D crystal formation, as well as location and assignment of the CP43 protein (11-13). In addition to reconstitution with native thylakoid lipids, DMPC has also been used with solubilized PSII complexes (14). These complexes contained the MSP extrinsic subunit, which was also visualized in the thylakoid lipid reconstituted PSII complexes (12). Along with MSP, two other extrinsic polypeptides, the 18- and 24-kDa proteins, are essential for optimal catalytic activity; however, a more complete PSII structure in higher plants with these subunits attached has not been solved yet.

A.4.2 SecYEG

SecYEG is a hetero-trimeric channel complex located in bacterial cytoplasmic membranes that functions in protein translocation. SecYEG is an interesting example of planar-tubular 2D crystals that form as a "sandwich" of two membranes. The membranes interact through cytoplasmic domains. The structure of SecYEG was solved to 8 Å resolution in 2002 (5). The 2D crystals were grown in the presence of 120 mM NaCl, and each of the two layers consisted of a sandwich of two interacting membranes, with a total of four membranes per planar-tubular crystal. Following 2D crystallization by reconstitution with E. coli purified phosphatidylethanolamine lipids, the assembly that consisted of the SecY, SecE, and SecG polypeptides was shown to be fully active.

A.4.3 RC-LHI

In photosynthetic purple bacteria, bacteriochlorophyll-binding light harvesting complexes (LHI and LHII) transfer energy to the reaction center (RC), which generates a transmembrane potential. Cryo-EM-derived projection maps of the RC-LHI complex of Rhodospirillum rubrum have been calculated to a resolution of 8.5 Å and obtained from two-dimensional crystals of two different symmetries (p1and p4212) (8). These maps revealed that the RC adopts preferred orientations within a ring of sixteen LHI subunits, rather than a continuous distribution of orientations, indicating specific interactions between the ring and the bound RC. Depending on the crystal type, the LHI ring adopted either circular or ellipsoidal conformations, implying that the structure was somewhat flexible in vivo.

A.5 Conclusions

Electron crystallography has supplied valuable information on the structure and function of several membrane protein complexes and will likely result in many more structures at increasing resolution as further complexes can be purified and stabilized. The technique lends itself to sensitive membrane proteins, such as eukaryotic proteins and complexes, because the reconstitution into phospholipid bilayers usually has a stabilizing effect. The 2D crystallization and the cryo-EM data collection follow roughly standard procedures, but structural and functional integrity need to be verified. In cryo-EM, thickness and sensitivity issues can be solved by the carbon sandwich technique. A range of methods has been outlined here that in combination or alone are used to confirm that subunits are not lost during any of the steps from protein purification to the final

collection of cryo-EM data. These verification techniques need to be repeated at the stage of purification, after 2D crystallization trials, and before screening of negatively stained samples by EM, as well as cryo-EM. These methods ensure that the correct number of subunits in the complete complex is seen in the final cryo-EM projection and 3D structures.

A.6 References

1. Henderson, R., and Unwin, P. N. T. (1975) Three-Dimensional Model of Purple Membrane Obtained by Electron Microscopy. *Nature* **257**, 28-32

2. McLuskey, K., Roszak, A. W., Zhu, Y. S., and Isaacs, N. W. (2010) Crystal structures of all-alpha type membrane proteins. *Eur. Biophys. J. Biophys. Lett.* **39**, 723-755

3. Nelson, N., and Yocum, C. F. (2006) Structure and function of photosystems I and II. in *Annual Review of Plant Biology*, Annual Reviews, Palo Alto. pp 521-565

4. Rhee, K.-H., Morris, E. P., Barber, J., and Kuhlbrandt, W. (1998) Three-dimensional structure of the plant photosystem II reaction centre at 8 A resolution. *Nature* **396**, 283-286

5. Breyton, C., Haase, W., Rapoport, T. A., Kuhlbrandt, W., and Collinson, I. (2002) Three-dimensional structure of the bacterial protein-translocation complex SecYEG. *Nature* **418**, 662- 665

6. Walz, T., and Ghosh, R. (1997) Two-dimensional crystallization of the light-harvesting I reaction centre photounit from Rhodospirillum rubrum. *J. Mol. Biol.* **265**, 107-111

7. Stahlberg, H., Dubochet, J., Vogel, H., and Ghosh, R. (1998) Are the light-harvesting I complexes from Rhodospirillum rubrum arranged around the reaction centre in a square geometry? *J. Mol. Biol.* **282**, 819-831

8. Jamieson, S. J., Wang, P. Y., Qian, P., Kirkland, J. Y., Conroy, M. J., Hunter, C. N., and Bullough, P. A. (2002) Projection structure of the photosynthetic reaction centre-antenna complex of Rhodospirillum rubrum at 8.5 angstrom resolution. *Embo J.* **21**, 3927-3935

9. Nakazato, K., Toyoshima, C., Enami, I., and Inoue, Y. (1996) Two-dimensional crystallization and cryo-electron microscopy of photosystem II. *J. Mol. Biol.* **257**, 225-232

10. Rhee, K.-H., Morris, E. P., Zheleva, D., Hankamer, B., Kuhlbrandt, W., and Barber, J. (1997) Two-dimentional structure of plant photosystem II at 8 A resolution. *Nature* **389**, 522-526

11. Morris, E. P., Hankamer, B., Zheleva, D., Friso, G., and Barber, J. (1997) The three-dimensional structure of a photosystem II core complex determined by electron crystallography. *Structure* **5**, 837- 849

12. Hankamer, B., Morris, E. P., and Barber, J. (1999) Revealing the structure of the oxygen-evolving core dimer of photosytem II by cryoelectron crystallography. *Nature Structural Biology* **6**, 560- 564

13. Hankamer, B., Morris, E. P., Nield, J., Gerle, C., and Barber, J. (2001) Three-dimensional structure of the photosystem II core dimer of higher plants determined by electron microscopy. *Journal of Structural Biology* **125**, 262- 269

14. Tsiotis, G., Walz, T., Spyridaki, A., Lustig, A., Engel, A., and Ghanotakis, D. (1996) Tubular Crystals of a Photosystem II Core Complex. *J. Mol. Biol.* **259**, 241- 248

15. da Fonseca, P., Morris, E. P., Hankamer, B., and Barber, J. (2002) Electron crystallographic study of photosystem II of the cyanobacterium Synechococcus elongatus. *Biochemistry* **41**, 5163-5167

16. Venien-Bryan, C., Lenne, P. F., Zakri, C., Renault, A., Brisson, A., Legrand, J. F., and Berge, B. (1998) Characterization of the growth of 2D protein crystals on a lipid monolayer by ellipsometry and rigidity measurements coupled to electron microscopy. *Biophys. J.* **74**, 2649-2657

17. Wang, D. N., and Kühlbrandt, W. (1991) High-Resolution Electron Crystallography of Light-Harvesting Chlorophyll *a/b*-Protein Complex in Three Different Media. *J. Mol. Biol.* **217**, 691-699

18. Schmidt-Krey, I. (2007) Electron crystallography of membrane proteins: Two-dimensional crystallization and screening by electron microscopy. *Methods* **41**, 417-426

19. Laemmli, U. K. (1970) Cleavage of Structural Proteins During Assembly of Head of Bacteriophage -T4. *Nature* **227**, 680-&

20. Morrissey, J. H. (1981) Silver stain for proteins in polyacrylamide gels- A modified procedure with enhanced uniform sensitivity. *Anal. Biochem.* **117**, 307-310

21. Berthold, D. A., Babcock, G. T., and Yocum, C. F. (1981) A highly resolved, oxygen- evolving photosystem II preparation from spinach thylakoid membranes. *FEBS Lett.* **134**, 231-234

22. Anderson, L. B., Ouellette, A. J. A., and Barry, B. A. (2000) Probing the structure of photosystem II with amines and phenylhydrazine. *J. Biol. Chem.* **275**, 4920-4927

23. Towbin, H., Staehelin, T., and Gordon, J. (1979) Electrophoretic Transfer of Proteins from Polyacrylamide Gels to Nitrocellulose Sheets- Procedure and Some Applications. *Proc. Natl. Acad. Sci. U. S. A.* **76**, 4350-4354

24. Leary, J. J., Brigati, D. J., and Ward, D. C. (1983) Rapid and senstive colorimetric method for visualizing biotin-labeled DNA probes hybridized to DNA or RNA on nitrocellulose- bio blots. *Proc. Natl. Acad. Sci. U. S. A.* **80**, 4045-4049

25. le Maire, M., Champeil, P., and Moller, J. V. (2000) Interaction of membrane proteins and lipids with solubilizing detergents. *Biochim. Biophys. Acta-Biomembr.* **1508**, 86-111

26. Kunji, E. R. S., Harding, M., Butler, P. J. G., and Akamine, P. (2008) Determination of the molecular mass and dimensions of membrane proteins by size exclusion chromatography. *Methods* **46**, 62-72

27. Zhao, G., Johnson, M. C., Schnell, J. R., Kanaoka, Y., Haase, W., Irikura, D., Lam, B. K., and Schmidt-Krey, I. (2010) Two-dimensional crystallization conditions of human leukotriene C(4) synthase requiring adjustment of a particularly large combination of specific parameters. *Journal of Structural Biology* **169**, 450-454

28. Koning, R. I., Oostergetel, G. T., and Brisson, A. (2003) Preparation of flat carbon support films. *Ultramicroscopy* **94**, 183-191

29. Gyobu, N., Tani, K., Hiroaki, Y., Kamegawa, A., Mitsuoka, K., and Fujiyoshi, Y. (2004) Improved specimen preparation for cryo-electron microscopy using a

symmetric carbon sandwich technique. *Journal of Structural Biology* **146**, 325-333

30. Ren, G., Cheng, A., Reddy, V., Melnyk, P., and Mitra, A. K. (2000) Three-dimensional fold of the human AQP1 water channel determined at 4 angstrom resolution by electron crystallography of two-dimensional crystals embedded in ice. *J. Mol. Biol.* **301**, 369-387

31. Schmidt-Krey, I., Haase, W., Mutucumarana, V., Stafford, D. W., and Kuhlbrandt, W. (2007) Two-dimensional crystallization of human vitamin K-dependent gamma-glutamyl carboxylase. *Journal of Structural Biology* **157**, 437-442

32. Rubinstein, J. L. (2007) Structural analysis of membrane protein complexes by single particle electron microscopy. *Methods* **41**, 409-416

33. Cheng, A., Leung, A., Fellmann, D., Quispe, J., Suloway, C., Pulokas, J., Abeyrathne, P. D., Lam, J. S., Carragher, B., and Potter, C. S. (2007) Towards automated screening of two-dimensional crystals. *Journal of Structural Biology* **160**, 324-331

34. Jap, B. K., Zulauf, M., Scheybani, T., Hefti, A., Baumeister, W., Aebi, U., and Engel, A. (1992) 2D crystallization- From art to science. *Ultramicroscopy* **46**, 45-84

35. Vink, M., Derr, K., Love, J., Stokes, D. L., and Ubarretxena-Belandia, T. (2007) A high-throughput strategy to screen 2D crystallization trials of membrane proteins. *Journal of Structural Biology* **160**, 295-304

36. Iacovache, I., Biasini, M., Kowal, J., Kukulski, W., Chami, M., van der Goot, F. G., Engel, A., and Remigy, H. W. (2010) The 2DX robot: A membrane protein 2D crystallization Swiss Army knife. *Journal of Structural Biology* **169**, 370-378

37. Potter, C. S., Pulokas, J., Smith, P., Suloway, C., and Carragher, B. (2004) Robotic grid loading system for a transmission electron microscope. *Journal of Structural Biology* **146**, 431-440

38. Suloway, C., Pulokas, J., Fellmann, D., Cheng, A., Guerra, F., Quispe, J., Stagg, S., Potter, C. S., and Carragher, B. (2005) Automated molecular microscopy: The new Leginon system. *Journal of Structural Biology* **151**, 41-60

39. Carragher, B., Kisseberth, N., Kriegman, D., Milligan, R. A., Potter, C. S., Pulokas, J., and Reilein, A. (2000) Leginon: An automated system for acquisition of images from vitreous ice specimens. *Journal of Structural Biology* **132**, 33-45

40. Potter, C. S., Chu, H., Frey, B., Green, C., Kisseberth, N., Madden, T. J., Miller, K. L., Nahrstedt, K., Pulokas, J., Reilein, A., Tcheng, D., Weber, D., and Carragher, B. (1999) Leginon: a system for fully automated acquisition of 1000 electron micrographs a day. *Ultramicroscopy* **77**, 153-161

41. Nakamura, N., Fujiyoshi, Y., Mitsuoka, K., Murata, M., and Shinkawa, T. (2003) An image evalutation system coupled with auto-TEM. *Microscopy and Microanalysis* **9**

VITA

TINA MICHELLE DREADEN KASSON

DREADEN KASSON was born in Atlanta, Georgia. She attended public schools in McDonough, Georgia and received a Bachelor of Science in Biology from The University of Georgia, Athens, Georgia in 2004 before coming to Georgia Tech to pursue a doctorate in Chemistry and Biochemistry. When she is not working on her research, Ms. Dreaden Kasson enjoys running and sampling exotic cuisine around the city.